Investigation into Key Pavement Materials and Local Calibration on MEPDG

A Dissertation Presented for the
Doctor of Philosophy
Degree
The University of Tennessee, Knoxville

Changjun Zhou
August 2013

ACKNOWLEDGEMENTS

The prime gratitude of mine would be given to my sincere gratitude to my advisor, Dr. Baoshan Huang, for his guidance, support, assistance, and encouragement throughout my doctoral study. I could not finish the research topics without his insightful suggestions and remarks.

I would also like to thank other professors in my doctoral committee, Dr. Eric D. Drumm, Dr. Khalid Alshibli, Dr. Z. John Ma, and Dr. Xiang Shu for taking their precious time to serve on my committee.

My special thanks go to Dr. Xiang Shu for his help and suggestions on my research. I would like to extend my appreciation to my colleagues and friends, Dr. Qiao Dong, Dr. Hao Wu, Dr. Jingsong Chen, Dr. Ximiao Jiang, Benjamin F. Bowers, Sheng Zhao, Dr. Shanshan Jin, Tyler Rutherford for their help and friendship.

I would also give my thanks to Pavement Design Division of Tennessee Department of Transportation for the financial support.

Finally, I would like to thank my parents and my sisters and brothers. They always show their strong support on my study and research. Their love and encouragement deserve special recognition.

ABSTRACT

The release of Mechanistic-Empirical Pavement Design Guide (MEPDG) in 2004 has been leading a transition from empirically-based pavement design to a mechanical-empirical procedure. The pavement performance prediction models in the MEPDG combines design inputs such as material properties, traffic, and climate to the observed field performance. Since the prediction models were primarily calibrated through inputs and pavement performance data from Long Term Pavement Performance database, local calibrations were highly recommended due to the potential differences between national and local conditions.

Key properties of pavement materials were investigated for the local calibration of the MEPDG, including the coefficient of thermal expansion (CTE) of cement concrete and the resilient modulus of soils. CTE values and other properties of concrete from eight concrete plants were investigated. A micromechanical model was proposed to predict concrete CTE considering the time and energy exhausted experimental methods. The thermal stress analysis was conducted on a composite material composed of aggregate and cement paste. Aggregate gradation was incorporated into the concrete CTE prediction model. The proposed model was validated by experimental data. Sensitivity analysis was also performed to explore the major factors affecting concrete CTE.

The MEPDG utilizes the generalized model to describe the subgrade stiffness. Coefficients of the generalized model were regressed from the cyclic triaxial load test

data for soils in Tennessee. Also the coefficients were correlated with soil physical properties and employed in evaluating the seasonal variation of subgrade resilient modulus. The influences of seasonal variation in subgrade resilient modulus on pavement performance were explored and found significant. Therefore, seasonal variation of soil resilient modulus should be considered in pavement design and analysis in MEPDG.

The highway pavement sections in the Tennessee pavement management system were analyzed using the MEPDG version 1.1. This analysis indicates that the national calibrated models predict pavement performance poorly in comparison with measured data. Local calibrations on rutting transfer functions were conducted on the two main types of pavements, i.e., asphalt overlay on cement concrete pavement and asphalt overlay on asphalt pavement. With the local coefficients provided, the MEPDG provides better agreement between predicted and measured rutting.

Keywords: MEPDG, Micromechanics, Concrete CTE, Soil Resilient Modulus, Verification, Local Calibration

TABLE OF CONTENTS

LIST OF TABLES

LIST OF FIGURES

LIST OF ACRONYMS

AADT: Annual Average Daily Traffic

AADTT: Annual Average Daily Truck Traffic

AASHTO: American Association of State Highway and Transportation Officials

CTE: Coefficient of Thermal Expansion

ESAL: Equivalent Single Axle Load

HMA: Hot Mixed Asphalt

IRI: International Roughness Index

LTPP: Long Term Pavement Program

MEPDG: Mechanical-Empirical Pavement Design Guide

NCHRP: National Cooperative Highway Research Program

OGFC: Open Graded Friction Course

PMS: Pavement Management System

PSI: Present Serviceability Index

TDOT: Tennessee Department of Transportation

PART 1 RESEARCH BACKGROUND AND OBJECTIVES

1.1 Research Background

The release of Mechanistic-Empirical Pavement Design Guide in 2004 under National Cooperative Highway Research Program Project 1-37A has been leading a transition from empirically-based pavement design to a mechanical-empirical procedure. The pavement performance prediction models in the MEPDG combines design inputs such as material properties, traffic, and climate to the observed field performance. Since the prediction models were primarily calibrated through inputs and pavement performance data from Long Term Pavement Performance (LTPP) database (ARA, 2004), local calibrations are highly recommended by AASHTO due to the potential differences between national and local conditions. Such activities have been taking places in multiple states prior to implementation.

The general procedure for calibrating the MEPDG follows the flow chart recommended by Von Quintus et al. (2009). With consideration of local conditions in Tennessee, the calibration of MEPDG in Tennessee was designed to be conducted as shown in Figure 1.1.

The first step toward local calibration of MEPDG is establishing inputs database for local materials. Concrete CTE and subgrade resilient modulus have been proven to significantly influence pavement performance. They are required in MEPDG as level 1 and/or 2 inputs. Concrete CTE directly affects thermal cracking and can accelerate other distresses like faulting and uneven settlement on rigid pavements. Resilient modulus of

subgrade presents the stiffness of subgrade. A sound support from subgrade is fundamental to the whole pavement structure and is a precondition for a pavement with a high service level.

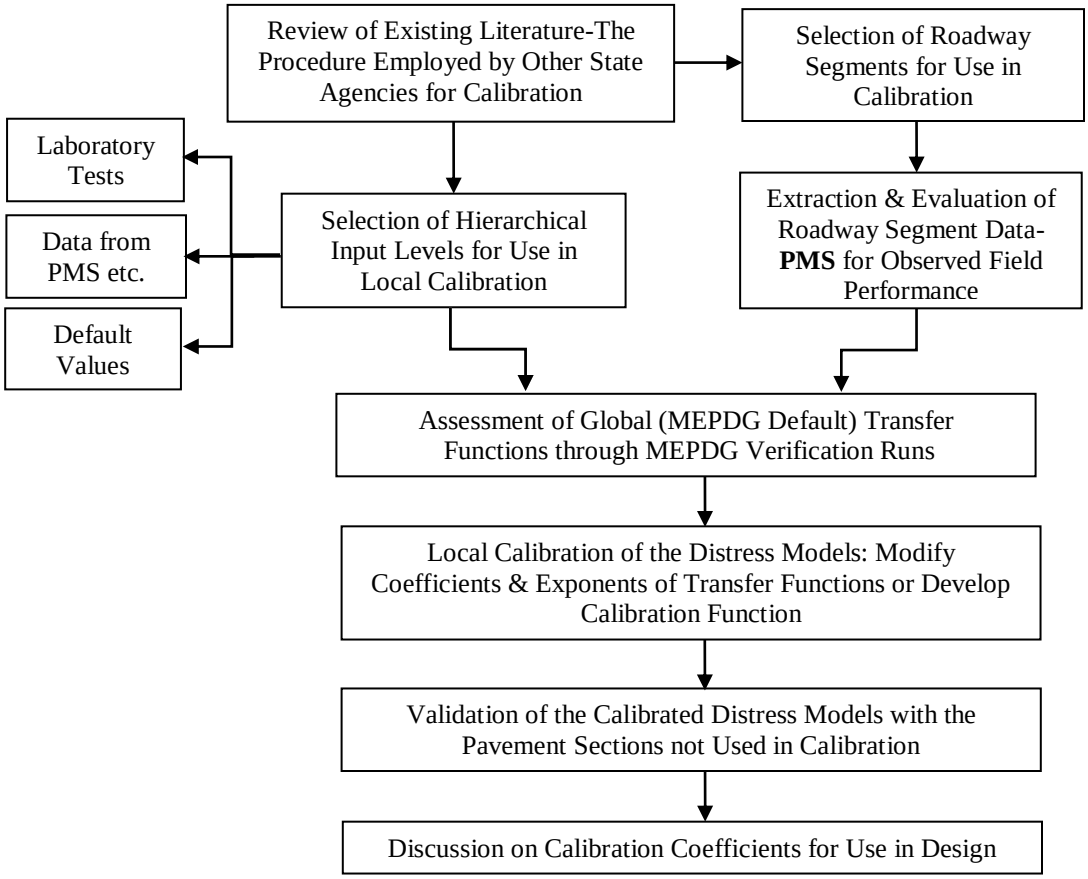

Figure 1.1 Procedure for Local Calibration in Tennessee

The transfer functions in MEPDG were developed based on LTPP, which covers the whole North America. The coefficients of the transfer functions or the functions themselves may not predict pavement performance in a specific state properly due to the variations on traffic, climate, pavement structures, and materials. Therefore, other

resources, like pavement management system (PMS) were utilized to validate and/or calibrate the distress prediction models in MEPDG.

1.2 Research Objectives and Scope

This dissertation is dedicated to the primary parts of the calibration procedure: investigating critical properties of typical pavement materials; collecting design inputs and field performance information from the Pavement Maintenance System (PMS) in Tennessee; and verification and calibration the MEPDG. Specifically, the objectives and the scope of this study include:

- To investigate the coefficient of thermal expansion of Portland cement concrete in TN

Raw materials of Portland cement concrete were collected from eight ready-mix concrete plants across Tennessee and transported to the Infrastructure Materials Laboratory of the University of Tennessee. Specimens were molded and tested in the laboratory for basic properties, such as compressive strength, elastic modulus, and CTE values at 28 days.
Due to its time and energy consuming characteristics of the experimental method of CTE, an alternate method, micromechanical model, was proposed. Thermal stress analysis was conducted on composite material composing with aggregate and cement paste. Aggregate gradation was incorporated in the model for CTE prediction. The proposed model was

validated by experimental data in Tennessee and other states. Sensitivity analysis was also performed to explore the major factors affecting concrete CTE.

- To investigate the resilient modulus of soils in TN

From test data of cyclic triaxial load tests for fourteen soils in Tennessee (Drumm, et al. 1996 & 1997), the coefficients of the generalized model were obtained. The coefficients were correlated with soil physical properties and employed in evaluating the seasonal variation of subgrade resilient modulus. The influences of seasonal variation in subgrade resilient modulus on pavement performance were explored.

- To verify and calibrate MEPDG in TN

The pavement performance of highway pavement sections in Tennessee was analyzed using the MEPDG version 1.1. Concrete CTE, subgrade resilient modulus, and other properties of local materials were utilized as inputs in MEPDG. The rutting transfer functions in MEPDG were validated and calibrated with the measured pavement performance data in PMS in Tennessee.

1.3 Research Procedure

Generally, the research procedure can be shown in Figure 1.2. Material inputs in MEPDG such as concrete CTE and soil resilient modulus, and other properties were collected in laboratory. Alternate approaches were developed in reaching concrete CTE and soil

resilient modulus, which potentially provide great benefits. Then typical pavement sections from TDOT PMS were selected and inputs such as pavement structure and traffic were collected. The MEPDG version 1.1 ran and local calibration and validation were conducted through the comparison between predicted distresses and measured distresses from TDOT PMS.

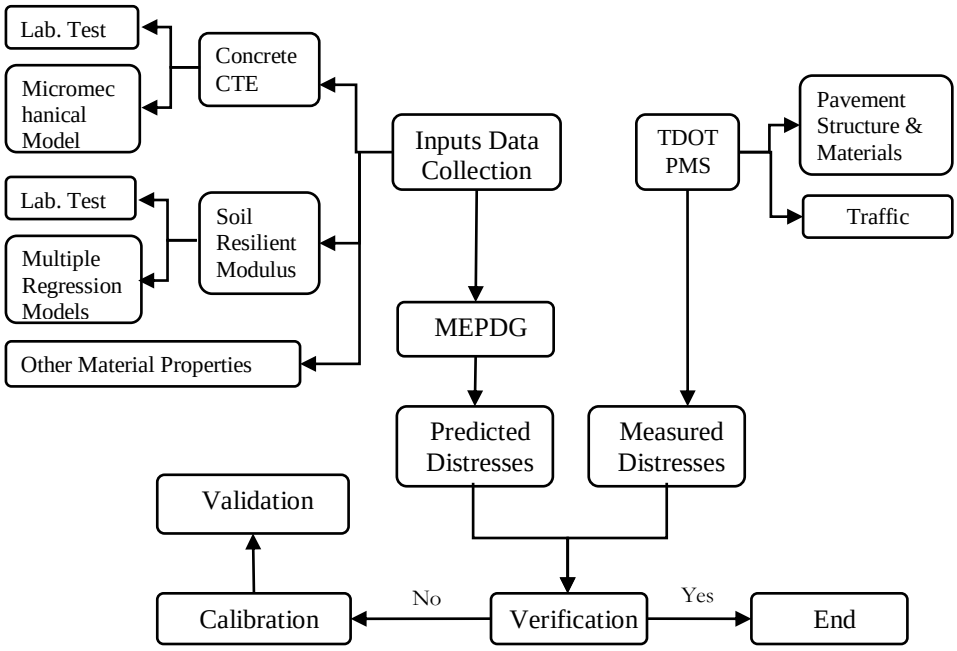

Figure 1.2 Procedure of the research

1.4 Significance Original contributions

Database of the two key properties of pavement materials, CTE of concrete and Mr of subgrade soil, were established, which is a fundamental step toward the calibration of MEPDG in Tennessee.

Micromechanics was firstly introduced into predicting concrete CTE. Comparing other empirical methods for predicting concrete CTE, the proposed model reveals the mechanism of concrete thermal expansion. The influences of factors such as aggregates' CTE, gradation, and water cement ratio on the CTE of concrete were investigated through the proposed model. Considering the time-consuming and energy-exhausting characteristics of experimental methods for concrete CTE, the proposed model has great potential benefits from views of economy and construction.

Concern to the generalized model utilized in MEPDG for subgrade resilient modulus, regressed models between coefficients of the generalized model to physical properties of soils in TN were firstly developed. These models are very helpful to evaluate the seasonal variation of subgrade resilient modulus, and also can be an alternate approach to obtain resilient modulus of soil if experimental apparatus are not available.

Key properties of typical pavement materials obtained from the laboratory were adopted into MEPDG as inputs. Pavement sections in PMS in TN were investigated and information including basic inputs and measured pavement performance were utilized in the verification and local calibration on MEPDG. The mechanism of the rutting transfer function in asphalt layers was discussed and a foundation was found on individual local calibration for each of the two different pavement structures: asphalt overlay on PCC pavements and flexible pavements. Then the rutting transfer function of the asphalt layer

was successfully calibrated utilizing PMS data in Tennessee. This is the first activity on the calibration of MEPDG in TN.

1.5 References

ARA Inc. (2004). "National Cooperative Highway Research Program (NCHRP) 1-37A, Guide for the Mechanistic-Empirical Design for New and Rehabilitated Pavement Structures." Transportation Research Board, Washington, DC.

Drumm, E.C., Li, Z., Reeves, J.S., and Madgett, M.R. (1996). "Alternative Test Method for Resilient Modulus of Fine-Grained Subgrades." Geotechnical Testing Journal, 19(2), pp. 141-154.

Drumm, E.C., Reeves, J.S., Madgett, M.R. and Trolinger, W.D. (1997). "Subgrade Resilient Modulus Correction for Saturation Effects." Journal of Geotechnical and Geoenvironmental Engineering, 123(7), pp. 663-670.

Mallela, J., Glover, L. T., Darter, M. I., Quintus, H. V., Gotlif, A., Stanley, M. and Sadasivam, S. (2009). "Guidelines for Implementing NCHRP 1-37A M-E Design Procedures in Ohio", Applied Research Associates, Inc., ODOT, U.S.DOT, FHA.

PART 2 INVESTIGATION ON CONCRETE COEFFICIENT OF THERMAL EXPANSION WITH A MICROMECHANICAL MODEL

This part is revised partially based on a paper published by Changjun Zhou, Baoshan Huang, and Xiang Shu:

Zhou, C., Huang, B., and Shu, X. (2012). " A Micromechanical Model for Predicting Coefficient of Thermal Expansion of Concrete." Journal of Materials in Civil Engineering (doi: 10.1061/(ASCE)MT.1943-5533.0000663).

My primary contributions to this paper include (1) development of the problem into a work, (2) identification of the study objective and scope, (3) deducing equations and developing the prediction model, (4) fulfilling comments from co-authors in the paper, (5) the writing.

2.1 Abstract

The transition from AASHTO 1993 design guide to new Mechanistic-Empirical Pavement Design Guide (MEPDG) in United States seems to be an inevitable trend. The concrete coefficient of thermal expansion (CTE) represents the thermal expansion and/or contraction sensitivity of concrete slab and is a critical input for concrete pavement design and analysis in MEPDG. CTE values of typical concrete in TN were measured in the laboratory. However, test methods of concrete CTE are time-consuming. Based on the thermal mechanical analysis, a micromechanical model was developed to predict concrete CTE, which is different from most empirical models. The proposed model was validated by laboratory test results in Tennessee and Alabama. Factors influencing concrete CTE were studied utilizing the proposed model. The proposed model could be

helpful in evaluating concrete CTE in cement concrete pavement design and reaching concretes with low CTE values in concrete mixture design.

2.2 Introduction

When excessive temperature differences exist in a concrete pavement structure or its surroundings, the disequilibrium of the potential volumetric changes in the structure, when restrained, introduces inner tensile stresses. When these tensile stresses exceed the in-place concrete tensile strength, thermal cracks occur. The hairline thermal cracks could not be easily found and may not affect concrete pavement performance immediately. However, thermal cracks could be a durability problem for concrete pavements. Thermal cracks on pavement slabs change the stress states in concrete slabs and structural layers beneath them. Uneven settlement may occur on the two sides of cracks. Precipitation makes this situation worse due to the negative impact of moisture to the subgrade stiffness and the loss of fine particles through cracks under hydrodynamic pressures. In general, transverse cracks could shorten service lives of rigid pavements, decrease the service level, and increase maintenance cost.

The thermal expansion sensitivity of concrete can be reflected by its basic characteristic, the coefficient of thermal expansion (CTE). CTE, defined as the rate at which concrete contracts or expands as temperature changes, affects thermal cracking development in concrete pavements. Recently, the AASHTO mechanistic-empirical pavement design guide (MEPDG) requires CTE as a crucial input for concrete pavement design (ARA, Inc.

2004). Ceylan et al. (2013) conducted a comprehensive global sensitivity analyses (GSA) of jointed plain concrete pavement performance predictions to MEPDG design inputs. They found faulting, transverse cracking, and international roughness index (IRI) are very sensitive to the concrete CTE. Numerous studies investigated the CTE of PCC and its impact on concrete pavements (Shin and Chung 2011; Tran et al. 2008; Sakyi-Bekoe 2008).

There are mainly two types of approaches to obtain concrete CTE, i.e., laboratory tests and prediction models. AASHTO T336-09 (AASHTO 2009), updated from AASHTO TP 60-00 (AASHTO 2007), is the latest method for testing concrete CTE. In AASHTO T336-09, a saturated concrete specimen is set vertically in a metal frame. A water bath is used to change the temperature of the specimen and the frame. The length change of the specimen is measured to calculate CTE. However, a mistake was found in AASHTO TP60-00 and its impact was discussed (Tanesi et al., 2010). Won (2005) found that the accuracy and repeatability of the AASHTO TP60-00 test method relies greatly on the accuracy and stability of the length changes at the low and high temperature boundaries, i.e., 10℃ and 50℃. He suggested that the slope of the deformation versus temperature curve be used as concrete CTE, rather than the value determined just from the length difference under the upper and lower temperature boundaries. This modified method gives slightly higher values of CTE (Kohler et al. 2007). Other CTE test methods were also proposed but received less attention, such as CRD-C 39-81 (US CORPS OF ENGINEERS 1981), sealed beam-air heating method (Yeon et al. 2009), ASTM E831 (ASTM 2006), vibrating wire extensometer method (Kada et al. 2002).

It is found that concrete CTE depends upon many factors, such as the CTE values of raw materials, aggregate type (Mukhopadhyay et al. 2007; Sakyi-Bekoe 2008; Naik et al. 2011; Tran, N., et al. 2008), moisture (Jeong, et al. 2012; Yeon et al. 2009; Naik et al. 2011; Sellevold and Bjøntegaard 2006), age (Jeong, et al. 2012; Jahangirnejad et al. 2008; Yao and Zheng, 2007), and some other factors.

Generally, most of the existing concrete CTE prediction models are based on the rule-of mixtures, i.e., concrete CTE is the weighted average of its components' CTEs. Nevertheless, they are slightly different from each other. Emanuel and Hulsey (1977) proposed a prediction model for concrete CTE in which the following factors are included: the proportions and CTEs of individual components, moisture, age, and temperature. Neville and Brooks (1987) noted that composition and moisture condition at the time of temperature change affect concrete CTE. They proposed a prediction model with the following variables: CTEs of cement mortar and aggregates, the stiffness ratio of cement paste to aggregate, and the volume fractions of aggregate. Mukhopadhyay et al. (2007) proposed in the first step a model to predict aggregate CTE based on the calculated weight percentages, pure mineral CTEs, and their elastic moduli. The CTE of the pure mineral was measured by dilatometry. Then based on the concept of the Hirsch's composite model (Hirsch 1962), they developed in the second step a prediction model for concrete CTE in which aggregate CTE, mortar CTE, volume fractions of components, and elastic moduli of components are independent variables.

Laboratory testing, AASHTO T336-09 for instance, requires expensive apparatus and is time-consuming and energy-exhausting. Further, different laboratory tests usually provide varied concrete CTE values due to the variation of testing conditions, which introduces difficulties to define a "standardized" concrete CTE value for a specific concrete. On the other hand, the prediction models in Table 2.1 empirically evaluate concrete CTE values from physical and mechanical parameters based on the-rule-of mixtures. The mechanism of the thermal expansion of concrete was rarely investigated from a view of micromechanics. In addition, an important factor, aggregate gradation, has not been well demonstrated on its effect on concrete CTE.

2.3 Impact of Concrete CTE on Concrete Pavement Performance

The importance of concrete CTE to the concrete pavement performance should be investigated prior to the development of concrete CTE model. A concrete pavement section on I-40 interstate highway in Davidson County, Tennessee was selected for the analysis. The pavement structure includes 10in. concrete slab and 9in. granular base, beneath which is subgrade with a k-value of 145. The total number of equivalent single axle loads (ESALs) is 10.1million. The climate in the location was assumed to be the same as the climatic station in Nashville, Tennessee as they are very close geographically. A sensitivity analysis on the influence of concrete CTE on pavement performance was conducted. In the control group, the concrete CTE was assumed as national default one, $9.9\times10^{-6}/^{o}C$. In the test groups, concrete CTE values deviated from the default value in

10% and 20%. The Version 1.100 MEPDG software Version provided pavement performance, which was summarized in the Figure 2.1.

Table 2.1 Summary on concrete CTE prediction models

	Emanuel and Hulsey, 1977	Neville and Brooks, 1987	Mukhopadhyay et al., 2007
Factors Covered	(1) the proportions of individual components, (2) the CTEs of individual components, (3) moisture, (4) age, (5) temperature.	(1) the CTEs of individual components (2) the stiffness ratio of cement paste to aggregate, (3) the volume fractions of aggregate	**Step1: aggregate CTE** (1) calculated weight percentages, (2) pure mineral CTEs, (3) aggregate elastic moduli **Step2: concrete CTE** (1) aggregate CTE (2) mortar CTE (3) volume fractions of components, (4) elastic moduli of components

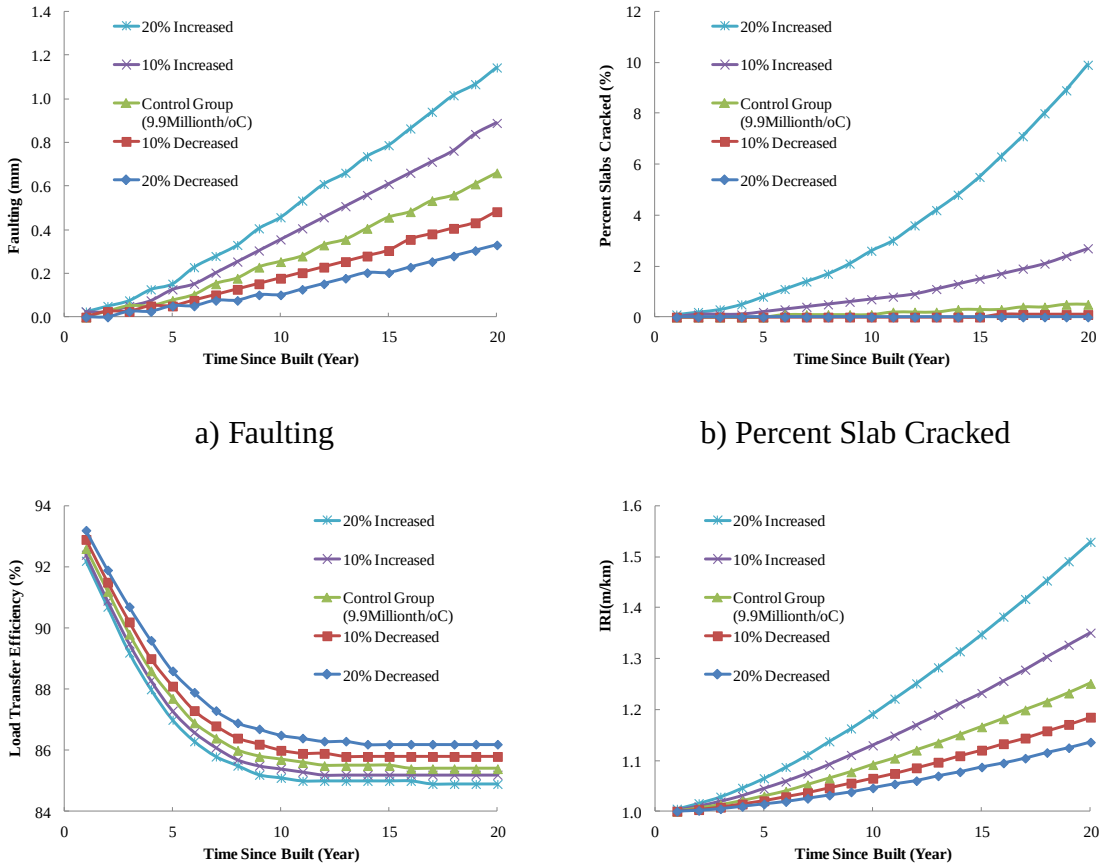

a) Faulting

b) Percent Slab Cracked

c) Load Transfer Efficiency

d) International Roughness Index (IRI)

Figure 2.1 Influence of concrete CTE on concrete pavement performance

It can be clearly seen that higher concrete CTE values introduce higher faulting, decrease load transfer efficiency, and increase concrete slab cracks, and therefore contribute to higher international roughness indices. The deterioration rate of concrete pavement accelerates when concrete CTE increases, especially slab cracks (appears as an exponential growth). On the other hand, a concrete slab with lower concrete CTE value could enhance the service level and extend the service lives of concrete pavements.

Therefore, it is very important to investigate the concrete CTE value and to take measurements to decrease the value before construction.

2.4 Study on Concrete CTE in Laboratory

In order to develop a concrete CTE value database in TN, raw materials from eight concrete plants (Figure 2.2) were collected. The plants were located at Memphis, Spring Hill, Nashville, Chattanooga, Sparta, Oak Ridge, Morristown, Blountville in Tennessee (from left to right on Figure 2.2), and cylinders (6 by 12 in.) were molded and tested for compressive strength, elastic modulus and CTE values at 28 and/or 60 days, according to ASTM C39 (ASTM, 2012), AASHTO T336 (AASHTO, 2009) , respectively. Test results were summarized in Table 2.2. Detailed information can be referred to in Appendix A.

Some articles claimed that the concrete coefficients of thermal expansion have an increasing trend since casting (Buch and Jahangirnejad, 2008). However, this conclusion is not solid. Experimental works conducted by Alungbe et al. (1992) show that the concrete CTE decreases with increasing age, from 28days' and 90 days' test results. Emanuel and Hulsey (1977) claimed that the concrete CTE decreases with increasing age for a Type I cement paste. Therefore, no general conclusion can be made on the effect of concrete age on concrete CTE currently.

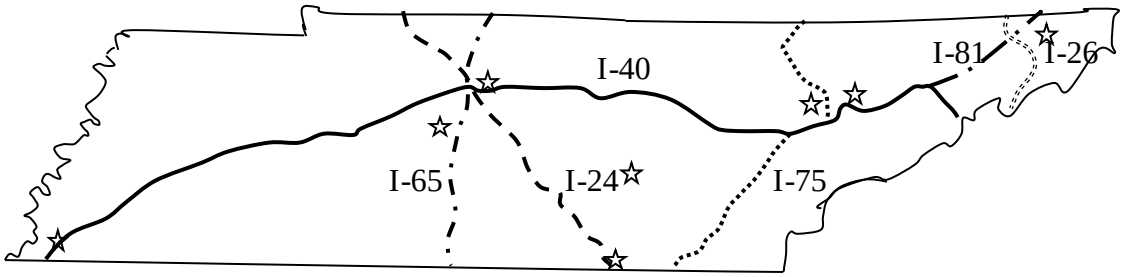

Figure 2.2 Concrete plants for concrete CTE database

Table 2.2 Summary on properties of concrete in TN

Contract No.	Location	Company	Compressive Strength (MPa), 28d	Elastic Modulus (GPa), 28d	CTE (10^{-6}/°C)	
					28d	60d
CNK 914	Harrison Anderson	APAC	23.5	23.4	9.21	9.39
CNK 014	Morristown	IMI	20.1	19.9	9.93	8.10
CNK 811	Spring Hill	IMI	21.0	20.7	7.44	7.19
PIN# 113411.00	Nashville	IMI	22.1	20.2	6.47	6.59
CNK 067	Memphis	APAC	20.3	19.9	8.57	8.50
CNJ 232	Chattanooga	Sequatchie	20.9	20.5	10.14	9.67
CNJ 060	Sparta	IMI	21.0	21.2	8.73	8.71

It is not practical to reach an "optimal" concrete mix design with lowest CTE value from laboratory experiments, considering too many influencing factors on the concrete CTE, such as water cement ratio, aggregate types, gradation, and so on. Whereas, a concrete CTE model could provide knowledge on the concrete CTE values prior to any laboratory experiments, and design a concrete mixture with a relative lower CTE value. In additions, it could be used as an alternate if laboratory experiments are restrained in some situations.

2.5 Development of Concrete CTE Model

Hardened cement concrete consists of aggregate particles and hydrated products of cement paste, which can be seen as a particulate filled composite material. An equivalent concrete medium is assumed to encircle such particulate filled composite material (Huang et al 2003, 2007; Shu and Huang 2007, 2008, 2009), as shown in Figure 2.3. Macroscopically, it can be seen as a homogenous material (Hao and Hao 2011; Li and Li 2011; Chou et al. 2011). The sketch of a typical unit is shown in Figure 2.4. Cement concrete and its components are assumed to be linear elastic. E_i, v_i, and $\propto_i$ are Young's modulus, Poisson's ratio, and CTE value, respectively (i=0 equivalent concrete; i=1 aggregate; i=2 cement paste). Aggregate particles are assumed to be spherical in shape. As shown in Figure 2.4, an aggregate particle with a radius a is coated with cement paste $b - a$ thick, which is further embedded in an equivalent concrete medium $c - b$ thick. The Poisson's ratio of concrete is quite stable, independent of temperature and moisture (Downie, 2005). A constant value 0.20 was adopted.

Assume the temperature of this composite material changes ΔT. This is a spherical symmetry problem with regard to stress, strain, and displacement. The normal stresses and strains in any two orthogonal tangential coordinate directions are identified by the subscript, t. The radial strain is $\epsilon_{\mathrm{r}} = \mathrm{du/dr}$, and the tangential strain is $\epsilon_{\mathrm{t}} = \mathrm{u/r}$. The stress-strain relationships in the inner solid sphere and the outer two hollow spheres are written as (Burgreen 1971):

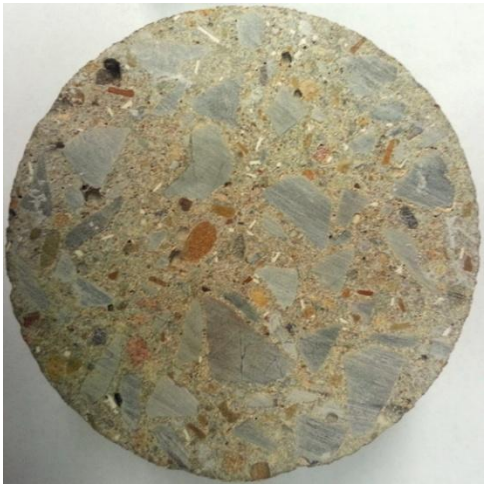

Figure 2.3 Composites of hardened cement concrete

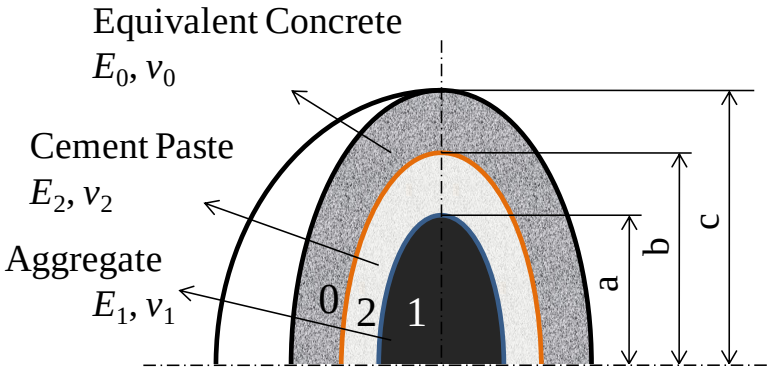

Figure 2.4 Sketch of a unit of aggregate-cement paste-equivalent concrete medium

$$\begin{cases} \epsilon_t = \frac{1}{E}[(1-v)\sigma_t - v\sigma_r] + \alpha\Delta T & (2.1) \\ \epsilon_r = \frac{1}{E}[\sigma_r - 2v\sigma_t] + \alpha\Delta T & (2.2) \end{cases}$$

The normal and tangential stresses can be expressed as Eqs. (2.3) and (2.4) (Burgreen, 1971). It is noteworthy that $\sigma_r + 2\sigma_t = \text{constant}$.

$$\begin{cases} \sigma_r = A - \dfrac{B}{r^3} & (2.3) \\ \sigma_t = A + \dfrac{B}{2r^3} & (2.4) \end{cases}$$

The boundary conditions are:

$$\sigma_{1r}(r = a) = -p;\ \sigma_{2r}(r = a) = -p;\ \sigma_{2r}(r = b) = -q;$$
$$\sigma_{0r}(r = b) = -q;\ \sigma_{0r}(r = c) = 0 \quad (2.5)$$

where: p =the radial pressure at the interface of aggregate and cement paste; q = the radial pressure at the interface of cement paste and equivalent concrete.

Substituting Eq. (2.5) into Eqs. (2.3) and (2.4) yields the stresses in terms of the still undetermined contact pressures p and q, as

$$\sigma_{1r} = -p \quad (2.6)$$

$$\sigma_{1t} = -p \quad (2.7)$$

$$\sigma_{2r} = -(q - p)\frac{b^3}{b^3 - a^3}\left(1 - \frac{a^3}{r^3}\right) - p \quad (2.8)$$

$$\sigma_{2t} = -(q - p)\frac{b^3}{b^3 - a^3}\left(1 + \frac{a^3}{2r^3}\right) - p \quad (2.9)$$

$$\sigma_{0r} = \frac{b^3 q}{c^3 - b^3}\left(1 - \frac{c^3}{r^3}\right) \quad (2.10)$$

$$\sigma_{0t} = \frac{b^3 q}{c^3 - b^3}\left(1 + \frac{c^3}{2r^3}\right) \quad (2.11)$$

It is noted that at the centre of the aggregate, in order to avoid singularity, B has to be 0.

Applying the continuity conditions, $r = a$, $\epsilon_{1r} = \epsilon_{2r}$, and $r = b$, $\epsilon_{2r} = \epsilon_{0r}$, we have

$$\frac{1}{E_1}[(1-v_1)\sigma_{1ta} - v_1\sigma_{1ra}] + \propto_1 \Delta T$$

$$= \frac{1}{E_2}[(1-v_2)\sigma_{2ta} - v_2\sigma_{2ra}] + \propto_2 \Delta T \tag{2.12}$$

$$\frac{1}{E_2}[(1-v_2)\sigma_{2tb} - v_2\sigma_{2rb}] + \propto_2 \Delta T$$

$$= \frac{1}{E_0(a)}[(1-v_0)\sigma_{0tb} - v_0\sigma_{0rb}] + \propto_0 (a)\Delta T \tag{2.13}$$

In Eqs. (2.6) through (2.9), we set $r = a$. The resulting interfacial stresses are substituted into Eq. (2.12), which yields

$$\left\{\frac{2v_1-1}{E_1} - \frac{1}{E_2}\frac{1}{2(b^3-a^3)}[b^3 + 2a^3 + (b^3-4a^3)v_2]\right\}p + \frac{1-v_2}{E_2}\frac{3b^3}{2(b^3-a^3)}q + (\propto_1 - \propto_2)\Delta T = 0 \tag{2.14}$$

Similarly, in Eqs. (2.8) through (2.11), we set $r = b$. The resulting interfacial stresses are substituted into Eq. (2.13), which yields

$$\frac{1-v_2}{E_2}\frac{3a^3}{2(b^3-a^3)}p + \left\{\frac{1}{E_2}\frac{1}{2(b^3-a^3)}[-a^3 - 2b^3 + (4b^3-a^3)v_2] - \frac{1}{E_0(a)}\frac{1}{2(c^3-b^3)}[2b^3 + c^3 + (c^3-4b^3)v_0]\right\}q - \propto_0 (a)\Delta T + \propto_2 \Delta T = 0 \tag{2.15}$$

Considering the size of the equivalent concrete medium surrounding aggregate particle is much larger than aggregate itself, i.e., c $\gg b$, Eq.(2.15) can be simplified as:

$$\frac{1-v_2}{E_2}\frac{3a^3}{2(b^3-a^3)}p+\left\{\frac{1}{E_2}\frac{1}{2(b^3-a^3)}[-a^3-2b^3+(4b^3-a^3)v_2]-\frac{1}{E_0(a)}\frac{1+v_0}{2}\right\}q-$$

$$\propto_0(a)\Delta T+\propto_2\Delta T=0 \tag{2.16}$$

Integration of the radial strain throughout aggregate and cement paste gives the total deformation in the radial direction:

$$u(a)=\int_0^a\epsilon_{1r}\mathrm{dr}+\int_a^b\epsilon_{2r}\mathrm{dr} \tag{2.17}$$

Macroscopically, the deformation of aggregate and cement paste also can be expressed as:

$$u(a)=b*\Delta T*\propto_0(a) \tag{2.18}$$

Then

$$b*\Delta T*\propto(\mathrm{a})=\int_0^a\epsilon_{1r}\mathrm{dr}+\int_a^b\epsilon_{2r}\mathrm{dr} \tag{2.19}$$

Substituting Eqs. (2.6)-(2.9) into Eq.(2.2) and then substituting Eq.(2.2) into Eq.(2.19) yields

$$\left\{\frac{2v_1-1}{E_1}a+\frac{1}{2E_2}\frac{1}{a^2+ab+b^2}[(2a^3-ab(b+a))-(4\mathrm{a}^3+\mathrm{ab(a+b)})v_2]\right\}p+$$

$$\frac{1}{2E_2}\frac{1}{a^2+ab+b^2}\{[-2b^3+ab(a+b)]+[4\mathrm{b}^3+\mathrm{ab(a+b)}]v_2\}\mathrm{q}-\mathrm{b}\Delta T\propto_0(a)+$$

$$[a\alpha_1+(b-a)\alpha_2]\Delta T=0 \tag{2.20}$$

Combining Eqs(2.14), (2.16), and (2.20), $\propto_0(a)$ can be solved as:

$$\propto_0 (a) = \left(D - \frac{BC}{A}\right)\frac{Aa + Cb - F}{(F - Cb)B - (G - Db)A}(\alpha_1 - \alpha_2) - \frac{C}{A}(\alpha_1 - \alpha_2) + \alpha_2 \tag{2.21}$$

where:

$$\mathrm{A} = \frac{2\mathrm{v}_1 - 1}{\mathrm{E}_1} - \frac{1}{\mathrm{E}_2}\frac{1}{2(\mathrm{b}^3 - \mathrm{a}^3)}[\mathrm{b}^3 + 2\mathrm{a}^3 + (\mathrm{b}^3 - 4\mathrm{a}^3)\mathrm{v}_2]$$

$$\mathrm{B} = \frac{1 - \mathrm{v}_2}{\mathrm{E}_2}\frac{3\mathrm{b}^3}{2(\mathrm{b}^3 - \mathrm{a}^3)}$$

$$\mathrm{C} = \frac{1 - \mathrm{v}_2}{\mathrm{E}_2}\frac{3\mathrm{a}^3}{2(\mathrm{b}^3 - \mathrm{a}^3)}$$

$$\mathrm{D} = \frac{1}{\mathrm{E}_2}\frac{1}{2(\mathrm{b}^3 - \mathrm{a}^3)}[-\mathrm{a}^3 - 2\mathrm{b}^3 + (4\mathrm{b}^3 - \mathrm{a}^3)\mathrm{v}_2] - \frac{1}{\mathrm{E}_0(\mathrm{a})}\frac{1 + \mathrm{v}_0}{2}$$

$$\mathrm{F} = \frac{2\mathrm{v}_1 - 1}{\mathrm{E}_1}\mathrm{a} + \frac{1}{2\mathrm{E}_2}\frac{1}{\mathrm{a}^2 + \mathrm{ab} + \mathrm{b}^2}[(2\mathrm{a}^3 - \mathrm{ab}(\mathrm{b} + \mathrm{a})) - (4\mathrm{a}^3 + \mathrm{ab}(\mathrm{a} + \mathrm{b}))\mathrm{v}_2]$$

$$\mathrm{G} = \frac{1}{2\mathrm{E}_2}\frac{1}{\mathrm{a}^2 + \mathrm{ab} + \mathrm{b}^2}\{[-2\mathrm{b}^3 + \mathrm{ab}(\mathrm{a} + \mathrm{b})] + [4\mathrm{b}^3 + \mathrm{ab}(\mathrm{a} + \mathrm{b})]\mathrm{v}_2\}$$

The elastic modulus of the equivalent concrete, $\mathrm{E}_0(\mathrm{a})$, according to Shu and Huang (2008), is calculated as:

$$\mathrm{E}_0(\mathrm{a}) = \frac{E_2(1-n)(1-2\mathrm{v}_0)}{x_1 - \frac{9E_1 n(1-\mathrm{v}_2)^2}{4E_2(1-2\mathrm{v}_1)(1-n)+4E_1 x_2}} \tag{2.22}$$

where: n = volume of concentration of aggregate in concrete, $(a/b)^3$; $x_1 = 1/2 * n(1 + \mathrm{v}_2) + (1 - \mathrm{v}_2)$; and $x_2 = 1/2 * (1 + \mathrm{v}_2) + n(1 - 2\mathrm{v}_2)$.

The CTE of the composite is influenced by many parameters such as temperature, aggregate size, cement paste thickness as well as elastic modulus, Poisson's ratio, CTE values of aggregate and cement paste. Every aggregate of a specified size gives its contribution to the overall CTE of the concrete. In order to take aggregate gradation into account, CTE of the concrete can be expressed as follows:

$$\alpha = \int_{a_{min}}^{a_{max}} \propto (a) dP(a) \tag{2.23}$$

where: a_{min}=minimum aggregate radius; and a_{max}=maximum aggregate radius.

The integration is too complex. A numerical summation, as an approximation to the integration, is adopted as follows:

$$\alpha = \sum_{i=1}^{N-1} \sum_{j=1}^{M=2} \{ \frac{1}{2} [\propto (a_{ij}) + \propto (a_{(i+1)j})][P(a_{ij}) - P(a_{(i+1)j})]\} \tag{2.24}$$

$$a_i = \frac{S_i + S_{i+1}}{4} \tag{2.25}$$

where:

$\propto (a_{ij})$=CTE corresponding to the composite with type *j* aggregate with radius a_i and its cement paste;

$\propto (a_{(i+1)j})$=CTE corresponding to the composite with type *j* aggregate with radius a_{i+1} and its cement paste;

$P(a_{ij})$=volume fraction of type *j* aggregates passing through the No.*i* sieve;

$P(a_{(i+1)j})$=volume fraction of type *j* aggregates passing through the No.*i+1* sieve; and

S_i=the size of the i^{th} sieve, (*i*=1, 2, 3,…N), mm.

An approach from Li et al. (1999) was used to determine the thickness of cement paste, i.e., *b*-*a*. This method assumes that all aggregate particles are coated with the same thickness of cement paste. The thickness can be determined from Eq. (2.26).

$$b - a = \frac{F_1}{12F_2 \sum_{i=1}^{N-1} \frac{[P(a_i) - P(a_{i+1})]}{S_i + S_{i+1}}} \tag{2.26}$$

where: F_1=volume fraction of cement paste in PCC; and F_2=volume fraction of aggregate in PCC.

With air voids in concrete neglected, the following relationship remains:

$$F_1 + F_2 = 1 \tag{2.27}$$

$$F_1 = \frac{V_1}{V_1 + V_2} \tag{2.28}$$

where: V_1=volume of cement paste in concrete, and V_2= volume of aggregates in concrete.

The volumes of hydrated cement paste and aggregates can be calculated with Eqs (2.29) (Mindess et al. 2003) and (2.30).

$$V_1 = 0.68\beta * m_{cm}\ cm^3 \tag{2.29}$$

$$V_2 = \sum_{i=1}^{N} \frac{m_i}{G_{sbi}}\ cm^3 \tag{2.30}$$

where: β = the degree of hydration, 1.0 in this paper; m_{cm}=the mass of cement paste in one unit concrete; m_i=the mass of one kind of aggregate in one unite concrete; and G_{sbi}=the specific gravity of the corresponding aggregate.

2.6 Validation on the Proposed Model

2.6.1 Investigation on CTE Values of Cement Paste

The proposed concrete CTE model requires CTE values of cement paste as inputs. Type I portland cement, as the most common commercial cement in the United States, was used to mold cement paste cylinders (4 by 8 inches) under four different water cement ratio, i.e., 0.32, 0.38, 0.44, and 0.48. Under each w/c ratio (except 0.48), three replicated samples were tested on CTE and results were shown in Figure 2.5. It indicates that among the range of 0.32 to 0.48, the CTE of cement paste decreases as w/c ratio increases. According to the *t*-test, the influence of w/c ratio on CTE of cement paste is insignificant at 5% significance level.

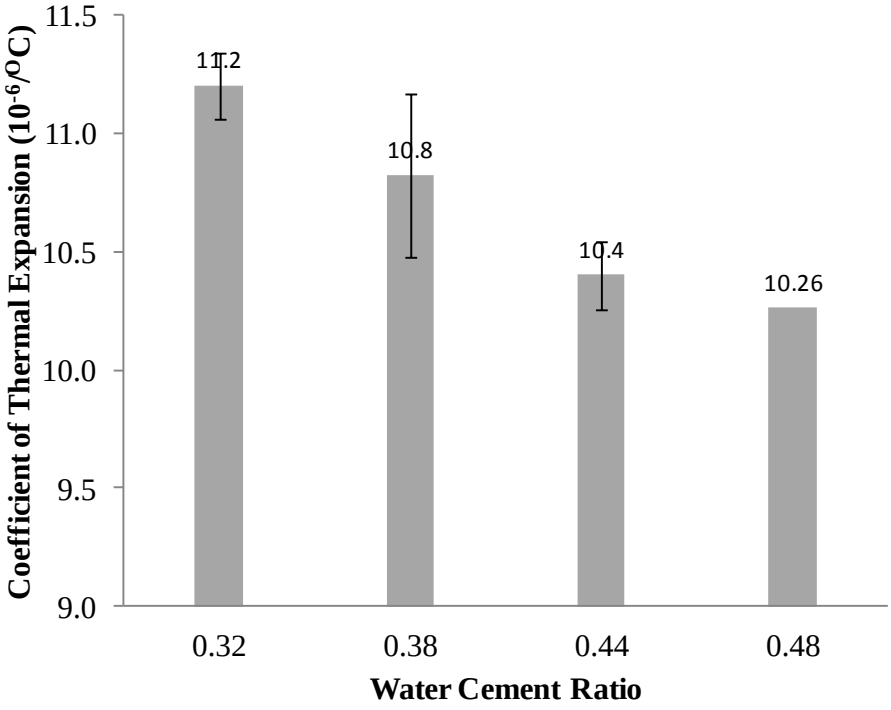

Figure 2.5 CTE of cement paste under varied w/c ratios

2.6.2 Validation of the CTE Model on Cement Mortar

Cement mortar is widely used in civil engineering and is an important component in cement concrete. The thermal behavior of cement mortar influences the mechanical performance of the structure, therefore should be investigated. Cement Mortar cylinders (4 by 8 inches) were molded and the CTE tests were conducted at 28 days. The fine aggregate is graded standard sand and the gradation can be referred from ASTM C778. On the other hand, the CTE model proposed in this paper predicted CTE values of cement paste. The inputs of the graded standard sand were listed in Table 2.3 as siliceous sand. Comparison of the measured and the predicted CTE values of cement paste were shown in Figure 2.6. It can be seen the predicted medium CTE values of cement mortar are very close to the measured values with no more than 5% variation. There is no obvious trend on the variation of CTE values of cement paste with w/c ratios ranged from 0.32 to 0.48.

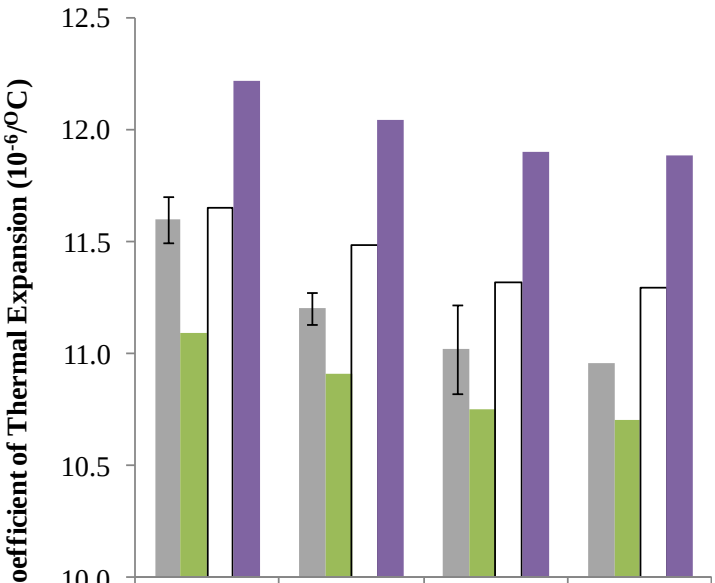

	0.32	0.38	0.44	0.48
Measured CTE (10-6/oC)	11.6	11.2	11.0	11.0
predicted Min.	11.1	10.9	10.8	10.7
Predicted Med.	11.7	11.5	11.3	11.3
Predicted Max.	12.2	12.0	11.9	11.9

Figure 2.6 Comparison of measured and predicted CTE values of cement paste

2.6.3 Validation of the CTE Model on Cement Concrete

The concrete data from Sakyi-Bekoe (2008) were utilized to validate the proposed CTE model. Concrete with two types of coarse aggregates, i.e., dolomitic limestone (DL) and granite (GR) were utilized in this paper. Siliceous sand was used for fine aggregate in all of concrete. Table 2.3 offers gradation and bulk specific gravity of each material. In each type of concrete, three water cement ratio (0.32, 0.38, 0.44) and three volumetric ratios of coarse aggregate to fine aggregate (60:40, 55:45, 50:50) were adopted. Therefore, in each type of concrete there are six different concretes.

Table 2.3 Gradation and bulk specific gravity of aggregates

Size	Mass % Passing Sieves		
	Dolomitic Limestone (DL)	Granite (GR)	Siliceous Sand
1"	100	100	100
3/4"	93	93	100
3/8"	32	29	100
#4	3	3	99
#8	1	1	92
#16	0	0	80
#30	0	0	50
#50	0	0	15
#100	0	0	5
#200	0	0	0
Bulk Specific Gravity	2.753	2.687	2.626

The inputs of cement paste (Yang, et al., 1997), aggregate and natural sand (Britannica Encyclopedia, 2013) were listed in Table 2.4 including CTE values and elastic moduli. It should be mentioned that CTE values of cement paste were assumed to be the same with the ones obtained in the laboratory above, since the same type of cement was used in (Sakyi-Bekoe 2008).

Three typical values among the CTE ranges of aggregates in Table 2.4 were substituted into the proposed model, i.e., minimum, maximum, and medium values. The predicted concrete CTE values were compared with the measured ones, as shown in Figure 2.7. It can be seen that the top boundaries of aggregate CTE values provide the maximum values of concrete CTE, while the bottom boundaries provide the minimum values of concrete CTE. Among them locate concrete CTE values predicted from other combinations of aggregate CTE values. It can be also seen that the differences between

the predicted concrete CTE values and the measured ones are no more than 15%. It indicates that the proposed model is valid.

Table 2.4 CTE values, elastic moduli and Poisson's ratios of concrete components

Properties	DL	GR	Siliceous Sand	Cement Paste		
				0.32	0.38	0.44
CTE Range (10^{-6}/°C)	7-10	7-9	11-13	-	-	-
Medium CTE (10^{-6}/°C)	8.5	8	12	11.2	10.8	10.4
Elastic Modulus (GPa)	20	60.0	20	20.87	18.42	15.97

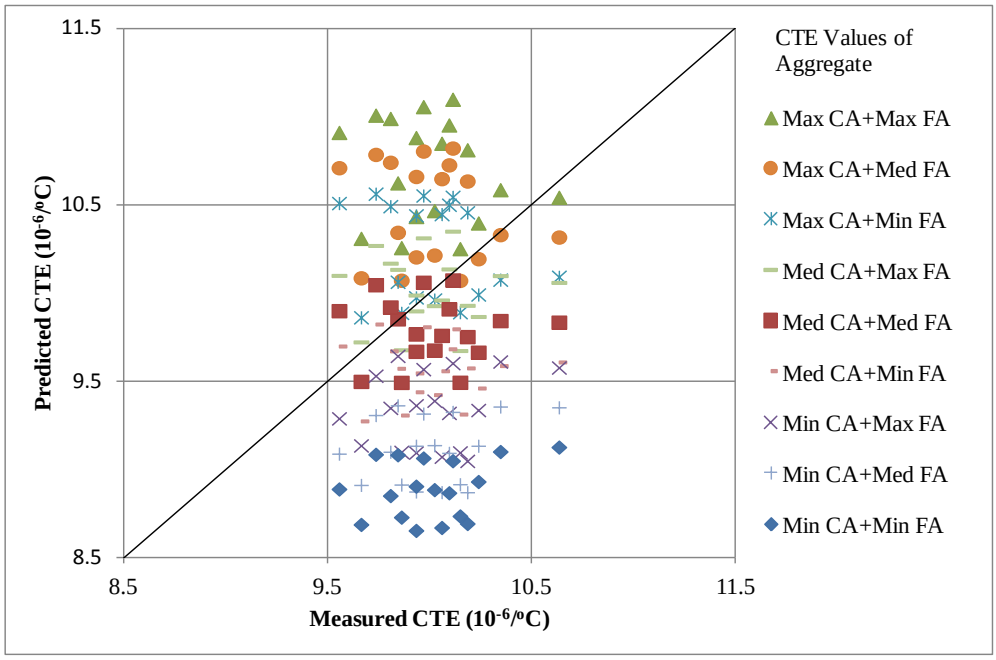

Figure 2.7 Comparison between predicted and measured concrete CTE values

2.7 Sensitivity Analysis on Factors Influencing Concrete CTE

Factors such as water cement ratio, aggregate type, and aggregate gradation were investigated on their effects on concrete CTE. The data from the Alabama concrete, as shown above, were used to evaluate the effects of different factors on concrete CTE using the proposed model.

2.7.1 Water cement ratio

With the range of water cement ratio from 0.32 to 0.44, there was no obvious change of concrete CTE observed. In fact, the cement paste CTE decreased as water cement ratio increased slightly, according to the test results in Figure 2.5. Since the cement paste merely occupy a small volumetric part of cement concrete and its CTE value does not drift away from the ones of aggregates, no significant variation was found on the concrete CTE under different water cement ratios.

2.7.2 Aggregate Type and Gradation

In order to investigate the influences of aggregate type and gradation on concrete CTE, five types of coarse aggregate were selected. They are marble (CTE: 4-7 $\times 10^{-6}/℃$), basalt (CTE: 6-8 $\times 10^{-6}/℃$), granite (CTE: 7-9 $\times 10^{-6}/℃$), dolomitic limestone (CTE: 7-10 $\times 10^{-6}/℃$), and quartzite (CTE: 11-13 $\times 10^{-6}/℃$). Siliceous sand (CTE: 13 $\times 10^{-6}/℃$) was used as fine aggregate. The water cement ratio in all concrete was assumed as 0.32. All kinds of coarse aggregate obey the size distribution as granite in Table 2.3 and the siliceous sand obey the one in Table 2.3 as well. In each kind of

concrete, the aggregate gradation varies as the proportions of coarse aggregate and fine aggregate changed, as shown in Figure 2.8.

The predicted concrete CTE values were summarized in Table 2.5, including the upper and lower boundaries of concrete CTE values relative to the maximum and minimum values of coarse aggregates. It can be seen that as the aggregate gradation become finer the concrete CTE slightly increases. For the aggregate type, the concretes with aggregates having lower CTE values, such as marble and basalt, are lower than the concretes with aggregates having higher CTE values, such as quartzite. However, the CTE values of concretes are very close to each other when their raw materials have the same CTE values even though different Young's moduli adopted, for example marble and granite with the same CTE value of $7 \times 10^{-6}/℃$. It indicates that the CTE values of raw materials are the most significant factor that influences concrete CTE value. The stiffness of raw materials was found not sensitive to the concrete CTE.

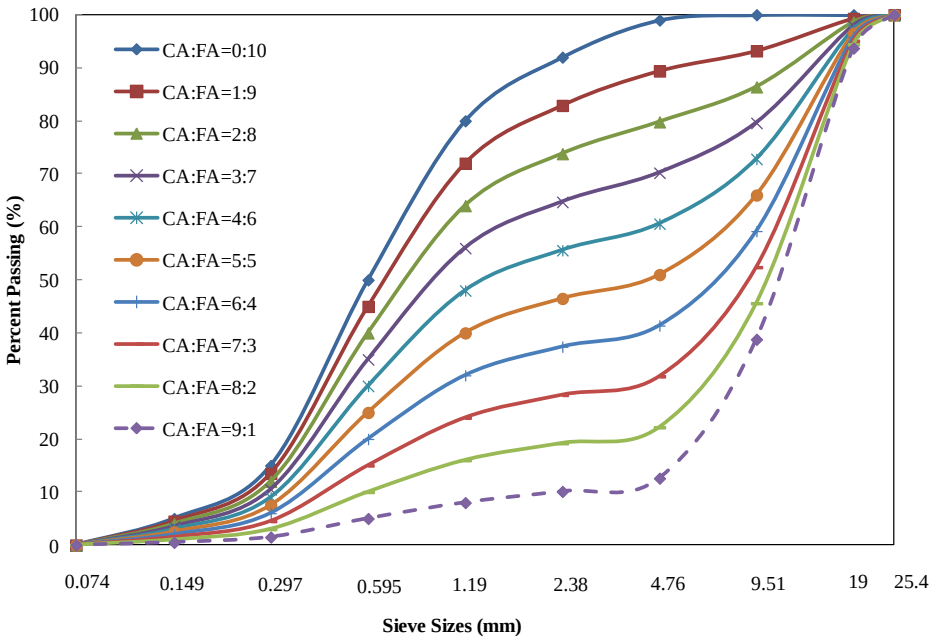

Figure 2.8 Aggregate gradations used in sensitivity analysis

Table 2.5 CTE values of concrete with different types of coarse aggregate ($10^{-6}/^{o}C$)

	Coarse Aggregate Type									
CA:	Marble		Basalt		Granite		DL		Quartzite	
FA	4	7	6	8	7	9	7	10	11	13
0:10	7.40	9.19	8.58	9.78	9.19	10.38	9.18	10.97	11.57	12.76
1:9	7.39	9.18	8.57	9.76	9.18	10.37	9.17	10.96	11.56	12.74
2:8	7.38	9.17	8.56	9.75	9.17	10.35	9.16	10.94	11.54	12.72
3:7	7.37	9.15	8.54	9.73	9.15	10.33	9.14	10.92	11.52	12.69
4:6	7.36	9.13	8.53	9.71	9.14	10.31	9.12	10.90	11.49	12.67
5:5	7.35	9.11	8.51	9.69	9.12	10.29	9.11	10.87	11.47	12.63
6:4	7.34	9.09	8.49	9.66	9.10	10.26	9.08	10.84	11.43	12.58
7:3	7.34	9.07	8.47	9.63	9.08	10.23	9.06	10.80	11.39	12.52
8:2	7.32	9.06	8.46	9.60	9.07	10.20	9.04	10.75	11.33	12.44
9:1	7.31	9.05	8.45	9.59	9.06	10.18	9.03	10.70	11.25	12.31

Note: CA:FA presents the ratio of the mass of coarse aggregate to the mass of fine aggregate in concrete.

2.8 Summary and Conclusions

The influence of concrete CTE on the concrete pavement performance was evaluated in version 1.100 MEPDG software. Typical concrete in TN were tested on their CTE in the laboratory. A concrete CTE prediction model was developed based on micromechanics. Data obtained from laboratory and literature was used to validate the proposed CTE model on cement mortar and cement concrete. Also the sensitivity analysis on the factors influencing concrete CTE values was investigated. The following conclusions can be drawn from the study:

- Concrete pavement performances are very sensitive to concrete CTE values. Pavement deteriorations, especially concrete slab cracks, accelerate when concrete CTE increases.
- The concrete CTE model was validated on cement paste from laboratory and cement concrete from literature. The differences between measured and predicted CTE values on cement paste and cement concrete are no more than 5% and 15%, respectively.
- The proposed model is effective in evaluating concrete CTE.

Based on the sensitivity analysis, the following conclusions can be drawn:

- The aggregate type, i.e., the aggregate CTE value, is the most important factor that affects concrete CTE. Higher CTE values of raw materials lead to higher concrete CTE values.
- CTE increases slightly as the aggregate gradation become finer.

- With the water cement ratio varied from 0.32 to 0.44, the concrete CTE was not found to change significantly.

2.9 References

AASHTO T 336, (2009). “Standard Test Method for the Coefficient of Thermal Expansion of Hydraulic Cement Concrete.” Washington, D.C.

AASHTO TP 60-00 (2007). “Provisional Test Method for the Coefficient of Thermal Expansion of Hydraulic Cement Concrete.” Washington, D.C.

Alungbe, G. D., Tia, M., and Bloomquist, D.G. (1992). "Effect of aggregate, water-cement ratio, and curing on the coefficient of linear thermal expansion of concrete." Journal of the Transportation Research Record 1335: 44-51.

ARA, Inc. (2004). “National Cooperative Highway Research Program (NCHRP) 1-37A, Guide for the Mechanistic-Empirical Design for New and Rehabilitated Pavement Structures.” *Transportation Research Board of the National Academies*, Washington, D.C.

ASTM C 39-12a (2012). “Standard Test Method for Compressive Strength of Cylindrical Concrete Specimens.” International, P.A.

ASTM C 778-12 (2012). “Standard Specification for Standard Sand.” ASTM International, P.A.

ASTM E 831-06 (2006). “Standard Test Method for Linear Thermal Expansion of Solid Materials by Thermomechanical Analysis.” *ASTM Inter*national, PA.

Buch, N. and Jahangirnejad S. (2008). "Quantifying coefficient of thermal expansion values of typical hydraulic cement concrete paving mixtures." Final report submitted to the Michigan Department of Transportation. Michigan State University.

Burgreen D. (1971) “Elements of Thermal Stress Analysis”. C.P. Press, N.Y.

Ceylan, H., Gopalakrishnan, K., Kim, S., Schwartz, C.W., and Li, R., (2013). "Global Sensitivity Analysis of Jointed Plain Concrete Pavement Mechanistic-Empirical Performance Predictions." *Transportation Research Record: Journal of the Transportation Research Board, No. 2690*, TRB, National Research Council, Washington, D.C.

Childs, P., Wong, A.C.L., Gowripalan, N., and Peng, G.D. (2007). "Measurement of Coefficient of Thermal Expansion of Ultra-High Strength Cementitious Composites Using Fibre Optic Sensors." Cement and Concrete Research, 37(5), 789-795.

Chou, J., Chiu, C., Farfoura, M., and Al-Taharwa, I. (2011). "Optimizing the Prediction Accuracy of Concrete Compressive Strength Based on a Comparison of Data-Mining Techniques." J. Compt. Civ. Eng., 25(3), 242-253

Downie, B. (2005). "Effect of Moisture and Temperature on the Mechanical Properties of Concrete ." Master thesis, West Virginia University

Emanuel, J. H. and Hulsey, J. L. (1977). "Prediction of the Thermal Coefficient of Expansion of Concrete" J. Amer. Conc. Inst. 74, 149–155.

Emanuel, J. H. and Hulsey, J.L. (1977). "Prediction of the thermal coefficient of expansion of concrete." Journal of the American Concrete Institute 74, No.4: 149-155.

Encyclopædia Britannica (2013) "rock" Encyclopædia Britannica Online. Encyclopædia Britannica Inc. <http://www.britannica.com/EBchecked/topic/505970/rock/80190/Stress-strain-relationships>.

Federal Highway Administration (2011) "Portland Cement Concrete Pavements Research-Thermal Coefficient of Portland Cement Concrete." <http://www.fhwa.dot.gov/pavement/pccp/thermal.cfm>

Hao, Y. and Hao, H. (2011) "Numerical Evaluation of the Influence of Aggregates on Concrete Compressive Strength at High Strain Rate." Int'l. J. Prot. Stru., 2(2), 177-206

Huang, B., Li, G., and Mohammad, L.N. (2003) "Analytical Modeling and Experimental Study of Tensile Strength of Asphalt Concrete Composite at Low Temperatures." Composites: Part B 34: 705-714

Huang, B., Shu, X., Li, G., and Chen, L. (2007). "Analytical modeling of three-layered HMA mixtures." Int. J. Geomech., 7(2), 140–148.

Jahangirnejad, S., Buch, N., and Kravchenko, A. (2008). "Laboratory Investigation of Effects of Aggregate Geology and Sample Age on Coefficient of Thermal Expansion of Portland Cement Concrete." *Transp. Res. Rec.: J. Transp. Res. Board*, 2388, *Transp. Res. Board Nat'l Acad*., WA, D.C.

Kada, H., Lachemi, M., Petrov, N., Bonneau, O., and Aitcin, P.C., (2002). "Determination of the Coefficient of Thermal Expansion of High Performance Concrete from Initial Setting." *Mate. and Struct.* 35: 35–41.

Li, G., Li, Y., Metcalf, J. B., and Pang, S. S. (1999). "Elastic Modulus Prediction of Asphalt Concrete." *ASCE J Mater. Civ. Eng.*, 11(3), 236–241.

Li, M. and Li, V.C. (2011). "Cracking and Healing of Engineered Cementitious Composites under Chloride Environment." ACI *Mater. J.*, 108 (3), 333-340

Mindess, S., Young, J. F., and Darwin, D. (2003) "Concrete", 2nd Edition. *Pearson Education, Inc.* N.J.

Mukhopadhyay, A. K., Neekhra, S., and Zollinger, D. G. (2007). "Preliminary Characterization of Aggregate Coefficient of Thermal Expansion and Gradation for Paving Concrete." *Texas Transportation Institute* (*TTI*), Colledge Statation, TX.

Naik, T. R., Kraus, R. N., and Kumar, R. (2011) "Influence of Types of Coarse Aggregates on the Coefficient of Thermal Expansion of Concrete." *J Mater. Civ. Eng.*, 467-472.

Neville, A. M., and Brooks, J. J. (1987). "Concrete *Technology*." Essex, UK: Longman Scientific and Technical

Sakyi-Bekoe K. O. (2008). "Assessment of the Coefficient of Thermal Expansion of Alabama Concrete." M.S. thesis, Auburn Univ., Auburn, Al.

Sellevold, E. and Bjøntegaard, Ø. (2006). "Coefficient of Thermal Expansion of Cement Paste and Concrete: Mechanisms of Moisture Interaction." *Materials and Structures*, 39 (9), 809-815.

Shin, H. and Chung Y. (2011). "Determination of Coefficient of Thermal Expansion Effects on Louisiana's PCC Pavement Design." L.A. State Univ., Baton Rouge, LA 70803.

Shu, X. and Huang, B. (2007) "Micromechanics-Based Dynamic Modulus Prediction of Polymeric Asphalt Concrete Mixtures." Composite: Part B 39: 704-713

Shu, X. and Huang, B. (2008) "Dynamic Modulus Prediction of HMA Mixtures Based on the Viscoelastic Micromechanical Model" *ASCE J Mater. Civ. Eng.*, 20(8), 530–538.

Shu, X. and Huang, B. (2009) "Predicting Dynamic Modulus of Asphalt Mixtures with Differential Method." Road Materials and Pavement Design, Vol. 10, No. 2, 337 – 359.

Tran, N. H., Hall, K. D., and James, M., (2008). “Coefficient of Thermal Expansion of Concrete Materials: Characterization to Support Implementation of the Mechanistic–Empirical Pavement Design Guide.” *Transp. Res. Rec.: J. Transp. Res. Board*, 2087, 51-56, *Transp. Res. Board Nat’l Acad*., WA, D.C.

US CORPS OF ENGINEERS. CRD-C 39-81. (1981) “Test Method for Coefficient of Linear Thermal Expansion of Concrete.”

Won, M. (2005). “Improvements of Testing Procedures for Concrete Coefficient of Thermal Expansion.” *Transp. Res. Rec.: J. Transp. Res. Board,* 1919:23-28, *Transp. Res. Board Nat’l Acad*., WA, D.C.

Yang, C., Yang, Y., and Huang, R. (1997). “The Effect of Aggregate Volume Ratio on the Elastic Modulus and Compressive Strength of Lightweight Concrete.” J. Marine Sci. and Tech., 5(1), 31-38

Yao, W. and Zheng, X. (2007). "Effect of Mix Proportion on Coefficient of Thermal Expansion of Concrete." Journal of Tongji University, 35(1), 77: 81-87

Yeon, J. H., Choi, S., and Won, M. C. (2009). “Effect of Relative Humidity on Coefficient of Thermal Expansion of Hardened Cement Paste and Concrete.” *Transp. Res. Rec.: J. Transp. Res. Board*, 2113, 83-91, *Transp.* Res. *Board Nat’l Acad*., WA, D.C.

PART 3 SEASONAL VARIATION IN RESILIENT MODULUS OF TYPICAL SOILS IN TENNESSEE AND ITS EFFECTS ON ASPHALT PAVEMENT PERFORMANCE

3.1 Abstract

Subgrade soil, as the critical underlying support for other pavement layers and traffic loads, should be stiff enough to maintain the integrity of pavement structures and the smoothness of pavement surface. The resilient modulus, as an indicator of subgrade stiffness, is an essential input in the AASHTO Mechanistic-Empirical Pavement Design Guide (MEPDG). At input level 1 of MEPDG, the MEPDG generalized model is required to describe resilient modulus of subgrade soil and the coefficients for this model are used for pavement design. The change of the resilient modulus model has raised the interest of many state highway agencies and makes it necessary to convert old resilient modulus test data into new ones required by the MEPDG model. In this study, the coefficients of the generalized and the universal models for soil resilient modulus were obtained through regression of the results of 14 soils in Tennessee. The coefficients of the two models were also compared. The coefficients of the generalized model were correlated to soil physical properties, which provided an alternate time-saving and economical method to obtain soil resilient modulus as level 2 inputs. The coefficients were obtained at different post-compaction water contents, to allow the estimation of pavement response under seasonal moisture variation of subgrade. Two typical pavement sections, I-40 Knox and SR-36 Washington, were employed for the evaluation of pavement performance utilizing a multiple layered software WESLEA 3.0 and the MEPDG software (version 1.1). The results show that moisture variation had a significant effect on subgrade resilient modulus and subsequently on pavement performance. It is

recommended that seasonal change in soil resilient modulus be considered in the analysis on pavement performance.

3.2 Introduction

Mechanical-empirical pavement design methods require the stiffness of subgrade soils as a basic input to analyze the dynamic response and fatigue behavior of pavement materials under vehicle loading. The 1986 AASHTO guide for design of flexible pavement (AASHTO, 1986) suggests resilient modulus (M_R) for characterizing subgrade soil. M_R is defined as the deviatoric stress divided by the resilient or recoverable axial strain under cyclic axial loading.

Currently, the Mechanistic-Empirical Pavement Design Guide (MEPDG) allows use of AASHTO T307 test standard (AASHTO, 1999) or the NCHRP 1-28A procedure (NCHRP, 2003) to evaluate resilient modulus of soil. The two methods are almost the same except for the tolerance of moisture and density among replicate samples. In repeated load triaxial tests, three different levels of confining stresses (41.4, 27.6, and 13.8kPa for subgrade soil) are applied on cylindrical specimens, simulating overburden pressure and wheel load. A series of load pulses (13.8, 27.6, 41.4, 55.2, and 68.9 kPa for subgrade soil) are applied with a distinct rest period on soil specimens, simulating the stresses from multiple wheels moving on the pavement. In the field, subgrade soil at different depth experiences varied bulk stresses, depending on the stiffness, thickness, and other factors of the pavement overlayers.

Due to the complexity and tediousness of laboratory testing, in-situ tests are preferred as long as reliable correlations could be established. Factors such as stress state, soil type and its structure, natural water content, density, and gradation are usually considered when analyzing M_r of soil. The California Bearing Ratio (CBR) is commonly used to estimate M_r (Hopkins, et al., 2004). The new MEPDG Level 2 input provides the options of estimating M_r from CBR, R value, (Bayomy, et al., 2012) and layer coefficient, respectively. In-situ apparatuses, such as field static plate bearing load test (Ping and Sheng, 2011; Ahn, et al., 2009) and falling weight deflectometer (Mohammad, et al., 2007; Nazzal and Mohammad, 2010; Dawson, et al., 2009) can be used to obtain field resilient modulus. Usually relationships between resilient modulus and CBR or other mechanical properties obtained in the field can be established.

The relationships between resilient modulus and the material stress state have been studied for decades. The K-θ model (Seed, et al., 1967), generally used for granular materials, does not consider shear stress and shear strain developed during loading. The K-σ_d model (Moossazadeh and Witczak, 1981) is adequate for cohesive soils found at shallow depths. The universal model (Uzan, et al., 1992) covers the effects of shear, confining, and deviator stresses and gives a better explanation for the stress state of soils. Later the generalized model (Von Quintus and Killingsworth, 1998) was adopted in MEPDG. After the coefficients for the constitutive models are determined from laboratory test results, soil resilient modulus can be estimated for any specific stress state. Generally, the coefficients of the generalized model can be obtained from laboratory

repeated load test results, as in MEPDG input level 1, or by correlating the coefficients with soil physical properties (Hossain, 2008; Titi, et al., 2006; Malla and Joshi, 2006; Mohammad, et al., 1999), and both the effects of season and stress sensitivity can be considered.

3.3 Comparison between the Universal Model and the Generalized Model

Soils from 14 locations in Tennessee were collected, as shown in Figure 3.1, and the physical properties and resilient modulus were tested in the laboratory according to SHRP Protocol P46 (Drumm, Reeves, and Madgett, 1995, 1999; Drumm, Li, Reeves, and Madgett 1996). Among these 14 soils, 3 are silty soils and 11 are clayey soils. The resilient moduli of the 11 clayey soils were evaluated under three different water contents: optimum water content and two higher water contents (changing water contents after compaction at optimum water content). The results of the laboratory tests were given in terms of the three coefficients (k_1, k_2, k_3) of the universal model (Uzan, Witczak, Scullion and Lytton, 1992) as follows:

$$M_r = k_1 P_a \left(\frac{\theta}{P_a}\right)^{k_2} \left(\frac{\tau_{oct}}{P_a}\right)^{k_3} \quad (3.1)$$

However, the generalized model of soil resilient modulus, as shown in Eq. (3.1), is used in the current MEPDG.

$$M_r = k_1 P_a \left(\frac{\theta}{P_a}\right)^{k_2} \left(1 + \frac{\tau_{oct}}{P_a}\right)^{k_3} \quad (3.2)$$

where: M_r= resilient modulus; θ= bulk stress; $\sigma_1 + \sigma_2 + \sigma_3$; $\sigma_1, \sigma_2, \sigma_3$= principal stresses; τ_{oct}= octahedral shear stress, $\frac{1}{3}\sqrt{(\sigma_1 - \sigma_2)^2 + (\sigma_2 - \sigma_3)^2 + (\sigma_3 - \sigma_1)^2}$; P_a=atmospheric pressure; k_1, k_2, k_3= regression coefficients.

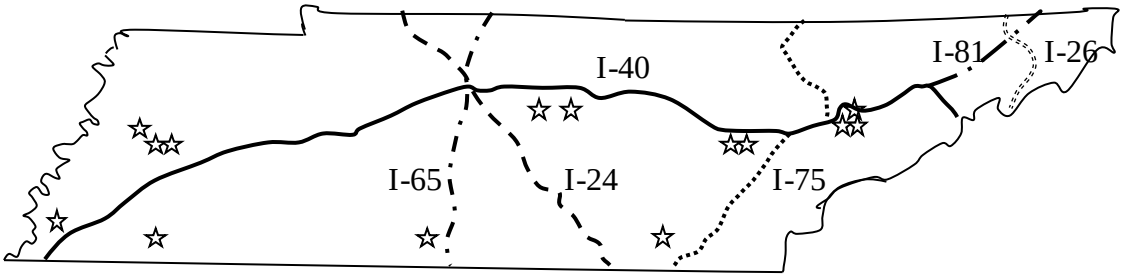

Figure 3.1 Distribution of soil samples in Tennessee

The soil resilient modulus data were regressed to obtain the coefficients (k_1, k_2, k_3) for the generalized model. Table 1 presents the regressed coefficients for the universal and generalized models of resilient modulus. The coefficients in the first row were for optimum water content, i.e. for the resilient modulus at the MEPDG input level 1, while coefficients in the other rows can be used to predict resilient modulus of soils with higher water contents. The ratios of coefficients of the universal model to those of the generalized model were shown in Figure 3.2. It can be seen that there was almost no change in k_2, whereas k_1 and k_3 varied significantly. The distribution of k_1 was more scattered than those of k_2 and k_3.

Table 3.1 Coefficients of the Generalized Model and the Universal Model for Soils in Tennessee

Location	AASHTO Classification	Water content, %	Dry Density, g/cm^3	Generalized Model				Universal Model			
				k_1	k_2	k_3	R^2	k_1	k_2	k_3	R^2
Crockett Co. Sta 781	A-4	16.3	1.668	1241.1	0.5230	-1.7450	0.90	596.3	0.5312	-0.2411	0.96
		18.0	1.668	1099.3	0.6670	-2.2540	0.92	428.6	0.6754	-0.3082	0.95
		18.9	1.675	781.4	0.5480	-0.9840	0.92	512.7	0.5550	-0.1399	0.95
Shelby Co. Sta 9	A-4	14.5	1.762	1028.7	0.2050	-1.1200	0.88	640.9	0.2062	-0.1558	0.94
		15.8	1.746	705.2	0.1720	-1.2670	0.86	417.6	0.1686	-0.1710	0.88
		15.8	1.763	586.5	0.2850	-2.2790	0.79	220.1	0.2938	-0.3259	0.92
Roane Co. Sta 85	A-4	12.5	1.845	1288.2	0.2831	-2.3644	0.93	485.7	0.2875	-0.3167	0.98
		13.5	1.843	1319.2	0.6359	-3.6189	0.90	290.5	0.6435	-0.5000	0.94
		13.5	1.873	763.7	0.7011	-2.8356	0.88	231.8	0.7138	-0.3911	0.96
Hamilton Co. Sta 578	A-6	15.3	1.763	1960.3	0.0970	-1.2050	0.88	1153.2	0.0971	-0.1646	0.92
Roane Co. Sta 47	A-6	17.3	1.747	1576.5	0.1780	-3.0340	0.94	455.7	0.1752	-0.4022	0.97
		17.8	1.766	1493.8	0.2670	-4.3010	0.89	253.7	0.2790	-0.5762	0.95
		17.8	1.777	1342.1	0.3635	-4.4842	0.95	216.9	0.3648	-0.5879	0.99
Crockett Co. Sta 925	A-6	16.3	1.718	913.1	0.0526	-1.1202	0.87	564.8	0.0586	-0.1595	0.79
		18.0	1.702	721.1	0.2031	-2.5360	0.71	245.0	0.2156	-0.3568	0.96
		19.2	1.709	419.2	0.2547	-1.8506	0.77	191.4	0.2585	-0.2587	0.83
Crockett Co. Sta 1081	A-6	17.9	1.715	913.3	0.1015	-2.1690	0.96	376.4	0.1004	-0.2858	0.98
		18.9	1.704	858.2	0.2191	-3.0697	0.95	245.1	0.2197	-0.4050	0.98
		20.0	1.689	975.7	0.6333	-3.7124	0.94	182.9	0.0633	-0.5731	0.98

Table 3.1 Coefficients of the Generalized Model and the Universal Model for Soils in Tennessee (Continued)

Location	AASHTO Classification	Water content, %	Dry Density, g/cm^3	Generalized Model				Universal Model			
				k_1	k_2	k_3	R^2	k_1	k_2	k_3	R^2
White Co. Sta 652	A-6	18.8	1.673	1369.9	-0.0369	-0.3829	0.26	1136.3	-0.0251	-0.0665	0.34
Giles Co. Sta 270	A-7-5	23.8	1.502	1487.3	0.1860	-1.3950	0.69	831.6	0.1858	-0.1905	0.72
		24.6	1.512	1299	-0.0440	-1.6850	0.93	644.6	-0.0455	-0.2284	0.96
		26.2	1.510	758.9	0.1030	-3.1000	0.96	210.1	0.0974	-0.4201	0.97
Knox Co. Sta 400	A-7-5	29.4	1.449	1568.2	0.0736	-1.6451	0.97	818.5	0.0683	-0.2058	0.92
		30.1	1.444	1099.3	0.2596	-2.7053	0.97	438	0.2504	-0.3382	0.95
		30.6	1.446	993.6	0.0924	-3.2551	0.95	265.9	0.0903	-0.4226	0.96
VanBuren Co. Sta 618	A-7-6	21.3	1.597	1241.1	0.5230	-1.7450	0.90	1360.2	0.1622	-0.1864	0.87
Knox Co. Sta Rutledge Pike	A-7-6	35.6	1.306	1610.6	0.2120	-1.6019	0.87	841.6	0.2099	-0.2086	0.87
		35.6	1.322	1347.7	-0.2068	-1.1694	0.49	834.8	-0.2057	-0.1551	0.50
		35.8	1.329	1032.2	0.1126	-2.3845	0.98	399.5	0.1063	-0.3018	0.95
Knox Co. Sta 500	A-7-6	18.6	1.715	2251.6	0.2510	-2.2020	0.98	926.6	0.2468	-0.2848	0.96
		19.7	1.705	1320.1	0.3430	-4.0470	0.94	248.3	0.3434	-0.5445	0.98
		19.9	1.707	1159.6	0.3230	-3.9450	0.93	230.5	0.3243	-0.5234	0.97

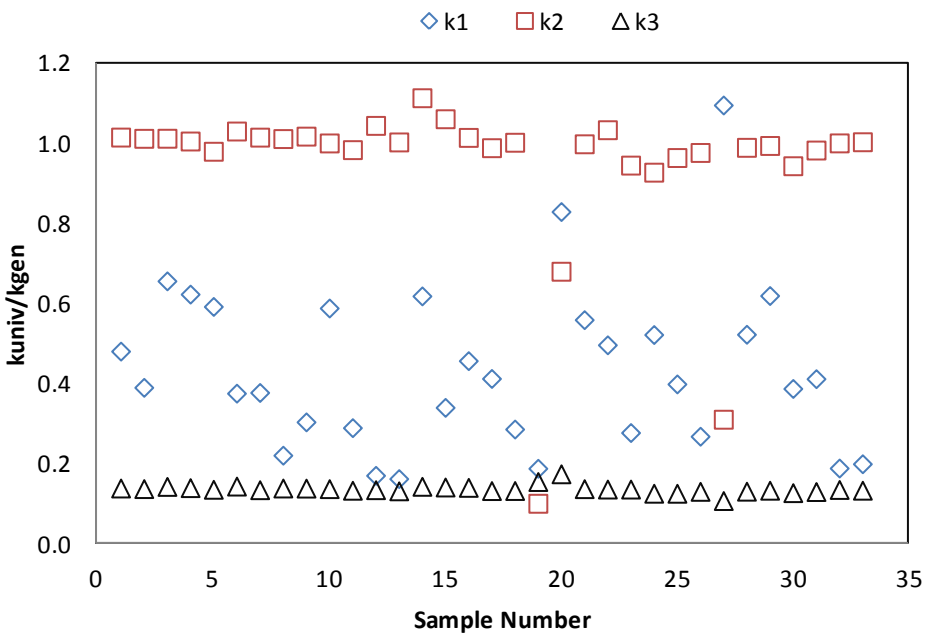

Figure 3.2 Coefficient ratios of the universal model to the generalized model

It is obvious that the coefficients of the universal model should not be adopted directly in the MEPDG software. Instead, highway agencies have to convert the coefficients from the universal model to those for the generalized model, if the original resilient modulus data are missing. They can do so by following the procedures described below: (1) Establish a series of resilient modulus data using the universal model with the associated coefficients; (2) Obtain the coefficients for the generalized model with the resilient modulus data through linear regression method.

3.4 Coefficients of the Generalized Model Regressed from Physical Properties

The establishment of relationships between coefficients of the generalized model and soil physical properties provides a convenient and economical way to evaluate resilient modulus of a new soil as long as this soil is similar to the ones used in the regressions. The physical properties commonly used in developing the relationship are water content, degree of saturation, plasticity index, material passing the #200 sieve, and dry density. Based on sensitivity analysis, George (2004) found that the most important input variable is water content, followed by materials passing #200 sieve, plastic index and sample density. However, the order is likely to vary for different soils and different stress conditions.

Drumm et al. (1995) reported values of soil physical properties such as Atterberg limits, specific gravity, gradation, water content and dry density, which were used as independent variables and $\log(k_1)$, k_2, and k_3 obtained from cyclic triaxial tests were dependent variables. 11 clayey soils, i.e. A-6 and A-7, and 3 silty soils, i.e. A-4, were used. As samples with three different water contents of each soil were included, the seasonal moisture variation of soils could be considered.

Since there are many independent variables, an ever-present danger is that of selecting a model that overfits the "training" data used in the fitting process, yielding a model with poor predictive performance. Using *k*-fold cross validation is one way to assess the

predictive performance of the model. The PRESS statistic was used here among the models whose variables were selected based on entry and stay significance levels (both are 0.15, as defaulted). The regressed models were shown in Table 3.2.

Table 3.2 Regressed models of coefficients from physical properties for soils in Tennessee

Model	R^2	F Value
Clayey Soils		
$\log k_1 = 0.7495 - 0.0080\text{PL} + 0.0038\text{Clay} - 0.0043\text{Passing\#200} + 1.0625\text{SG} - 2.0635\lvert 1 - w_c/w_{opt}\rvert$	0.74	12.85
$k_2 = 0.3680 + 0.0072\text{LL} - 0.0121\text{Clay}$	0.38	7.57
$k_3 = 77.999 + 0.0275\text{Clay} - 38.915\gamma_{max} + 0.7971 w_{opt} - 1.6667 w_c + 25.450\lvert 1 - w_c/w_{opt}\rvert$	0.89	37.43
Silty Soils		
$\log k_1 = 7.1074 - 1.5396\text{SG} - 1.6200\lvert 1 - w_c/w_{opt}\rvert$	0.47	2.68
$k_2 = 0.6595 - 3.2335\text{SG}$	0.66	13.56

Note: PL presents plastic limit; LL presents liquid limit; Clay presents the percentage of clay in soil; Passing#200 presents the percentage of soil particles passing #200 sieve; γ_{max} presents the maximum dry density under optimal water content, w_{opt}; w_c presents current water content of soil; SG presents the specific gravity of soil.

It can be seen from Table 3.2 that physical properties such as plastic limit, percentage of clay, percentage passing #200 sieve, specific gravity, liquid limit, optimum water content, maximum density, and water content had significant effects on the resilient modulus of clayey soils, while specific gravity, water content, and percentage passing #4 sieve significantly affected the resilient modulus of silty soils. Also it can be seen that resilient modulus of soils decreased as the water content increased from optimum water content. It

should be noted that only 9 samples were used when developing the regressed coefficients for silty soils, and more confidence would be achieved if more samples were included.

The coefficients estimated from the physical properties were compared with those based on experimental data, as shown in Figure 3.3. It can be seen that physical properties provided fairly good predictions on the coefficients of the generalized model.

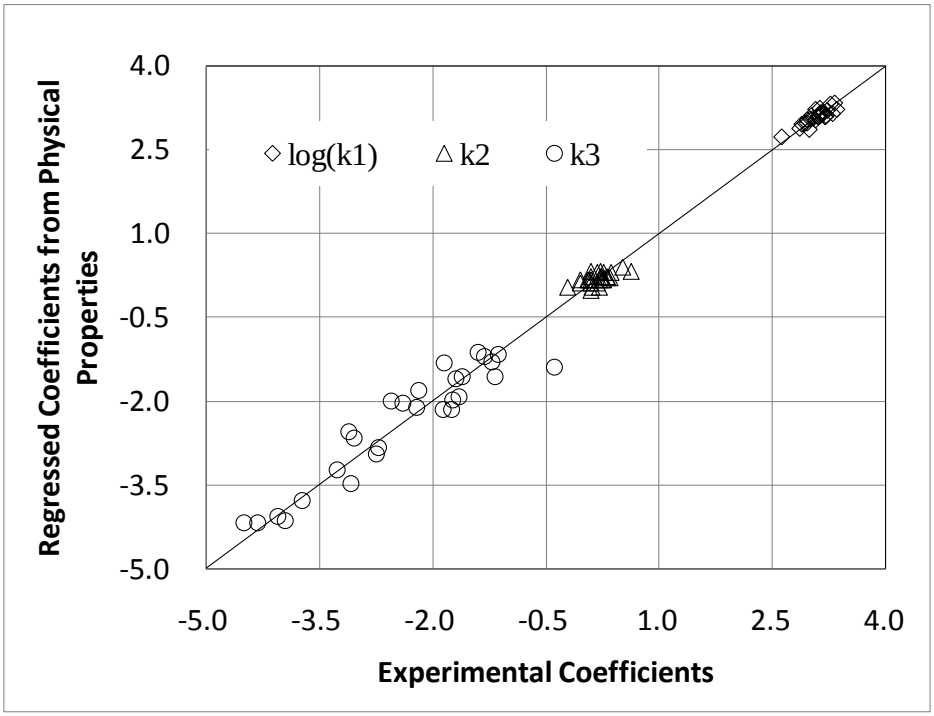

Figure 3.3 Experimental coefficients versus regressed coefficients

The resilient moduli of the clayey soils were calculated from the regressed coefficients, the cyclic stresses, and confining pressures (referred to as regressed resilient moduli hereafter). Figure 3.4 shows the comparison between regressed and experimental resilient

moduli of clayey soils. In general, the majority of regressed resilient moduli were close to the experimental values. Therefore, the relationships for clayey soils in Table 3.2 can be utilized as a time-saving and economical method to evaluate coefficients in the generalized model and the resilient moduli of clayey soils.

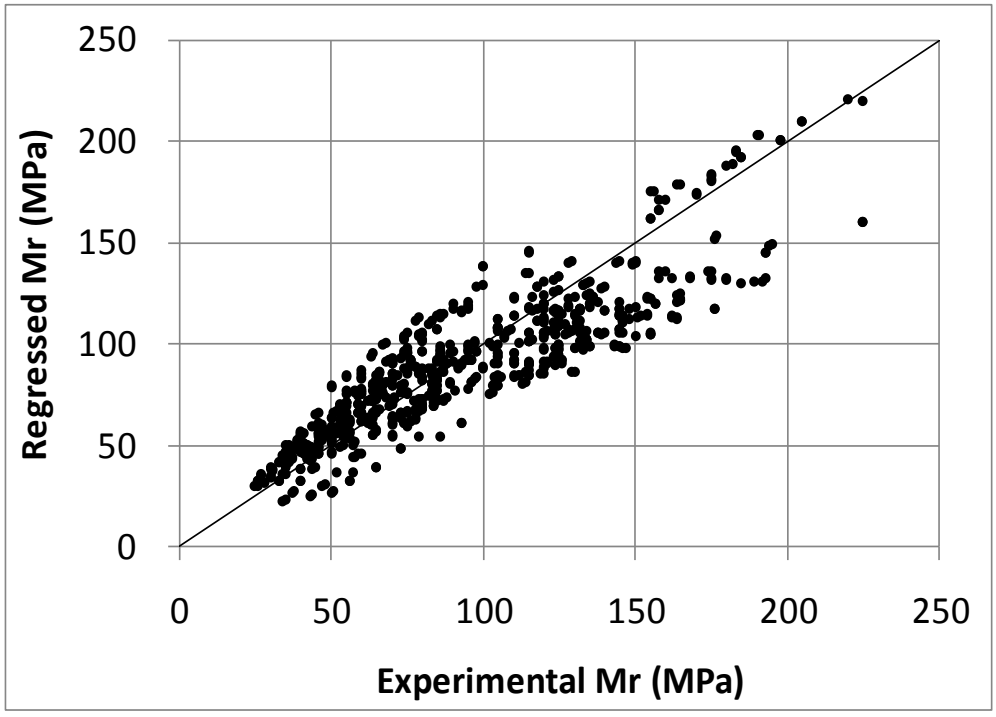

Figure 3.4 Experimental resilient moduli versus regressed resilient moduli

3.5 Seasonal Variation of Clayey Soil Resilient Moduli in Tennessee

In pavement design, resilient modulus of soil at optimum water content (standard Proctor) is usually adopted. However, soil resilient modulus is highly dependent on moisture content (George, 2004; Figueroa, 2001; Shalaby, 2010). Zuo (2007) selected four locations in Tennessee and monitored moisture variation in subgrade. Among these four

locations, the subgrade soil from Blount County was classified as A-7-5, which is the same as the soil in Knox. Co. Sta. 400. These two counties are geographically close and have similar climate. California Bearing Ratio (CBR) of the subgrade soil was defaulted as 7.0, according to pavement design experience in Tennessee. The empirical model in Eq. (3.3) (ARA, 2004) gives a representative resilient modulus of 61.2 MPa for the following pavement response analysis.

$$M_r\ (\text{psi}) = 2555 * (\text{CBR})^{0.64} \tag{3.3}$$

In order to evaluate the influence of soil moisture on soil resilient modulus, Knox. Co. Sta. 400 soil in Table 3.1 was selected and assumed to experience the annual moisture variation, as shown in Figure 3.5, which was the change of moisture 0.15 m under the subgrade surface at the Blount County pavement site (Zuo, 2007). Water contents in the soil shown in Figure 3.5 were higher than the optimum water content (29.4%) in Table 3.1. The coefficients of the generalized model for Knox. Co. Sta. 400 soil were determined from the regressed models in Table 3.2 and the results were shown in Figure 3.5. It can be seen from Figure 3.5 that $\log(k_1)$ and k_2 decreased while subgrade moisture increased, vice versa.

As recommended by AASHTO T307, fifteen stress states were applied to the Knox Sta.400 soil, as shown in Figure 3.6. As the subgrade depth increased, confining pressure increased while deviator stress decreased. As the horizontal distance increased from the site of the traffic load, the deviator stress in soil decreased. Figures 3.7 and 3.8 show the

seasonal change of soil resilient modulus. They indicate that when the water content was higher than the optimum one, there was an inverse correlation between resilient modulus and water content. Similar results were reported elsewhere (Ceratti, et al., 2004). The variation of soil resilient modulus was around 10 MPa. It can also be seen that soils vertically under traffic loads exhibited smaller resilient modulus than those located deeper (Figure 3.8) or horizontally farther away from traffic loads (Figure 3.7).

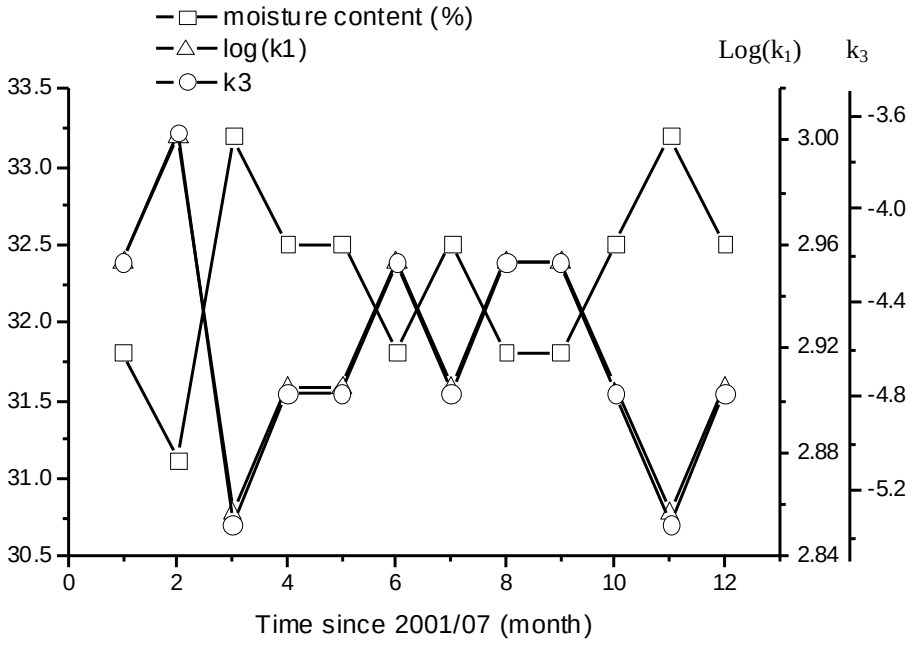

Figure 3.5 Annual changes of coefficients of the generalized model with seasonal moisture variation in subgrade on Knoxville Sta. 400

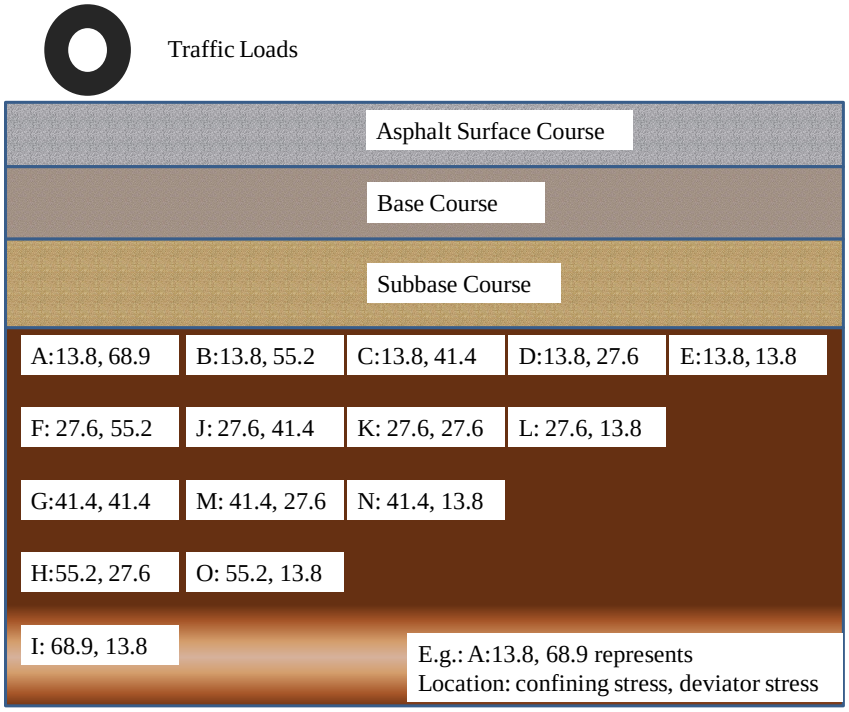

Figure 3.6 Sketch of stress state in subgrade

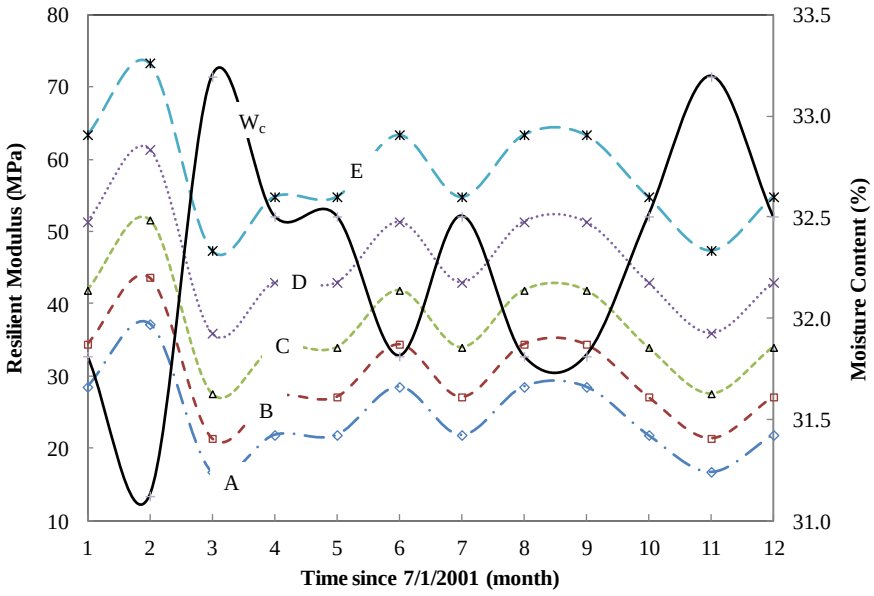

Figure 3.7 Seasonal variation of soil resilient modulus at different horizontal location in the same depth

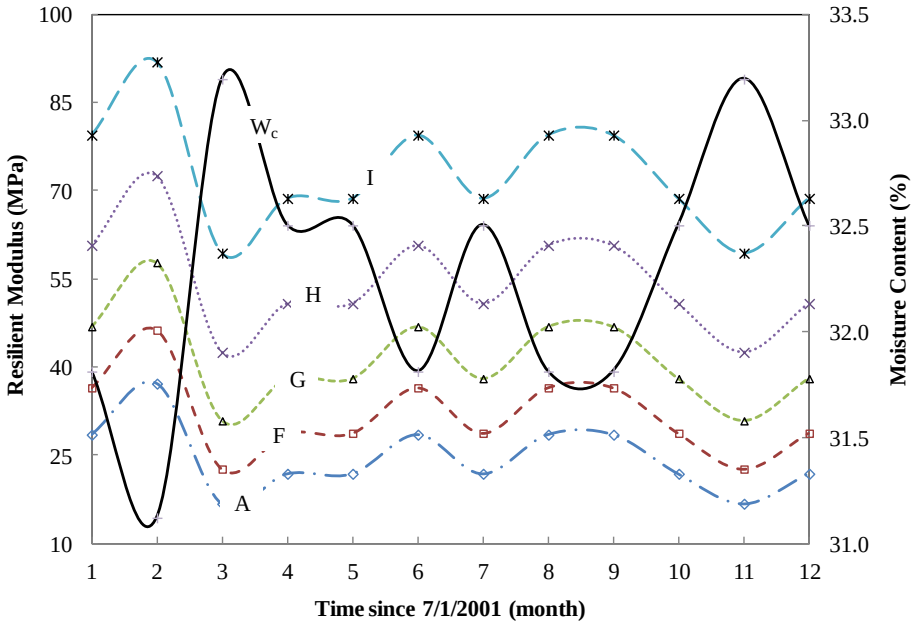

Figure 3.8 Seasonal variation of soil resilient modulus at different depths under traffic load

3.6 Influence of Soil Resilient Modulus on Flexible Pavement Performance

As shown above, the stiffness of the subgrade varied seasonally. Therefore, the support of soil to pavement structure would also change, which would subsequently affect pavement performance. Two typical pavement structures, interstate highway I-40 at Knoxville (I-40 Knox.) and state route 36 (SR-36 Washington) were selected to investigate the influence of soil resilient modulus variation on pavement performance. The details of pavement sections and material properties are listed in Table 3.3.

Table 3.3 Pavement structures and material properties

Layers	Thickness (cm)		Elastic Modulus (MPa)	Poison's Ratio
	I-40 Knox	SR-36 Washington		
Asphalt Surface Course	31.1	17.8	3445	0.35
Asphalt Base Course	8.9	8.9	2412	0.35
Granular Base	20	20	138	0.40
Subgrade	-	-	Varied	0.45

A multiple elastic-layered software, WESLEA 3.0 was adopted to analyze the tensile strain in the upper asphalt layer, the compressive strain on the top of subgrade, and the fatigue life of pavement. The default values of elastic moduli and Poisson's ratio were used. It should be pointed out that since the mechanical properties of asphalt mixtures are highly related to temperature, the use of constant elastic moduli may not reflect the seasonal modulus variation of the asphalt layers in the field. Adoption of constant elastic moduli was only to investigate the effect of subgrade resilient modulus variation on pavement performance. Due to this simplification, the analysis from WESLEA 3.0 here only indicated the trend of the impact of seasonal soil resilient modulus variation on pavement performance rather than the full seasonal variation on pavement performance.

It was assumed that the subgrade soils under the two pavement sections had the same properties as the Knox Sta. 400 in Table 3.1. In general, pavement section in SR-36 Washington County has a 18in. thick pavement structure, while pavement section in I-40 Knox. has a 24in. thick pavement structure., the subgrade soil is typically subjected to between 48.3 kPa (7 psi) and 68.9 kPa (10 psi) vertical stresses from an 18,000-lb single-

axle load. Therefore, a deviatoric stress of 68.9 kPa (10 psi) was used in the analysis in order to simulate field conditions. Since the goal was to obtain the trend, not the specific values of pavement responses, only a confining pressure of 41.4 kPa (6 psi) was used.

A transfer function developed at the University of Illinois using Mn/ROAD fatigue crack data was used in WESLEA 3.0 to predict fatigue life of asphalt pavement, as shown in Eq.(3.4).

$$N_f = 2.83 * 10^{-6} * (\frac{10^6}{\varepsilon_t})^{3.148} \quad (3.4)$$

where: N_f= number of repeated loads under current structural conditions before a fatigue crack will form; ε_t= maximum horizontal tensile strain at bottom of first layer caused by one pass of current wheel configuration, expressed in microstrain.

Figures 3.9 and 3.10 showed the seasonal variation of longitudinal strain at the bottom of the first asphalt layer and compressive strain on the subgrade surface for both pavement sections. The fatigue lives corresponding to different resilient moduli of subgrade through one year are shown in Figure 3.11. It can be seen that as the subgrade resilient modulus decreased, the longitudinal tensile strain at the bottom of the first asphalt layer and the compressive strain on the top of subgrade increased, and the fatigue life decreased by 15% - 40% compared to that with optimal water content. West et al. (2012) reported a similar trend on longitudinal strain at the bottom of asphalt layer and also on subgrade pressure

on an Open-Graded Friction Course (OGFC) test track. The possible reasons they offered for this change are layer slippage and/or cracking extending deeper into the pavement structure. Actually, comparing to the climate data record from National Climatic Data Center, a positive correlation can be observed between the longitudinal strain at the bottom of asphalt layer and precipitation in that area. A reasonable explanation for the phenomenon is the high precipitation increased moisture content in subgrade through cracks on the pavement and weakened the stiffness of soil, and furtherly redistribute the traffic loads in the pavement structure and the subgrade. Therefore, pavement responses in the asphalt pavement structure were enlarged by moisture increase in subgrade.

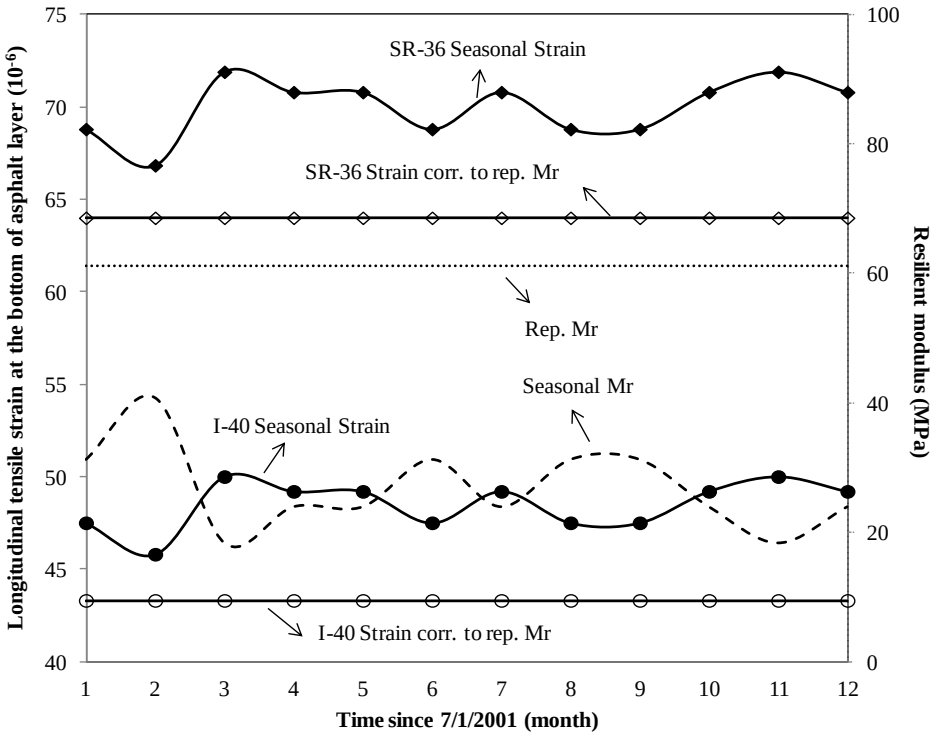

Figure 3.9 Seasonal variation of longitudinal tensile strain at the bottom of the first asphalt layer

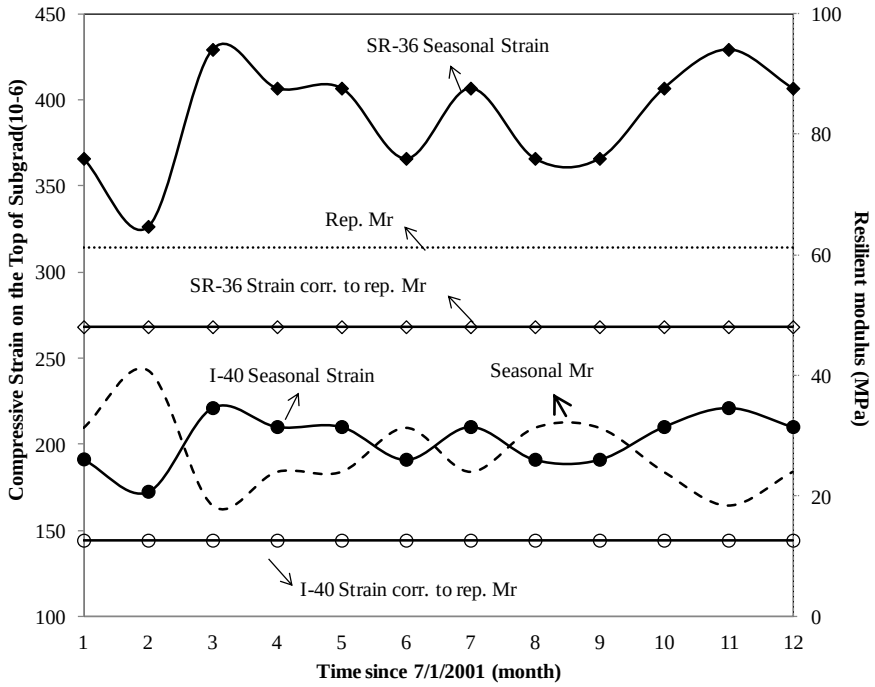

Figure 3.10 Seasonal variation of compressive strain at the top of subgrade

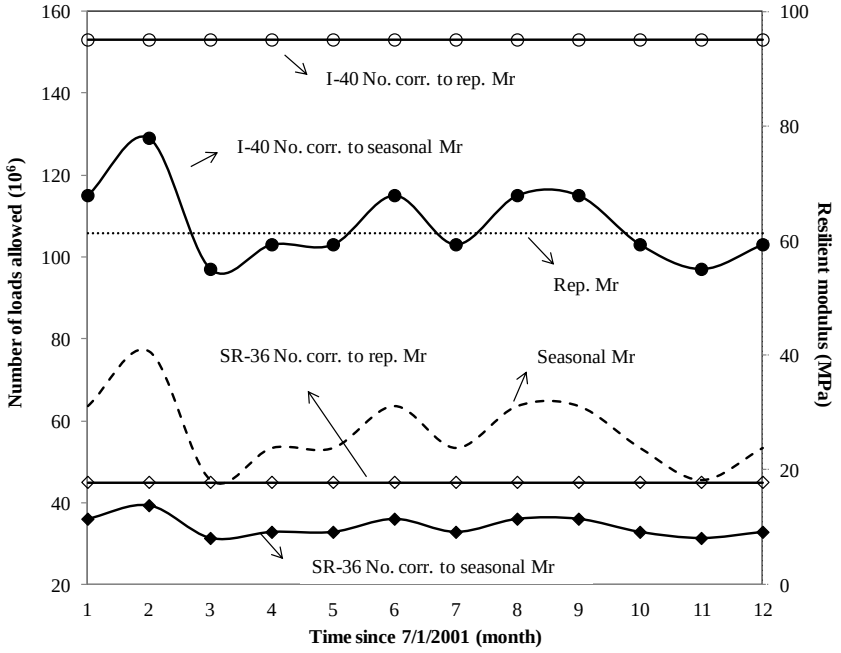

Figure 3.11 Seasonal variations on fatigue life of the two pavement sections

Compared to the I-40 Knox. pavement section, the thinner pavement section, the SR-36 section in Washington presented a higher tensile strain at the bottom of the upper asphalt layer and a higher compressive strain at the surface of the subgrade. There was no evidence to show that pavement responses of a thick pavement were less sensitive to the variation of resilient modulus than those of a thin pavement. Therefore, resilient modulus variation due to seasonal moisture change in subgrade should be fully taken into account on both low and high traffic volume highways.

Rutting development of the two pavement sections was evaluated using the MEPDG software (version 1.1) with an input level 2 on subgrade resilient modulus property and with input level 3 with all other input factors on traffic, climate and material properties. The same traffic was applied on both sections, with an initial 380 AADTT (average annual daily truck traffic). Rutting development of SR-36 Washington pavement section, as an example, is shown in Figure 3.12. It can be seen that when seasonally varying resilient modulus instead of a representative resilient modulus was taken into account, a relatively higher rutting depth would occur on subgrade. An interesting result was observed: the portion of the rutting contributed by the asphalt layers and base was about the same with or without seasonal resilient moduli considered. This may not be true in the field. A weak support from subgrade would force the pavement structure carry more parts of loads than a strong support, which would usually lead to accelerated pavement deteriorations, including rutting. From this point of view, the MEPDG software version 1.1 may not capture the impact of seasonal resilient moduli on the rutting of pavement structure.

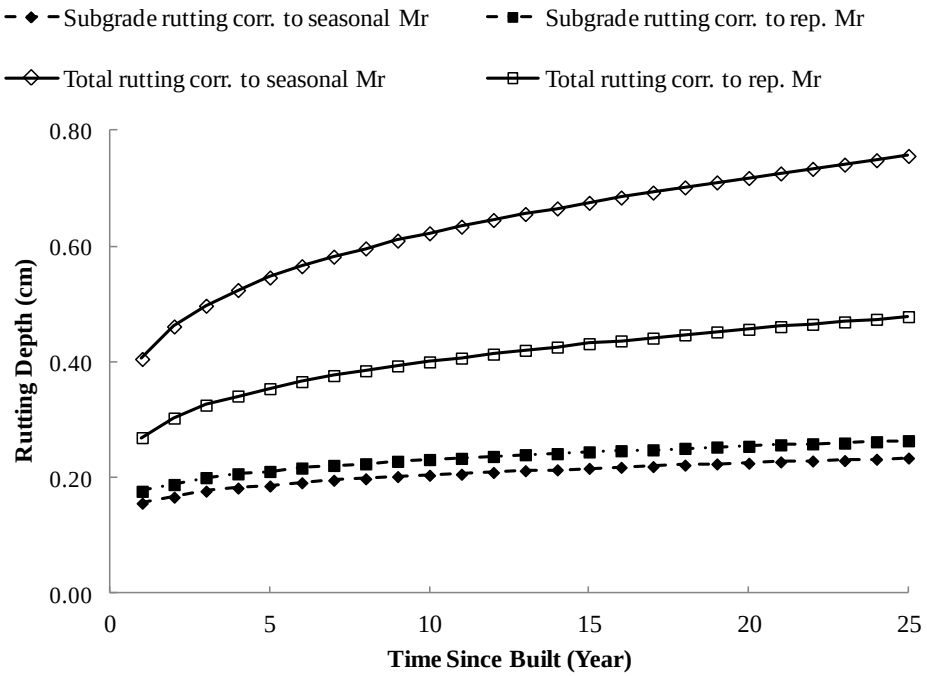

Figure 3.12 Rutting development of SR-36 Washington pavement section

Since the pavement responses caused by the seasonal variation of the subgrade resilient modulus vary significantly, it is recommended that the resilient modulus at input Level 2 and the coefficients of the generalized model at input Level 1 should be substituted by the seasonally changing resilient modulus and coefficients of the generalized model, respectively, when the information is available.

3.7 Conclusions and Recommendations

Based on the triaxial cyclic test results of fourteen soils in Tennessee, the coefficients of the generalized model and the universal model were obtained through multiple linear regressions and their values compared. The variation of soil resilient modulus due to

seasonal moisture change was explored and its effect on pavement performance was investigated. The following conclusions and recommendations can be drawn from the study:

- The relationships between the coefficients of the generalized model and the physical properties for clayey soils were developed and validated to be a time-saving and economical way to estimate the resilient modulus of clayey soils.
- There existed an inverse correlation between soil resilient modulus and water content higher than optimal moisture content. The higher the water content, the lower the soil resilient modulus.
- The seasonal variation of subgrade resilient modulus due to the moisture change enhanced the computed longitudinal tensile strain at the bottom of the asphalt layers and compressive strain on subgrade surface, decreased fatigue life of the flexible pavements, and increased the rutting depth in the subgrade.
- The fatigue life of both low volume and heavy volume pavements was significantly affected by subgrade resilient modulus reductions due to moisture change.
- It is recommended that seasonal changes in soil resilient modulus and the coefficients of the generalized model be included in MEPDG software.

3.8 References

Ahn, J., Cote, B.M., Robinson, B., Gabr, M.A. and Borden, R.H. (2009). "Inverse Analysis of Plate Load Tests to Assess Subgrade Resilient Modulus." *Transportation Research Record: Journal of the Transportation Research Board,* No. 2101, *TRB, National Research Council, Washington, D.C.* pp. 110-117.

American Association of State Highway and Transportation Officials (1986). " AASHTO Guide for Design of Pavement structures." Washington, D.C.

American Association of State Highway and Transportation Officials (1999). "AASHTO T307 Determining the Resilient Modulus of Soils and Aggregate Materials." Washington, D.C.

Bayomy, F., El-Badawy, S., and Awed, A. (2012). "Implementation of the MEPDG for Flexible Pavements in Idaho." National Institute for Advanced Transportation Technology , University of Idaho.

Ceratti J.A., Gehling, W.Y.Y., and Núñez, W.P. (2004). "Seasonal Variations of a Subgrade Soil Resilient Modulus in Southern Brazil." *Transportation Research Record: Journal of the Transportation Research Board,* No. 1874, *TRB, National Research Council, Washington, D.C.,* pp. 165–173.

Dawson, T.A., Baladi, G.Y., Sessions, C.P., and Haider, S.W. (2009). "Backcalculated and Laboratory-Measured Resilient Modulus Values." *Transportation Research Record: Journal of the Transportation Research Board,* No. 2094, pp. 71-78.

Drumm, E.C., Li, Z., Reeves, J.S., and Madgett, M.R. (1996). "Alternative Test Method for Resilient Modulus of Fine-Grained Subgrades." *Geotechnical Testing Journal*, Vol. 19, No. 2, pp. 141-154.

Drumm, E.C., Reeves, J.S., and Madgett, M.R. (1995). "Design Handbook of Index Properties and Resilient Response." Final Report to Tennessee Department of Transportation, *University of Tennessee, Knoxville*.

Drumm, E.C., Reeves, J.S., Madgett M.R., and Trolinger W.D. (1999). "Subgrade Resilient Modulus Correction for Saturation Effects." *Journal of Geotechnical and Geoenvironmental Engineering*, Vol. 123, No. 7, pp. 663-670.

Figueroa, J.L. (2001) "Monitoring and Analysis of Data Obtained from Moisture Temperature Recording Stations." Final Report to *the Ohio Department of Transportation, Case Western Reserve University*.

George, K.P. (2004). "Prediction of Resilient Modulus from Soil Index Properties." Final Report to *Mississippi Department of Transportation Research Division*.

Hopkins, T.C., Beckham, T.L., and Sun, C. (2004). "Resilient Modulus of Kentucky Soils." *University of Kentucky*.

Hossain, M.S. (2008). "Characterization of Subgrade Resilient Modulus for Virginia Soils and Its Correlation with the Results of Other Soil Tests." *Virginia Transportation Research Council*.

Malla, R.B. and Joshi, S. (2006).). "Establish Subgrade Support Values for Typical Soils in New England." Final Report to the New England Transportation Consortium, *University of Connecticut, Storrs, Connecticut*.

Mohammad L. N., Huang, B., Puppala, A J., and Allen, A. (1999) "Regression Model for Resilient Modulus of Subgrade Soils." *Transportation Research Record: Journal of the Transportation Research Board*, No. 1442, *TRB, National Research Council, Washington, D.C.* pp. 47-54.

Mohammad, L.N., Gaspard, K., Herath, A., and Nazzal. M.D. (2007). "Comparative Evaluation of Subgrade Resilient Modulus from Non-destructive, In-situ, and Laboratory Methods." *Louisiana Transportation Research Center*.

Moossazadeh, J. and Witczak, M.W. (1981). "Prediction of Subgrade Moduli for Soil that Exhibits Nonlinear Behavior." *Transportation Research Record: Journal of the Transportation Research Board*, No. 810, *TRB, National Research Council, Washington, D.C.* pp. 9-17.

National Cooperative Highway Research Program (2003) "NCHRP project 1-28A, Appendix A, Procedure for Resilient Modulus of Unstabilized Aggregate Base and Subgrade Materials." *Transportation Research Board*.

National Cooperative Highway Research Program (2004) "NCHRP project 1-37A, Guide for Mechanistic-Empirical Design of New and Rehabilitated Pavement Structures." *Transportation Research Board*.

Nazzal. M.D. and Mohammad, L.N. (2010). "Estimation of Resilient Modulus of Subgrade Soils Using Falling Weight Deflectometer." *Transportation Research Record: Journal of the Transportation Research Board*, No. 2701, pp. 1-10.

Ping, W.V. and Sheng, B. (2011). "Developing Correlation Relationship between Modulus of Subgrade Reaction and *Resilient* Modulus for Florida Subgrade Soils."

Transportation Research Record: Journal of the Transportation Research Board, No. 2232, *TRB, National Research Council, Washington, D.C.*, pp. 95-107.

Seed, H.B., Mitry, F.G., Monismith, C.L. and Chan, C. K. (1967). "Prediction of Pavement Deflection from Laboratory Repeated Load Tests." *NCHRP Transportation Research Board* Report 35.

Shalaby, A. (2010). "Sensitivity of Sbugrade Resilient Modulus to Moisture Variation." *Annual Conference of the Transportation Association of Canada*.

SHRP Protocol P-46. (1993). "Resilient Modulus of Granular Base\Subbase Materials and Subgrade Soils." *Strategic Highway Research Program*, SHRP-LAPP Laboratory Material Testing Guide.

Titi, H.H., Elias, M.B., and Helwany, S. (2006). "Determination of Typical Resilient Modulus Values for Selected Soils in Wisconsin." Final Report to Wisconsin Department of Transportation. *University of Wisconsin - Milwaukee.*

Uzan, J., Witczak, M.W., Scullion, T. & Lytton, R.L. (1992). "Development and validation of Realistic Pavement Response Models." *7th International Conference on Asphalt Pavement, Nottingham, UK*, Vol.1, pp. 334-350.

Von Quintus, H. and Killingsworth, B. (1998). "Analyses Relating to Pavement Material Characterizations and Their Effects on Pavement Performance." A Report to Federal Highway Administration, *U.S. Department of Transportation*.

West R., Timm, D., Willis, R., Powell, B., Tran, N., Watson, D., Sakhaeifar, M., Brown, R., Robbins, M., Vargas-Nordcbeck, A., Villacorta, F.L., Guo, X., and Nelson, J. (2012). "Phase IV NCAT Pavement Test Track Findings." Final Report, National Center for Asphalt Technology, Auburn, Alabama.

Zuo, G., Drumm, E.C., and Meier R.W. (2007). “Environmental Effects on the Predicted Service Life of Flexible Pavements.” Journal of Transportation Engineering, ASCE, 133 (1), 47-56.

PART 4 VERIFICATION ON MECHANICAL-EMPIRICAL PAVEMENT DESIGN GUIDE WITH PMA DATABASE IN TENNESSEE

This part is revised based on a paper published by Changjun Zhou, Baoshan Huang, Xiang Shu, and Qiao Dong:

Zhou, C., Huang, B., Shu, X., and Dong, Q. (2013). "Validating MEPDG with Tennessee Pavement Performance Data." Journal of Transportation Engineering, 139(3): 306-312 (doi: 10.1061/(ASCE)TE.1943-5436.0000487).

My primary contributions to this paper include (1) development of the problem into a work, (2) identification of the study objective and scope, (3) data collection, analysis and interpretation, (4) fulfilling comments from co-authors in the paper, (5) the writing.

4.1 Abstract

To implement the Mechanistic-Empirical Pavement Design Guide (MEPDG) developed by AASHTO for pavement construction and rehabilitation, it is necessary to evaluate its performance prediction models utilizing actual pavement performance data, material properties, traffic information, and environmental factors. This paper verified the MEPDG models utilizing the performance of typical pavements in the state of Tennessee from pavement management system (PMS). With traffic and pavement structural information collected from PMS, the performance of selected highway pavement sections was analyzed with MEPDG Version 1.100 software. The predicted Present Serviceability Index (PSI) and rutting were compared with the actual measurement values. An initial value for the International Roughness Index (IRI) was suggested for Tennessee highways through investigation into the actual roughness data. The dynamic moduli of asphalt

mixtures for input Level 1 were obtained from laboratory testing. Those for input Level 3 were estimated with the Witczak model. The results show that rutting of asphalt concrete (AC) pavements was more accurately predicted at input Level 1, whereas it was over-predicted at input Level 3. Traffic level was found to be an important factor affecting predicted pavement roughness. It was also found that MEPDG software was relatively conservative for highway pavements of low traffic level. However, MEPDG with nationally averaged default parameters was not sensitive enough to differentiate between various climate, traffic and materials in Tennessee for the prediction of PSI.

4.2 Introduction

4.2.1 Research Background

The *AASHTO 1993 Guide for Design of Pavement Structures* (hereafter, AASHTO 1993 Guide) has been extensively employed in the United States for highway pavement design for decades (AASHTO 1993). Nevertheless, its development is based on limited pavement sections at one location of unique climate, specific materials and loads. Therefore, it does not reflect many current design inputs (ARA 2004). In 2004, a new Mechanistic-Empirical Pavement Design Guide (MEPDG) for New and Rehabilitated Pavements was developed by AASHTO. Compared to the AASHTO 1993 guide, this new MEPDG has made significant improvements in that it utilizes databases of traffic, climate, materials and structural analysis to predict pavement performance over a defined service life (ARA 2004). Mechanistic-empirical models use both volumetric and fundamental material properties to characterize pavement materials. This is in contrast to

the 1993 AASHTO Guide, which only uses resilient modulus for estimating structural layer coefficient. The new design guide can directly consider effects and interactions of inputs on structural distress and ride quality. In order to implement the new design guide, many states have begun data collecting, model testing (Garcia and Thompson, 2007; Banerjee et al., 2009; Saxena et al. 2010, Kutay and Jamrah, 2013), sensitivity analysis (Ayyala and Daniel 2010, Aguiar-Moya et al. 2010), software evaluation, validation, and calibration.

Schwartz et al. (2013) conducted a comprehensive global sensitivity analyses (GSA) of flexible pavement performance predictions to MEPDG design inputs under five climatic conditions and three traffic levels. Factors that greatly influence each pavement distresses were presented in the order of importance. The design inputs most consistently in the highest sensitivity categories across all distresses were the hot mix asphalt (HMA) dynamic modulus master curve, HMA thickness, surface shortwave absorptivity, and HMA Poisson's ratio. Longitudinal and alligator fatigue cracking were also very sensitive to granular base thickness and resilient modulus and subgrade resilient modulus. Similar GSA was conducted on the concrete pavements by Ceylan et al. (2013). Schwartz and Carvalho (2007a) analyzed the sensitivity of the MEPDG performance predictions to input parameters, including traffic, environmental conditions, and material properties for the state of Maryland. They found that MEPDG was very sensitive to climate variations and different material properties. They recommended local calibrations for different materials and every region. Mallela et al. (2009) conducted sensitivity analysis as well as local validation and calibration of MEPDG models with limited LTPP sections in Ohio.

The fatigue prediction models in the MEPDG for pavement rehabilitation in Oregon (Rahman, Williams, and Scholz, 2013) were calibrated and predictions of both alligator cracking and longitudinal cracking were improved by local calibration. However, after calibration a high variability still existed between the predicted distresses and observed distresses, especially for the longitudinal cracking. Kim, et al. (2013) calibrated DARWin-ME and MEPDG version 1.1 on the jointed plain concrete pavement performance prediction models in Iowa and suggested that few differences are observed between DARWin-ME and MEPDG with national and local calibrated models for faulting and transverse cracking predictions for JPCP, but not for International Roughness Index (IRI). The locally calibrated JPCP IRI prediction model for Iowa conditions could reduce the prediction differences between DARWin-ME and MEPDG.

Hall et al. (2011) conducted a local calibration of performance prediction models in MEPDG for Arkansas. They successfully calibrated rutting and alligator (bottom-up) cracking models while did not calibrate longitudinal (top-down) cracking and transverse cracking models due to the nature of the data. Velasquez et al. (2009) utilized field performance data from MnROAD pavement sections as well as other pavement sections located in Minnesota and neighboring states to modify the prediction models for rutting and the coefficients in alligator cracking and thermal cracking models. They recommended adopting the modified models to implement MEPDG in predicting relative distresses in Minnesota. They also suggested Level 3 as asphalt binder characterization. However, they did not recommend using MEPDG to predict longitudinal cracking and

roughness. Sunghwan et al. (2010) evaluated the accuracy of the MEPDG performance prediction models utilizing pavement sections with pavement performance data from the Iowa state's Pavement Management System (PMS) and the Long Term Pavement Performance (LTPP) database. They suggested a recalibration for the MEPDG performance models to Iowa conditions. Souliman et al. (2010) used 39 pavement sections in LTPP database to perform the calibration. They found that the national-calibrated MEPDG models under-predicted alligator cracking and rutting for Arizona conditions, whereas they over-predicted the longitudinal cracking and the subgrade rutting. Local-calibrated coefficients were proposed for rutting, fatigue cracking and IRI models. Li et al. (2009, 2010) established a pavement thickness design catalog for the Washington state Department of Transportation (DOT) based on the calibration of MEPDG software for their state condition. Actually, dynamic modulus and other fundamental tests were not included in the LTPP database when the national calibration conducted in the NCHRP 1-37A Report. Therefore, errors are expected when those properties of materials are adopted in the MEPDG software.

It can be summarized from the above-mentioned studies that local calibration for MEPDG is necessary in that the national-calibrated models for distresses and/or roughness either under-predicted or over-predicted pavement performance for each specific state. The frequently utilized pavement performance data sources include the Minnesota MnROAD test roads, states' PMS and LTPP database. Because materials, climate, and traffic all significantly affect pavement performance, it is of great significance to calibrate the MEPDG models for local transportation agencies.

4.2.2 Research Objectives and Methodology

The objective of the study is to verify the MEPDG prediction models of pavement performance in Tennessee. To achieve this goal, the pavement performance of 19 highway pavement sections in Tennessee was analyzed using the latest version of MEPDG software and compared to the data collected from the PMS of Tennessee.

The methodology for validating the MEPDG prediction models of pavement performance are shown in Figure 4.1. First, traffic, climate, pavement structures and material properties of selected highway pavement sections were collected from PMS, state's pavement construction records and MEPDG database. Then, two pavement performance parameters, PSI and rutting, were predicted with the MEPDG software and compared with the values obtained from PMS.

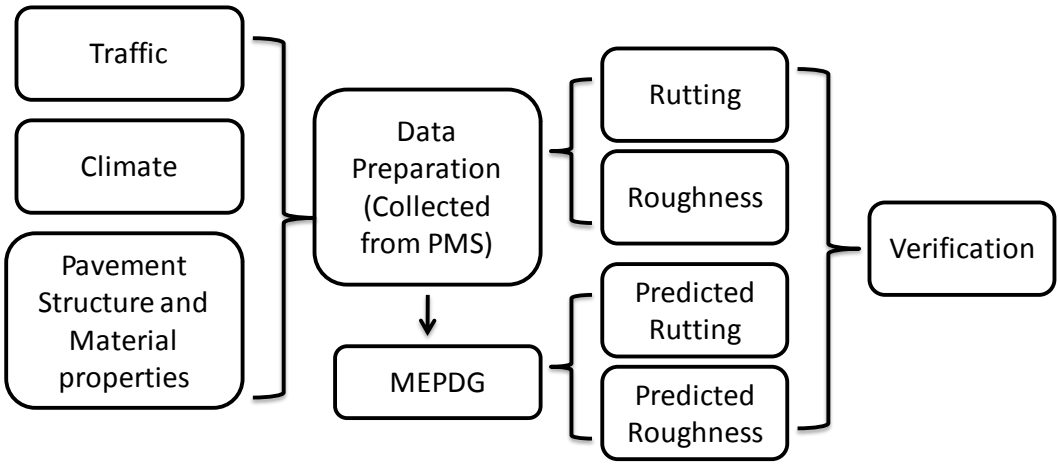

Figure 4.1 Procedure of verification on MEPDG

4.3 Data Preparation

The PMS in Tennessee contains structure, material and traffic information of pavement sections as well as pavement performance indices including PSI, IRI, and rutting depth. Pavement performance data are collected every year for interstates and every two years for state routes in Tennessee. The quality of data has a significant effect on the pavement performance prediction and evaluation. The data prepared in this study includes four parts, namely, traffic, climate, pavement structures and materials, and pavement performance.

4.3.1 Traffic

Axle load spectra was introduced into the MEPDG which requires truck counts by week days and months for all truck types from Class 4 to Class 13 (FHWA). The traffic volume adjustment factors for truck distribution, vehicle class distribution and axle load distribution factors are required. Some factors such as axle load distribution factor and percentage of vehicles in the design lane are very sensitive inputs (Oman 2010). However, due to the fact that the detailed information about axle load distribution is still unavailable from the Tennessee PMS, national default axle load spectra were used in this study. The Equivalent Single Axle Load (ESAL) acquired from the PMS was selected as a traffic level indicator. The initial Average Annual Daily Truck Traffics (AADTTs) were back-calculated from the respective ESALs.

4.3.2 Climate

The variation in climate condition has a significant influence on the MEPDG performance prediction of interstate highways (Schwartz and Carvalho 2007b). The default climate data of weather stations located in Tennessee was tested and found to be acceptable for the validation efforts. The stations with incomplete data cannot be used alone in MEPDG. Utilizing these stations when creating a virtual weather station through interpolation may only decrease the quality of prediction (Johanneck and Khazanovich 2010). It is observed that the weather station located in Knoxville, Tennessee missed some data in some months. Therefore, the nearest weather station with complete data was used instead of this station in the analysis. According to Tennessee Water Science Center, the groundwater table is 1.8 m deep or lower. Since distress predictions for AC pavement sections are not affected by depths greater than 1.2 m (Witczak et al. 2006, Zapata 2009), the depth of groundwater table was assumed to be 1.8 m for all pavement sections.

4.3.3 Pavement Structures and Material Properties

Most interstate highways in Tennessee were constructed before the 1970s. Since then, maintenance and rehabilitations have been continuously conducted to keep these highways up to an acceptable service level. The main interstates in Tennessee include I-40, I-24, I-65, I-75, I-26, and I-81. Totally, 19 pavement sections were selected throughout Tennessee for this study, including 18 interstate highway sections and one state route section (Figure 4.2). All these highway sections have an overlay thickness no thinner than 10cm in their last maintenance activities.

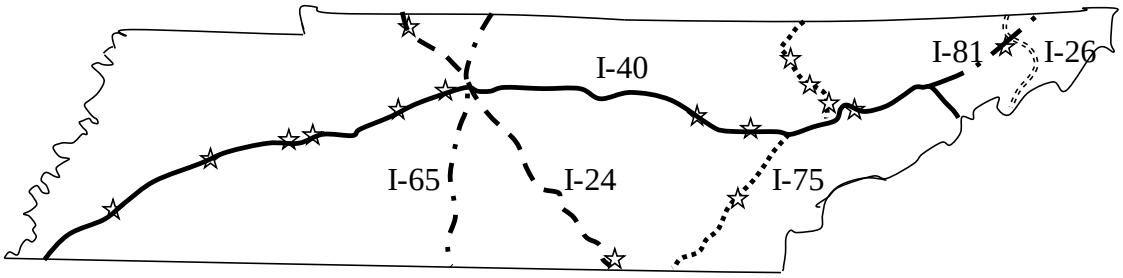

Figure 4.2 Pavement sections for evaluation in Tennessee

Basic information on the location, structure, construction and maintenance history, and soil properties of the selected highway pavement sections is presented in Table 4.1. Current MEPDG procedure is able to analyze pavement overlays. However, this overlay analysis has not yet been nationally calibrated and currently is not recommended for evaluation of existing pavements. Therefore, only the MEPDG new design procedure was used in this study. Because MEPDG can analyze no more than four AC layers, several old layers had to be merged into one layer for some selected pavement sections. In addition, MEPDG's new design procedure cannot analyze old portland cement concrete (PCC) pavements, which has to be converted into an equivalent crushed stone base with a proper thickness.

Table 4.1 Information of selected pavement sections for analysis

20-year ESALs	Highway	County	Mile	AADTT	Overlay (cm)	Existing AC/PCC (cm)	Crushed Stone (cm)
<4,500,000	I_40	Knoxville	0-6.9	250	--	31.1Asphalt Surface+8.9Asphalt Base	20.3
	SR_36	Washington	14.4-15.1	380	--	17.8Asphalt Surface+8.9Asphalt Base	20.3
	I_81	Greene	6.0-12.3	520	13.3Asphalt Surface	5.7Asphalt Surface+26.7Asphalt Base	7.6
	I_40	Roane	15.7-22.9	600	3.2GrD+6.4GrB+7.6GrA	18.4Asphalt Surface+17.8Asphalt Base	25.4
	I_40	Fayette	7.9-16.1	730	3.25Asphalt Surface+9Asphalt Base+31.1Crushed Stone	22.9PCC	20.3
	I_40	Benton	0-8	750	7.6Asphalt Surface+7.6Asphalt Base	25.4Asphalt Base	20.3
	I_75	Campell	27-30.4	750	7.6Asphalt Surface +15.2 Asphalt Base	25.4Asphalt Base	20.3
	I_40	Dickson	9.1-17.8	820	8.3Asphalt Surface +27.9Asphalt Base	17.8Asphalt Base	20.3
	I_75	McMinn	10.9-13.4	870	11.4Asphalt Surface	5.7Asphalt Surface+17.8Asphalt Base	20.3
	I_40	Cumberland	6.4-13.5	950	3.2Asphalt Surface +7.6Asphalt Base	6.4Asphalt Surface+31.8Asphalt Base	20.3
4,500,000-9,000,000	I_75	Knoxville	8.8-13.7	1050	7.6Asphalt Surface +26.7Asphalt Base	22.9PCC	41.9
	I_40	Davidson		1100	13.3Asphalt Surface	Milled Asphalt Surface off	35.6
	I_75	Anderson	8.3-10.2	1150	8.3Asphalt Surface +10.2Asphalt Base	17.8Asphalt Base	20.3
	I_24	Montgomery	11.7-17.2 M	1150	3.2Asphalt Surface +7.6GrA+7.6GrAS	45.7Asphalt Base	20.3
	I_40	Madison	7.4-12.4	1320	3.2Asphalt Surface +16.5Asphalt Base	22.9PCC	15.2
	I_24	Montgomery	11.7-17.2 P	1370	3.2Asphalt Surface +12.1Asphalt Base	19.7Asphalt Surface+8.9Asphalt Base	12.7
	I_65	Davidson	20.1-22.2	2000	3.2Asphalt Surface +15.2Asphalt Base	12.7Asphalt Base+22.9PCC	15.2
>9,000,000	I_40	Davidson	0-4.7	2900	9.5Asphalt Surface +8.9Asphalt Base	25.4PCC	15.2
	I_65	Davidson	0.4-3.5	4100	13.3Asphalt Surface	7.6Asphalt Base+22.9PCC	22.9

Two input levels were defined and used for the MEPDG analyses in this study. The first one was input Level 2.5, which means that input Level 3 was adopted for AC layers whereas input Level 2 was adopted for base and subgrade. The gradation, air voids, optimum binder content, performance grade of binder for AC layers were prepared at this level. The other one was input Level 1.5, which means that input Level 1 was used for AC layers and input Level 2 was used for base and subgrade. The dynamic moduli of asphalt mixtures and complex moduli of asphalt binders were prepared at Level 1.5. Currently, the level 1 input in MEPDG, i.e., coefficients of the generalized model for soil resilient modulus from the laboratory data, usually lead to death of MEPDG software. Communication with software developer (through Email) was conducted and no solutions were provided. Therefore, Level 2 inputs were adopted for the subgrade and base. The layer coefficient, California Bearing Ratio (CBR), and/or R-value for stone base, and CBR for subgrade were prepared at both levels.

4.3.4 Determination of Initial IRI

The initial IRI is one of the critical input parameters in the evaluation of the pavement roughness. MEPDG recommends 99.4cm/km as an initial IRI. PSI is a roughness index in the AASHTO 1993 design guide and has been used by TDOT for decades. For the convenience of communication with agencies that still use PSI as a roughness index in Tennessee and other states, PSI was used in this study to characterize pavement roughness. The relationship between PSI and IRI in Tennessee was used to calculate predicted PSI, as shown in Eq. (4.1) (McKenzie et al. 1982). Based on the data of the 19 pavement sections, the initial PSI in Tennessee was determined to be approximately 4.1

(Figure 4.3). The initial IRI in MEPDG software, back-calculated from Eq. (4.1), was determined to be 67.9 cm/km.

$$PSI = 5e^{-0.2925IRI} \quad (4.1)$$

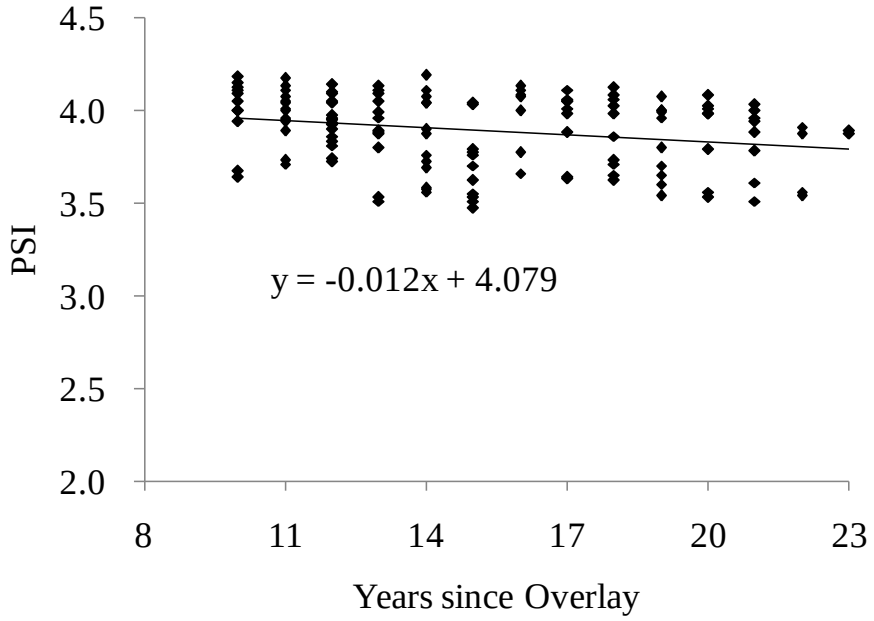

Figure 4.3 Development of roughness since overlay

4.4 Rutting Analysis

The MEPDG is able to predict rutting in every layer of pavement structure and subgrade. The collected rutting depths in PMS represent the rut depth for the total pavement structure and subgrade rather than each individual layer.

4.4.1 AC Overlay on PCC

Among selected pavement sections, six were initially PCC pavements. After overlays were constructed, rutting should accumulate only from the AC overlays since no rutting should occur in PCC slabs and layers beneath them. Therefore, the rutting from base and subgrade should be ignored in the comparison. Figure 4.4 shows the development of the measured and predicted rutting of one AC+PCC section. It can be seen from Figure 4.4 that at either input Level 2.5 or 1.5, total rutting predicted from the MEPDG was significantly higher than the measured one. However, the trend of the predicted AC rutting was found to be similar to that of the measured, indicating the MEPDG rutting prediction model could reasonably reflect rutting development. The predicted AC rutting at input Level 1.5 was slightly smaller than the one predicted at input Level 2.5.

Figure 4.5 compares the measured and predicted rutting at input Levels 2.5 and 1.5, respectively. It can be seen that the rutting predictions at input Level 1.5 were less scattered than those at input Level 2.5. Generally, input Level 2.5 over-predicted the rutting for the majority of the pavement sections. Input Level 1.5 gave a more accurate rutting prediction for these sections.

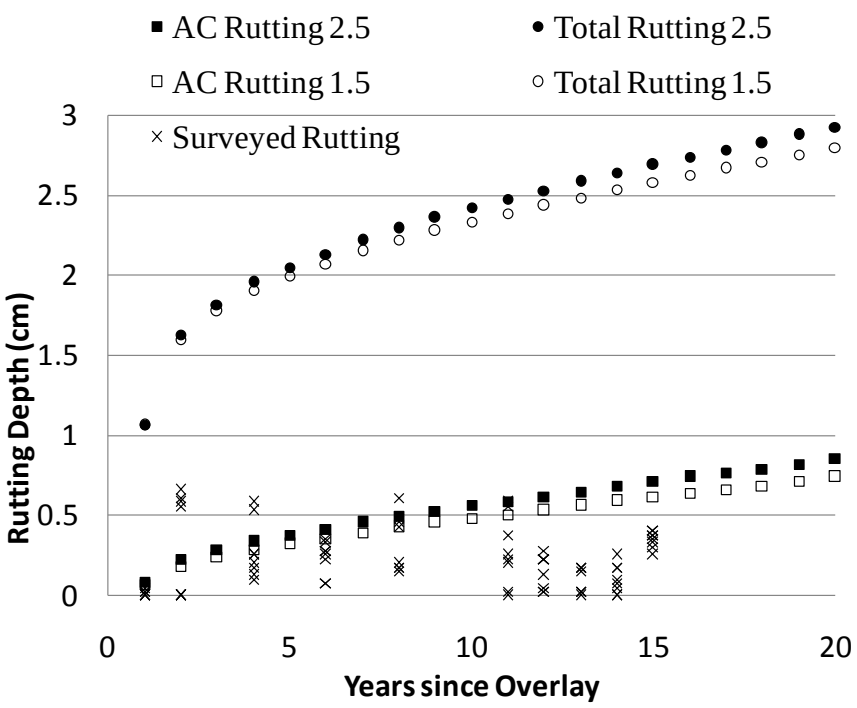

Figure 4.4 Development of measured and predicted rutting on an AC+PCC section

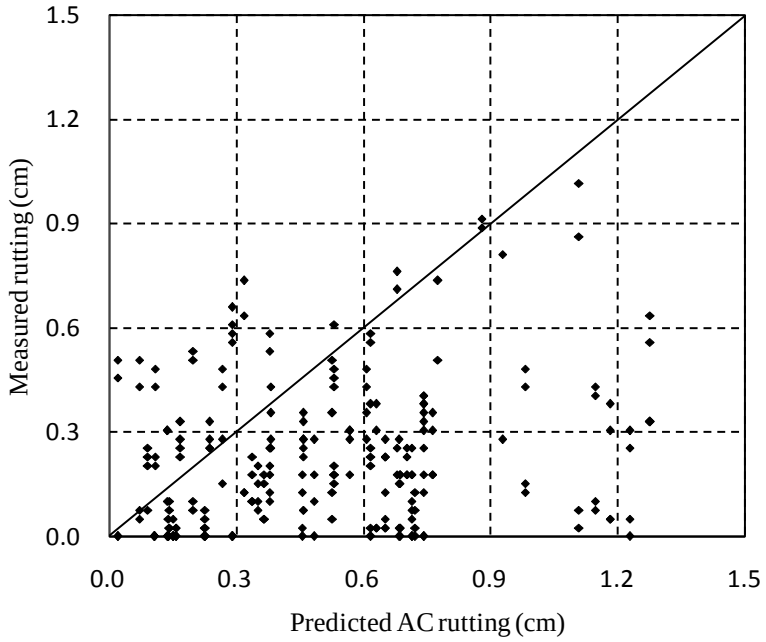

a) Under input **Level 2.5**

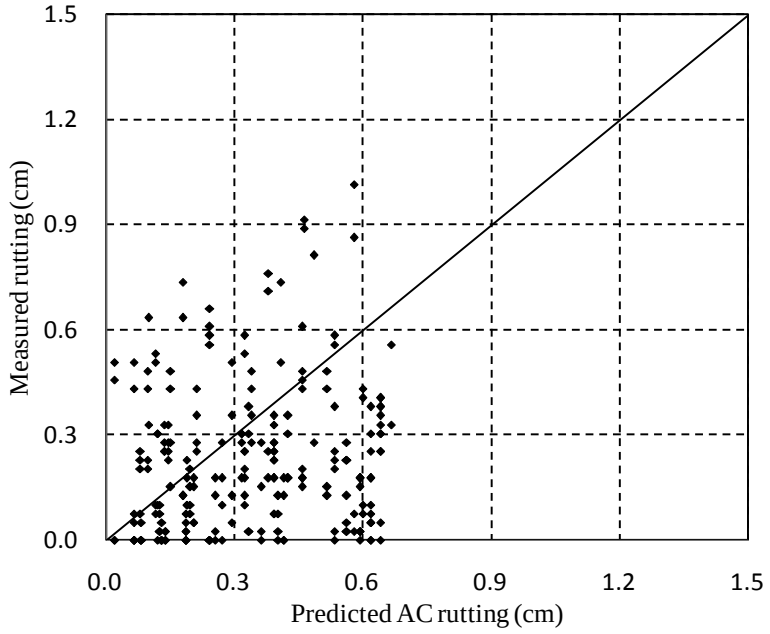

b) Under input **Level 1.5**

Figure 4.5 Comparison of measured and predicted rutting on AC+PCC sections a) under input Level 2.5 and b) under input Level 1.

4.4.2 AC Overlay on AC

Figure 4.6 shows the development of the measured and predicted total rutting of one AC+AC pavement section. The predicted total rutting for the AC+AC pavement section was significantly higher than the measured rutting. The predicted AC rutting at input Level 1.5 was slightly smaller than that at input Level 2.5.

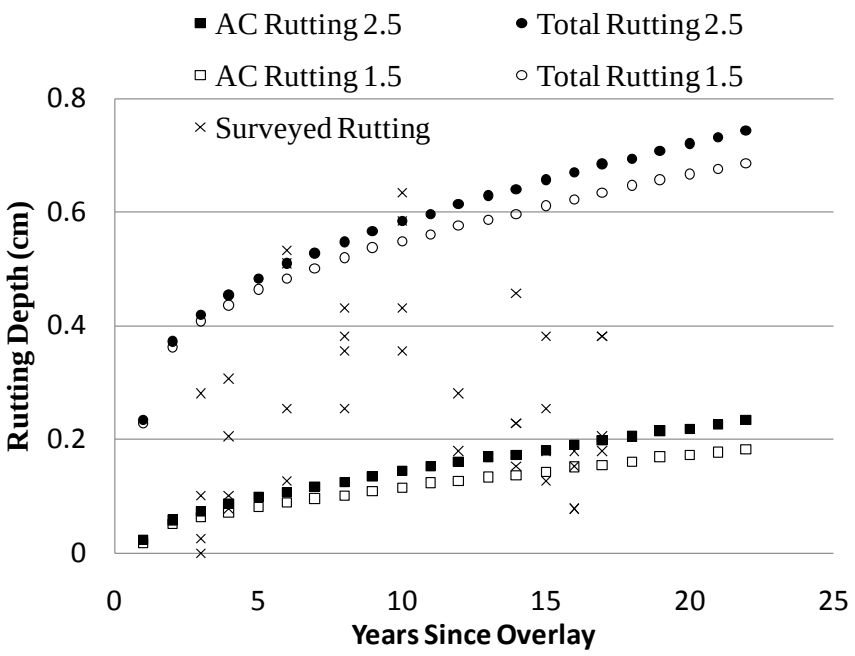

Figure 4.6 Development of measured versus predicted rutting on an AC+AC section

Figure 4.7 compares the measured and predicted total rutting of AC+AC pavement sections at input levels 2.5 and 1.5. It is observed that the majority of predicted rutting was higher than the measured one. Because the points in Figure 4.7 (b) were less scattered and closer to the line of equality than the points in Figure 4.7 (a), the MEPDG predicted rutting depths in AC layers at input Level 1.5 more reasonably than at input Level 2.5.

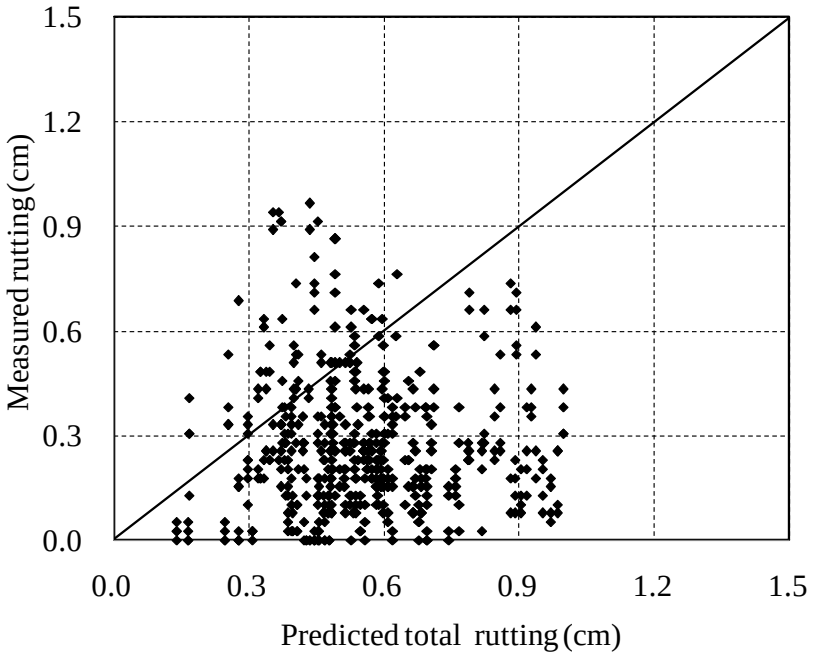

a) Under input Level **2.5**

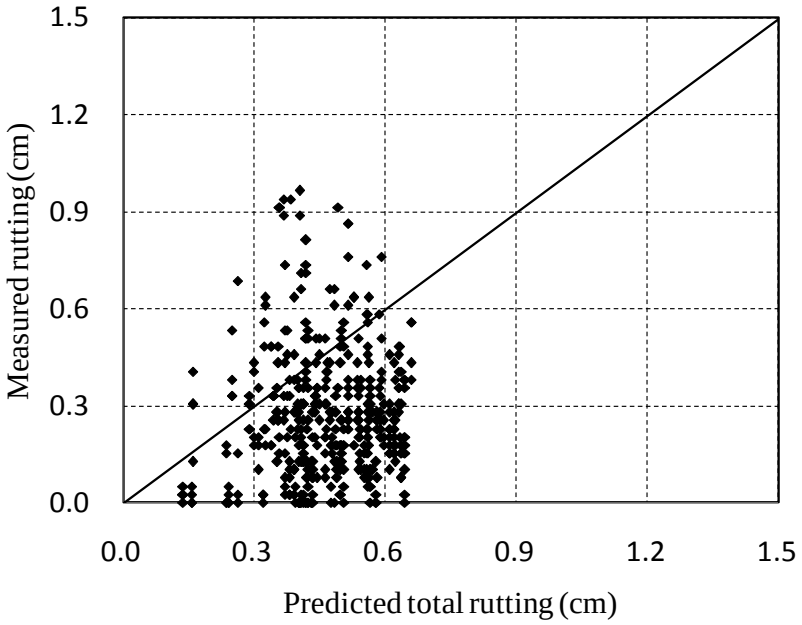

b) Under input Level **1.5**

Figure 4.7 Comparison of measured and predicted rutting on AC+AC sections a) under input Level 2.5 and b) under input Level 1.5

4.5 Roughness Analysis

Pavement roughness prediction in the MEPDG is dependent on rutting, fatigue cracking, thermal cracking, site factor, and other factors, as shown in Eq. (4.2) (NCHRP 1-37A 2004).

$$IRI = IRI_0 + C_1 * RD + C_2 * FC + C_3 * TC + C_4 * SF \quad (4.2)$$

Where:

IRI = International roughness Index, in/mile;

IRI_0 = Initial IRI after construction, in/mile;

RD = Rutting depth, in;

FC = Area of fatigue cracking, % of total lane area;

TC = Length of transverse cracking, ft/mile;

SF = Site Factor; and

C_1, C_2, C_3, C_4 = Local calibration coefficients.

The predicted IRI valued were converted into PSI values through Eq. (4.1) in order to comparison to the measured PSI values in PMS database. Figure 4.8 shows the predicted PSI at input Level 1.5 versus at input Level 2.5 for all selected pavement sections. It can be seen from Figure 4.8 that the predicted PSI at input Level 1.5 was almost the same as the one at input Level 2.5. In Eq. (4.2), rutting, fatigue cracking, and transverse cracking are all affected by the properties of AC layers. However, no longitudinal cracking or transverse cracking was predicted by the MEPDG at either input Level 2.5 or 1.5. Similar phenomena were found by Velasquez et al. (2009). The influence of AC layer properties

on alligator cracking was small. The same was true with rutting. For these concerns above, the predicted IRIs and PSIs at both input levels were very similar for the same pavement sections.

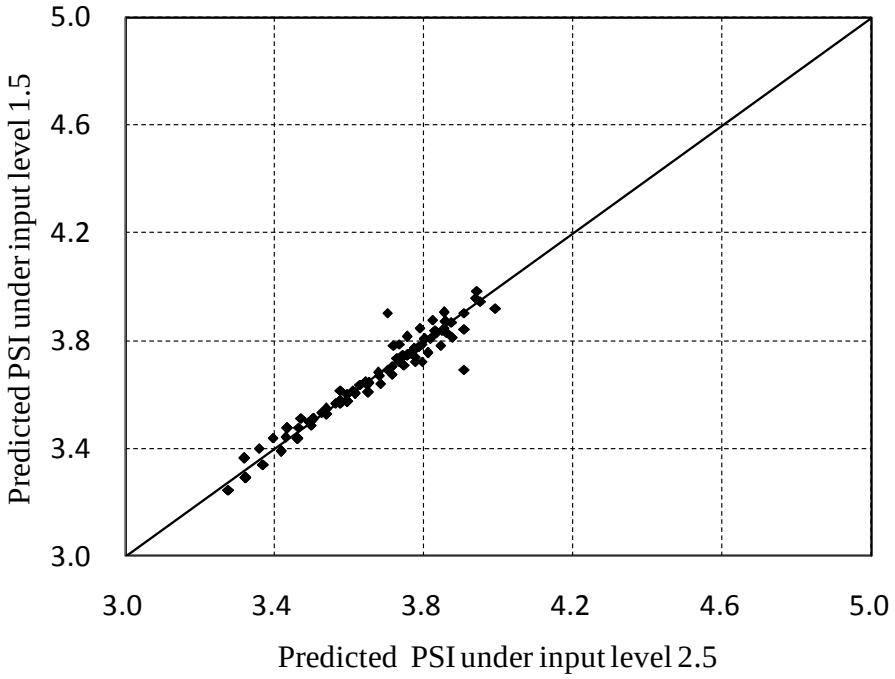

Figure 4.8 Predicted PSI (input Level 2.5 versus input Level 1.5)

Traffic level was found to affect PSI prediction significantly in this study. The analysis results of the pavement sections at different traffic levels, as presented in Table 4.1, are discussed below.

4.5.1 20-year ESALs 0-4.5million

The predicted and measured PSI at input Level 2.5 on the pavement sections with accumulated ESALs less than 4.5 million is shown in Figures 4.9 and 4.10. It is obvious

that the MEPDG under-predicted pavement roughness. It is noted from Figure 4.9 that the decreased rate of measured PSI was close to that of predicted PSI, which indicates that the MEPDG roughness prediction model is potentially applicable to Tennessee conditions. However, it is recommended that local coefficients be modified before application. More data are required for local calibration in Tennessee, which is beyond the objective of this paper.

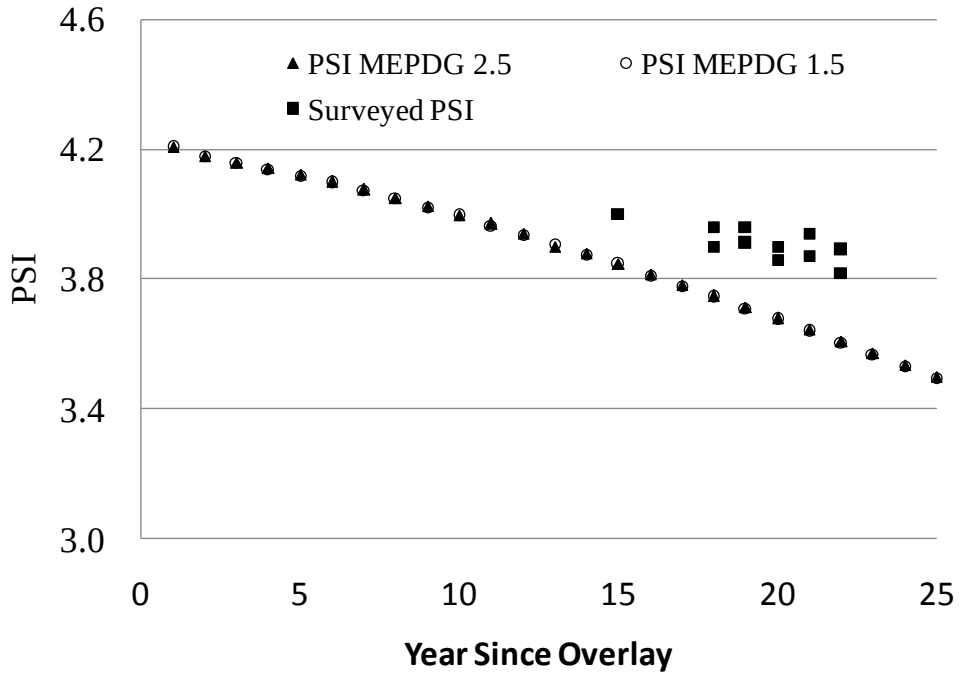

Figure 4.9 Development of measured PSI and predicted PSI on a section with ESAL 0-4.5million

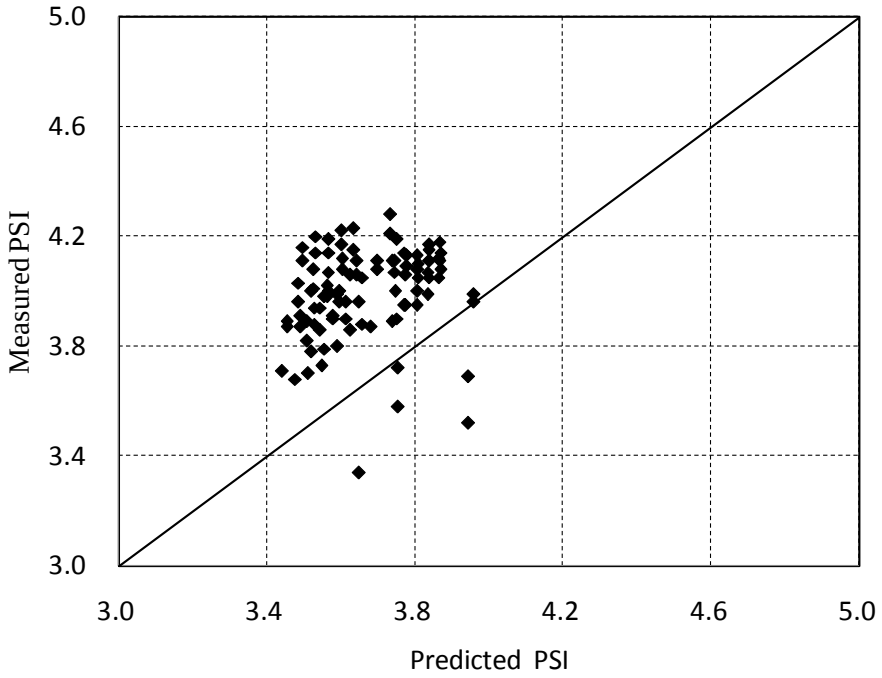

Figure 4.10 Measured PSI versus predicted PSI on all sections with ESAL 0-4.5million

4.5.2 20-year ESALs 4.5-9.0million

As shown in Figure 4.11, within this range of traffic, the predicted PSI agreed well with the measured data. However, Figure 4.12 shows the variation of the measured PSI was very high. It was observed that the predicted PSI in one section was very similar to other sections (Figure 4.13), though the measured PSIs between them were significantly different (Figure 4.14), indicating that MEPDG was not sensitive enough to reflect the variation of climate, traffic, and materials among sections on the prediction of PSI.

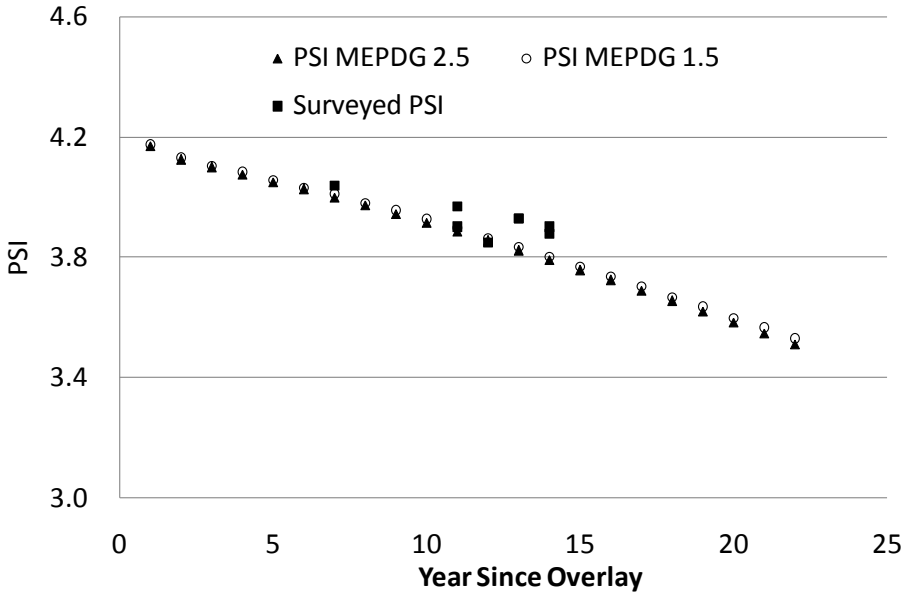

Figure 4.11 Development of measured PSI versus predicted PSI on a section with ESAL 4.5-9million

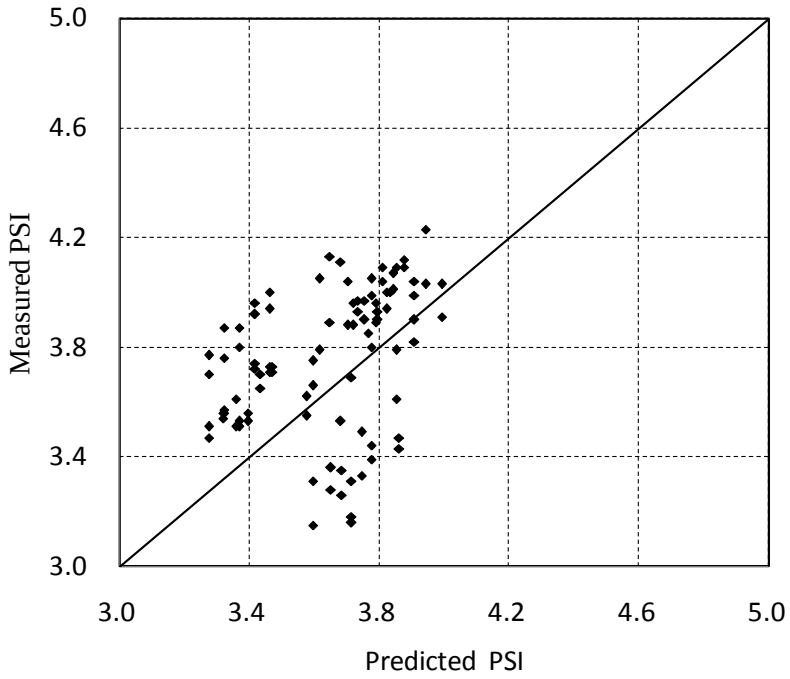

Figure 4.12 Measured PSI versus predicted PSI on all sections with ESAL 4.5-9million

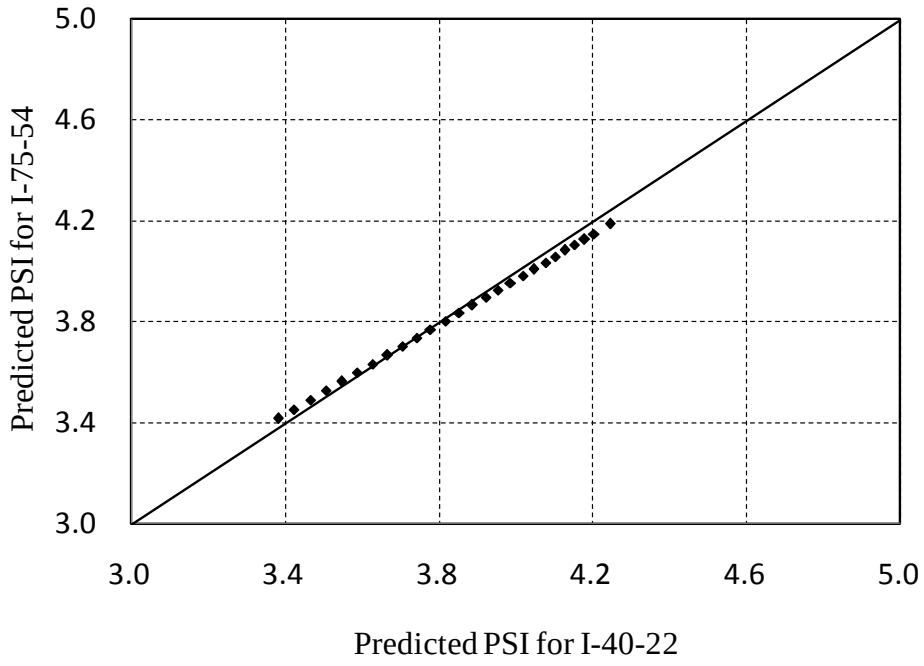

Figure 4.13 Predicted PSI (I-40-22 Dickson TN versus I-75-54 McMinn TN)

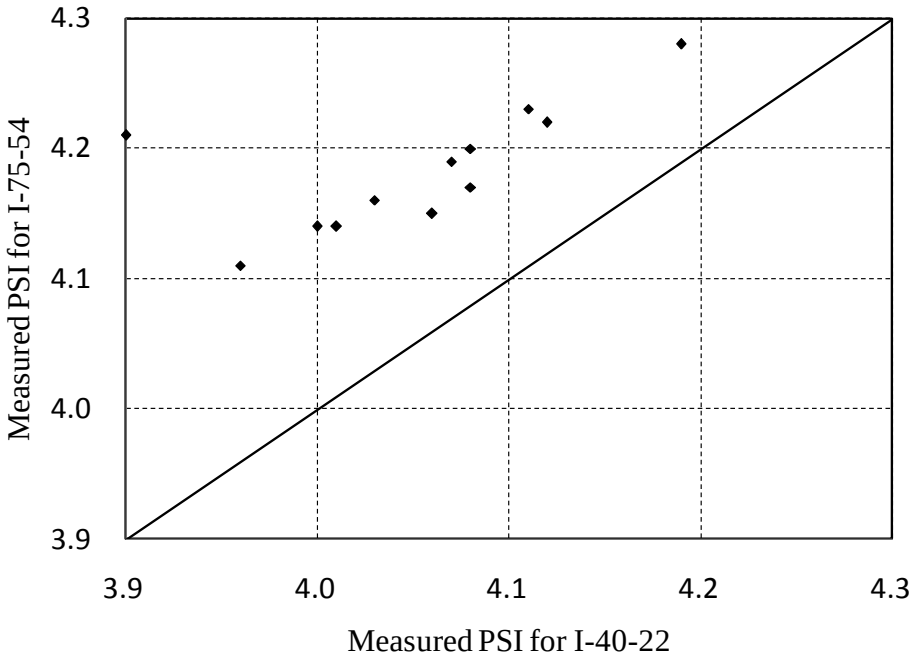

Figure 4.14 Measured PSI (I-40-22 Dickson TN versusI-75-54 McMinn TN)

4.6 Conclusions and Recommendations

Pavement performance of selected highway pavement sections in Tennessee was analyzed utilizing the latest MEPDG software and compared to the measurements acquired from PMS. The new pavement design procedure, instead of the overlay design procedure, of MEPDG was used to predict the pavement performance. Based on the analysis, the following conclusions and recommendations can be summarized:

- As an important input for the MEPDG, the initial IRI value for pavement performance prediction needs to be determined before calculation. The initial IRI value was determined to be 67.9 cm/km based on the PSI history data of the highway pavement sections used in this study.
- The MEPDG gave more satisfactory AC rutting predictions when input Level 1 was used for AC layers whereas it over-predicted AC rutting for input Level 3 on flexible pavements. The MEPDG also over-predicted rutting of base and subgrade for input Level 2.
- Traffic was found to be an important factor affecting predicted pavement roughness in MEPDG. The MEPDG design was relatively conservative for the design of low-traffic level highway pavements.
- MEPDG was not sensitive enough to reflect the variations in climate, traffic, and materials when predicting PSI for the some highway pavement sections in Tennessee.
- It is recommended that local calibration of MEPDG be performed for more accurate prediction models of pavement performance. To achieve this goal,

more data of material, traffic, and pavement distresses are required to meet the MEPDG requirements.

4.7 References

Aguiar-Moya, J., Banerjee, A. and Prozzi, J. (2010) "Sensitivity Analysis of the M-E PDG Using Measured Probability Distributions of Pavement Layer Thickness.", *Transportation Research Record, 0412*.

American Association of State Highway and Transportation Officials (AASHTO), (1993). "AASHTO Guide for Design of Pavement Structure." Washington, D.C.

Ayyala, D., Chehab,G. and Daniel, J. (2010). "Sensitivity of M-E PDG Level 2 and 3 Inputs using Statistical Analysis Techniques for New England States." *Transportation Research Record, 3694*.

Banerjee, A., Aguiar-Moya, J. and Prozzi, J. (2009) "Texas Experience using LTPP for Calibration of the MEPDG Permanent Deformation Models." *Transportation Research Record, 0829*.

Bayomy, F., El-Badawy, S., and Awed, A. (2012). "Implementation of the MEPDG for Flexible Pavements in Idaho." National Institute for Advanced Transportation Technology , University of Idaho.

Ceylan, H., Gopalakrishnan, K., Kim, S., Schwartz, C.W., and Li, R., (2013). "Global Sensitivity Analysis of Jointed Plain Concrete Pavement Mechanistic-Empirical Performance Predictions." *Transportation Research Record: Journal of the Transportation Research Board, No. 2690,* TRB, National Research Council, Washington, D.C.

Garcia, G. and Thompson, M. (2007). "HMA Dynamic Modulus Predictive Models - A Review. A Report of the findings of ICT-R39: Validation of Extended life HMA Design Concepts." Illinois Center for Transportation.

Johanneck, L., and Khazanovich, L. (2010). "A Comprehensive Evaluation of the Effect of Climate in MEPDG Predictions." *Transportation Research Record: Journal of the Transportation Research Board*, 2246, 45-55.

Kutay, M.E. and Jamrah A. (2013). "Preparation for Implementation of the Mechanistic-Empirical Pavement Design Guide in Michigan, Part 1: HMA Mixture Characterization." Final report to the Michigan Department of Transportation, Michigan State University.

Li, J., Pierce, L. and Uhlmeyer, J. (2010). "Use of the AASHTO 1993 Guide, MEPDG and Historical Performance to Update the WSDOT Pavement Design Catalog.", *Transportation Research Record, 2776*.

Li, J., Pierce, L., and Uhlmeyer, J. (2009). "Calibration of the Flexible Pavement Portion of the Mechanistic-Empirical Pavement Design Guide for the Washington State Department of Transportation." *Transportation Research Record, 2121, 73-83.*

Mallela, J., Glover, L. T., Darter, M. I., Quintus, H. V., Gotlif, A., Stanley, M. and Sadasivam, S. (2009). "Guidelines for Implementing NCHRP 1-37A M-E Design Procedures in Ohio." Applied Research Associates, Inc., ODOT, U.S.DOT, FHA.

McKenzie, D. W., Hudson, W. R. and Lee, C. E. (1982). "The Use of Road Profile Statistics for Maysmeter Calibration." Research Report 251-1, Center for Transportation Research, the University of Texas at Austin.

National Cooperative Highway Research Program (NCHRP) 1-37A, (2004). "Guide for the Mechanistic-Empirical Design for New and Rehabilitated Pavement Structures." Transportation Research Board, Washington, DC.

Oman, M. S. (2010). "MnROAD Traffic Characterization for the Mechanistic- Empirical Pavement Design Guide Using Weigh-in-Motion Data." *Transportation Research Record, 2903.*

Saxena, P., Tompkins D., Khazanovich, L. and Balbo, J. (2010). "Evaluation of Characterization and Performance Modeling of Cementitiously Stabilized Layers in the MEPDG." *Transportation Research Record: Journal of the Transportation Research Board*, 0550, 111-119.

Schwartz, C. W., and Carvalho, R. L. (2007a). "Implementation of the NCHRP 1-37A Design Guide, Volume 2: Evaluation of Mechanistic-Empirical Design Procedure." Final Report to Maryland State Highway Administration.

Schwartz C. W. and Carvalho, R. L. (2007b). "Implementation of the NCHRP 1-37A Design Guide, Volume 1: Summary of Findings and Implementation Plan." Final Report to Maryland State Highway Administration.

Schwartz, C.W., Li, R., Ceylan, H., Kim, S., and Gopalakrishnan, K. (2013) "Global Sensitivity Analysis of Mechanistic-Empirical Performance Predictions for Flexible Pavements." *Transportation Research Record: Journal of the Transportation Research Board, No. 1572*, TRB, National Research Council, Washington, D.C.

Souliman, M., Mamlouk, M., and El-Basyouny, M. (2010). "Calibration of the AASHTO MEPDG for Flexible Pavement for Arizona Conditions." *Transportation Research Record, 1817.*

Sunghwan, K., Ceylan, H., Gopalakrishnan, K., Smadi, O., Brakke, C. and Behnami, F. (2010). "Verification of Mechanistic-Empirical Pavement Design Guide (MEPDG) Performance Predictions Using Pavement Management Information System (PMIS)." *Transportation Research Record, 2395*.

Velasquez, R., Hoegh, K., Yut, I., Funk, N., Cochran, G., Marasteanu, M. and Khazanovich, L. (2009). "Implementation of the MEPDG for New and Rehabilitated Pavement Structures for Design of Concrete and Asphalt Paveemnts in Minnesota." Final Report to Minnesota Department of Transportation.

Witczak, M.W., Zapata, C. E. and Houston, W. N. (2006). "Models Incorporated into the Current Enhanced Integrated Climatic Model: NCHRP 9-23 Project Findings and Additional Changes after Version 0.7." Final Report, Project NCHRP 1-40D.

Zapata, C. E. (2009). "Considerations of Climate in the New AASHTO Mechanistic Empirical-Pavement Design Guide". *Transportation Research Record, 2254*.

PART 5 CALIBRATION ON MEPDG RUTTING TRANSFER FUNCTIONS USING PMS DATABASE IN TENNESSEE

5.1 Abstract

The rutting is a main type of distresses on flexible pavements. It can cause vehicle hydroplaning, especially when water exists. The deterioration of pavements could be accelerated due to the moisture in the ruts. The new MEPDG defined rutting as one of primary distresses on flexible pavements. Efforts have been taken to develop rutting models based on LTPP database, according to NCHRP 1-37A and NCHRP 1-40D. The national-calibrated models were further calibrated locally in states based on PMS or LTPP database. However, the local calibrations on the overlay pavements have not been well addressed. In Tennessee, almost all the highways were overlaid with asphalt layers in recent decades. In this paper, two main types of pavements, asphalt overlays on Portland cement concrete pavements and asphalt overlays on asphalt pavements were selected to calibrate the rutting models. The rutting transfer function for asphalt layers was discussed from a view of mechanisms. Separated local calibrations are recommended for the two pavement structures since strain states were found to vary significantly. Significant differences were observed between the measured rutting and the predicted rutting with the national calibrated rutting transfer functions. It was also found that the national calibrated rutting transfer function under predicted rutting of asphalt overlay on PCC pavements, especially for the pavements with low traffic, while over predicted the total rutting on the asphalt pavements. Local calibrations were conducted and better agreements were reached between the predicted and the measured rutting. The measured data in PMS are very scattered, therefore it is recommended that careful data mining should be conducted prior to use.

5.2 Introduction

5.2.1 Research Background

Since released under NCHRP 1-37A (Applied Research Associates, 2004) and 1-40D (Applied Research Associates, 2009), the new MEPDG has been seen as a new trend in pavement design and analysis and appointed as the substitution of AASHTO 1993 design guide (1993) in future. It has significantly improved the ability to model and simulate the effects of traffic, material properties, and climate on pavement damage, distress, and smoothness. The long term pavement performance (LTPP) database in North America was initially utilized as a resource for developing national transfer functions of distresses. Although the transfer functions were national calibrated based on LTPP database, local calibrations were strongly recommended due to the variation of traffic, environment, pavement structure and materials through states.

Tremendous efforts have to be put onto the local calibration, as shown in Figure 1.1. Based on the sensitivity analysis, critical properties of materials need to be collected in the laboratory. Then pavement sections from the LTPP database or local PMS databases are selected. And then measured pavement distresses such as rutting, cracking, and international roughness index were used to calibrate the transfer functions in MEPDG. In the final, extra pavement sections should be used to validate the local calibrated transfer functions.

For those agencies who want to utilize local PMS database to calibrate MEPDG, comparison between data in LTPP and in PMS should be conducted to see if differences exist. Kang (2007) prepared a regional pavement performance database for a Midwest implementation of the MEPDG from Michigan, Ohio, Iowa and Wisconsin State transportation agencies. They suggested a data cleaning process be conducted before applied to MEPDG calibration. They also found that the default national calibration values do not predict the distresses observed in the Midwest. Mamlouk and Zapata (2010) found the differences between the Arizona Department of Transportation (ADOT) PMS data and the LTPP database used in the original development and national calibration of the MEPDG distress models including rut measurements, asphalt cracking, IRI, and all layer backcalculated moduli found from NDT measurements done by ADOT and those of the LTPP.

Khazanovich, et al. (2013) investigated the MEPDG rutting model and the CalME procedure and introduced a procedure incorporating the CalME rutting model into the MEPDG framework for rutting in AC-PCC design and analysis. Jannat, et al. (2013) found DARWin-ME overpredicted the total rutting in asphalt pavements and they utilized clustering analysis based on functional class and geographical zone to improve the precision of the locally calibrated models. Glover and Mallela (2009) utilized LTPP projects in central Ohio to firstly compare the predicted pavement performance with the measured ones and found that hot mix asphalt (HMA) rutting on new flexible pavements and IRI models for both new flexible and rigid pavements need to be calibrated for Ohio conditions. Then the rutting models for the asphalt concrete layers, granular base, and the

subgrade were simultaneously calibrated through a simple linear regression. Fair agreement was reached between predicted rutting and the measured data and further comprehensive recalibration was recommended through plenty pavement sections in Ohio. Velasquez, et al. (2009) evaluated MEPDG rutting model with the measured rutting from Minnesota Road Research Project (MnROAD) and offered a novel approach to calibrate the rutting model: deducting the first month's rutting from the rutting of base. Li et al. (2009, 2010) calibrated transfer functions for AC fatigue cracking, longitudinal cracking, alligator cracking, AC rutting, and subgrade rutting based on data in Washington State Pavement Management System (WSPMS). They established a pavement thickness design catalog for the Washington state Department of Transportation (DOT) based on the calibration of MEPDG software for their state condition. Darter, et al. (2009) calibrated MEPDG for local conditions in Utah State. They claimed that the nationally calibrated rutting model predicted rutting adequately for older pavements constructed using viscosity binder grade (AC-10 and AC-20) and predicted rutting poorly on the new HMA pavements using the Superpave Binders. Therefore, they calibrated the rutting model with the older pavements constructed using viscosity binder grade and offered the locally calibrated coefficients for HMA, Base, and subgrade, respectively. Mallela, et al. (2009) summarized the flexible pavement local calibration value results of the MEPDG from NCHRP project 9-30 (2003), 1-40B (2013), and Montana DOT studies. Kim et al. (2007) conducted local calibration on rutting models for North Carolina. Schram and Abdelrahman (2006) conducted local calibration work on MEPDG in the project-level rather than a net-work level for Jointed Plain Concrete Pavement (JPCP) and HMA overlays of PCC pavements. Results indicate that

project-level calibrations reduced default model prediction error by nearly twice that of network-level calibration.

The verification runs in Part 4 with national-default calibration coefficients indicates differences between predicted rutting in MEPDG and measured rutting in PMS in Tennessee. This suggests an extensive local calibration is needed. Furthermore, asphalt overlay, as a most used type of maintenance, has not been well addressed as a subject of local calibration on rutting transfer functions.

5.2.2 Transfer Functions for Rutting

The permanent deformation is a main distress in the flexible pavements. A rut in the surface is the sum of permanent deformation in all or some layers and subgrade. In the MEPDG Version 1.1, the total rut is the sum of ruts from HMA layer, base, and subgrade, as shown in Equ. (5.1).

$$\mathrm{Rut_{tol}} = \mathrm{Rut_{AC}} + \mathrm{Rut_{Base}} + \mathrm{Rut_{SG}} \tag{5.1}$$

where $\mathrm{Rut_{tol}}$ presents the predicted total rutting, $\mathrm{Rut_{AC}}$, $\mathrm{Rut_{Base}}$, and $\mathrm{Rut_{SG}}$ present the rutting from the asphalt layer, base, and subgrade, respectively.

The MEPDG version 1.1 field-calibrated rutting transfer function is of the form:

$$\Delta_{pac} = \varepsilon_{pac} h_{ac} = \beta_{r1} k_z \varepsilon_{rac} 10^{k_1} T^{k_2 \beta_{r2}} n^{k_3 \beta_{r3}} h_{ac} \tag{5.2}$$

where,

Δ_{pac}=Accumulated permanent or plastic vertical deformation in the HMA layer/sublayer, inches;

ε_{pac}=Permanent or plastic axial strain in the HMA layer/sublayer, inches/inches;

ε_{rac}=resilient axial strain in the HMA layer/sublayer, inches/inches;

h_{ac}=Thichness of the HMA layer/sublayer, inches;

n =Number of axle load repetitions;

T=Mix or pavement temperature, ^{o}F;

k_z=Depth confinement factor, inches

$k_{1,2,3}$ =Global filed calibration parameters (from the NCHRP 1-40D recalibration; $k_1 = -3.35412, k_2 = 1.5606, k_3 = 0.4791$).

$\beta_{r1,2,3}$ =Local or mixture field calibration constants; for the global calibration, these constants were all set to 1.0.

$$k_z = (C_1 + C_2 D) \times 0.328196^{D} \quad (5.3)$$

$$C_1 = -0.1039(H_{ac})^2 + 2.4868 H_{ac} - 17.342 \quad (5.4)$$

$$C_2 = 00172(H_{ac})^2 - 1.7331 H_{ac} + 27.428 \quad (5.5)$$

where,

D=Depth below the surface, inches;

H_{ac}=Total HMA thickness, inches.

It is worth to mention that only the asphalt surface layer is divided into two sublayers: first 0.5 inches and the remains. No layers under the asphalt surface layer are divided during the calculation.

The rutting transfer function for the unbound pavement layers and the subgrade is shown in Equ. (5.6).

$$\delta_a(N) = \beta_{s1} k_1 \varepsilon_v h_{soil} (\varepsilon_0 / \varepsilon_r) e^{-(\frac{\rho}{n})^{\beta}} \quad (5.6)$$

where,

$\delta_a(N)$=Permanent or plastic deformation for the layer/sublayer, inches;

n= Number of axle load applications;

ε_0 =Intercept determined from laboratory repeated load permanent deformation tests, inches/inches;

ε_r=Resilient strain imposed in laboratory test to obtain material properties ε_0, β, and ρ, inches/inches;

h_{soil}=Thickness of the unbound layer/sublayer, inches;

k_1=Global calibration coefficients; $k_1 = 2.03$ for granular materials and 1.35 for fine-grained materials;

β_{s1}=Local calibration constant for the rutting in the unbound layers.

$$\log\beta = -0.61119 - 0.017638(W_e) \quad (5.7)$$

$$\rho = 10^9 \left(\frac{C_0}{1-(10^9)^{\beta}}\right)^{\frac{1}{\beta}} \quad (5.8)$$

$$C_0 = \mathrm{Ln}\left(\frac{a_1 M_r^{b1}}{a_9 M_r^{b9}}\right) \quad (5.9)$$

where,

W_e=water content, percent;

M_r=resilient modulus of the unbound layer and sublayer, psi;

$a_{1,9}$=regression constants; $a_1 = 0.15, a_9 = 20.0$;

$b_{1,9}$=regression constants, $b_1 = 0.0, b_9 = 0.0$.

5.2.3 Problem Statement

Currently, the pavement rehabilitation occupies the largest part of TDOT's activities on pavement. The pavement performance data in Tennessee started from 1993. Almost all data are for reconstruction and rehabilitation activities. Therefore, for Tennessee conditions, the local calibration should be mainly on overlay pavements, including asphalt overlays on PCC pavements and on asphalt pavements.

For asphalt layers, no matter on new flexible pavements or on asphalt overlays on rigid or flexible pavements, the same rutting transfer function is adopted, which is not well explained in research reports such as NCHRP 1-37A and NCHRP 1-40D or by other studies. The stress/strain states in these different pavement structures should be investigated to see whether these different pavement structures can be calibrated in the same group.

The local calibration on the rutting transfer functions in flexible pavements usually conducted a linear regression on the total measured rutting depth data from predicted rutting depth from sublayers, which failed to indicate the actual part of rutting depth contributed by asphalt layer. Without this information of asphalt layer, the limit on the asphalt layer rutting depth could not be claimed as a firm criterion for asphalt pavement design.

5.3 Objective and Scope

The objective of this study is to fulfill the calibration on rutting transfer function in MEPDG for local conditions in Tennessee.

Two types of pavements were selected from PMS database, asphalt overlays on PCC pavements and on asphalt pavements. Firstly, the mechanical behaviors of the two types of pavements were analyzed under the elastic layer system theory. The results will be used to decide whether these two pavement structures can be calibrated in the same group. Then local calibrations were conducted on the two types of pavements. Finally, the proposed calibrated rutting transfer functions were validated.

5.4 Investigation on the Vertical Compressive Strain in Asphalt Layers

As mentioned above, the same transfer function (Eq. (5.2)) is utilized in asphalt layers no matter for AC overlay on PCC pavements or for asphalt layers in the flexible pavements.

According to the rutting transfer function of asphalt layers, the vertical compressive plastic strain in the asphalt layers is directly affected by the vertical compressive elastic strain. Therefore, it is necessary to investigate the compressive strain in the asphalt layers in the two pavement structures. Two typical pavement structures were selected in Tennessee. The details were shown in Figure 5.1. The thickness of asphalt surface layers varies from 2in. to 8 in.

Assume the two pavement structures share the same climate and local materials. A multiple layered software WESLEA 3.0 based on elastic layered theory was utilized to analyze the strain trends underneath the contact area center of the standard wheel load (100psi, 5000lb). It should be mentioned that the MEPDG uses the maximum vertical compressive strain to calculate the rutting depth, which does not necessarily locate underneath the tire, whereas depends on many factors, such as load magnitude, tire pressure, pavement structure, and so on.

The vertical compressive strains in the asphalt surface layers of the two pavement structures were shown in Figure 5.2. It can be seen that the development of vertical compressive stain in the surface asphalt layers of flexible pavements is quite different with the one of the asphalt overlay on PCC pavements, especially when the asphalt layers are relatively thinner. The development trends of the vertical compressive strain in the thick surface asphalt layers are similar in the two pavement structures, which are still very different within the first 2 inches. Since the strain states in the surface asphalt layers of the two pavement structures are varied from each other, the rutting development trends

will not be similar. Therefore, the local calibration should be conducted on each pavement structure individually for the rutting transfer function of the asphalt layer. In addition, except the very thin asphalt layers, the maximum compressive strains locate around 2in. down to the surface, from which the main part of rutting accumulates (White, et al. 2002). However, the current dividing method in calculation of rutting does not describe the main contribution of this depth. It is recommended that the MEPDG increase the number of sublayers in the asphalt layer, especially in the depth from 1in. to 3in.

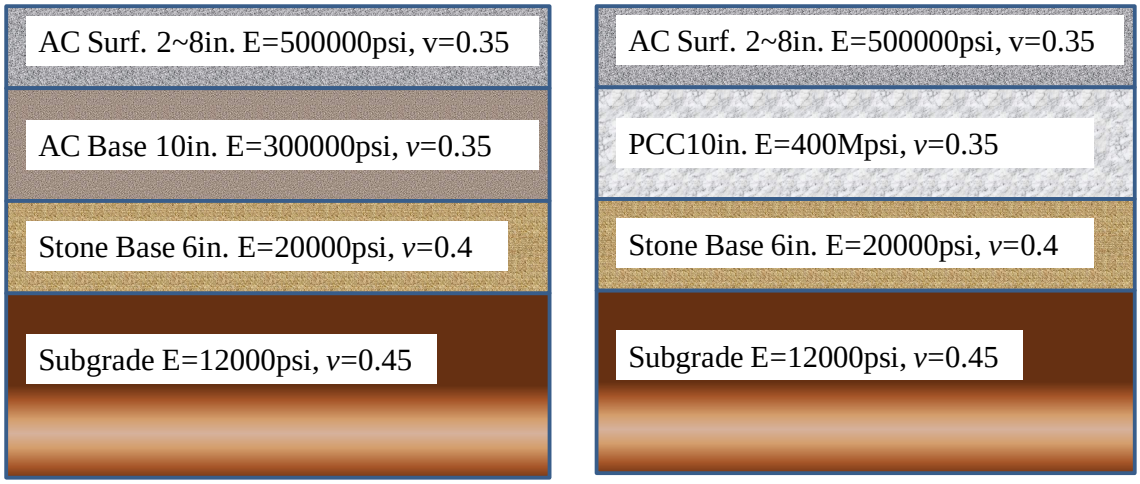

a) Asphalt Pavement b) Asphalt Overlay on PCC Pavement

Figure 5.1 Two typical pavement structures in Tennessee

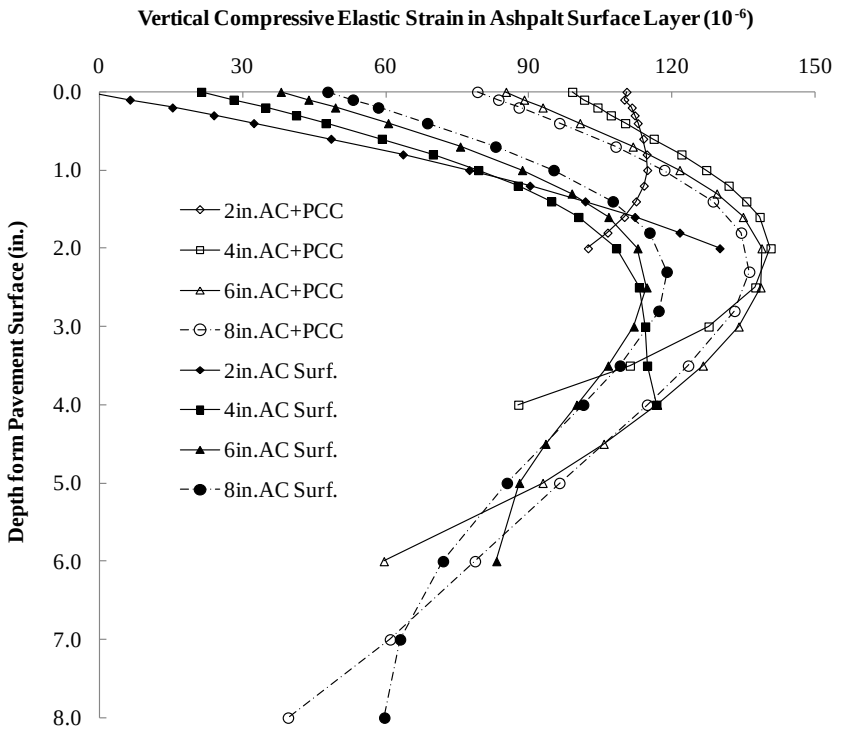

Figure 5.2 Vertical elastic compressive strain in the asphalt layer underneath the center of the tire-pavement contact area

5.5 Approach on Local Calibration

A simple comparison of the measured and predicted rutting was made by categorizing the results into groups to determine if the measured data stay in the same group with the predicted data and to recognize outliers in the measured data. Several groups may be made and conducted on local calibration if necessary. Then Microsoft Solver was used to eliminate the bias (to minimized the standard error of estimate (SEE)) between the measured and the predicted rutting values. The proposed local calibration was validated by extra pavement sections.

5.6 Calibration on Rutting Transfer Function for Asphalt Overlay on PCC Pavements

Due to the small amount of PCC pavements in Tennessee, there were totally six sections of asphalt overlays on PCC pavements collected from PMS database, as shown in Figure 5.3. As described in Chapter 4, information including pavement structures and materials, traffic, and measured rutting data were collected from PMS. The climate data for the selected sections were chosen as the same way in the Chapter 4, as well as the AADTT information. The detailed information of pavement sections was listed in Table 5.1.

For the asphalt overlays, level 1 inputs were used, including the dynamic modulus of asphalt mixtures and complex modulus of asphalt binders collected from laboratory in University of Tennessee. And for the PCC slab and the underneath base/subgrade, level 3 inputs, i.e., national defaulted values, were used including layer coefficients, California Bearing Ratio (CBR), and/or R-value for base, and CBR for subgrade.

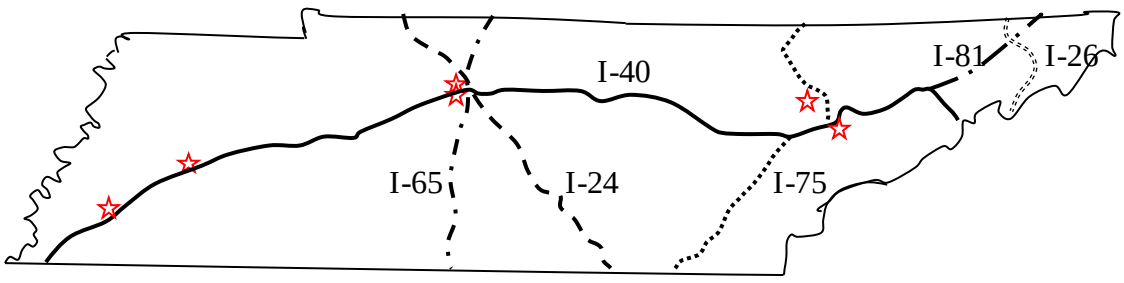

Figure 5.3 Pavement sections of asphalt overlays on PCC pavements

Table 5.1 AC overlay on PCC pavements Sections for local calibration on rutting model

Highway	County	Mileage	AADTT	Asphalt Overlay (cm)	Concrete Slab (cm)	Stone Base (cm)
I_40	Madison	7.4-12.4	710	3.2Asphalt Surface +15.2Asphalt Base	22.9	15.2
I_40	Davidson	25.4-28.4	1940	8.9Asphalt Surface+16.5Asphalt Base	25.4	15.2CTB
I_65	Davidson	0.4-3.5	2350	13.3Asphalt Surface+7.6Asphalt Base	22.9	22.9
I_65	Davidson	20.9-22.9	1120	7Asphalt Surface+14Asphalt Base	22.9	22.9
I_75	Knoxville	8.8-13.7	590	7.6Asphalt Surface +26.7Asphalt Base	22.9	41.9
I_40	Haywood	2.9-10.1	420	7.6Asphalt Surface+8.9Asphalt Base+38Concrete	22.9	15.2CTB

Note: CTB presents the cement treated base.

It should be mentioned that there is no rutting on PCC slabs and the layers underneath. Therefore, for the asphalt overlay on PCC pavements, the local calibration is actually focusing on the comparison between predicted rutting of asphalt overlay and the measured rutting on the pavement surface. Figure 5.4 shows the comparison between the measured rutting and the predicted rutting of asphalt overlay based on the national calibrated rutting transfer function. It indicates for the pavement sections with high traffic volume, i.e., 1000-2500 AADTT, the national calibrated model gave a fair result on rutting prediction. And for the low traffic volume i.e., 0-1000 AADTT, the national

calibrated model under predicted the rutting of asphalt overlay. Therefore, two groups were divided according to the traffic volume, as shown in Figure 5.4.

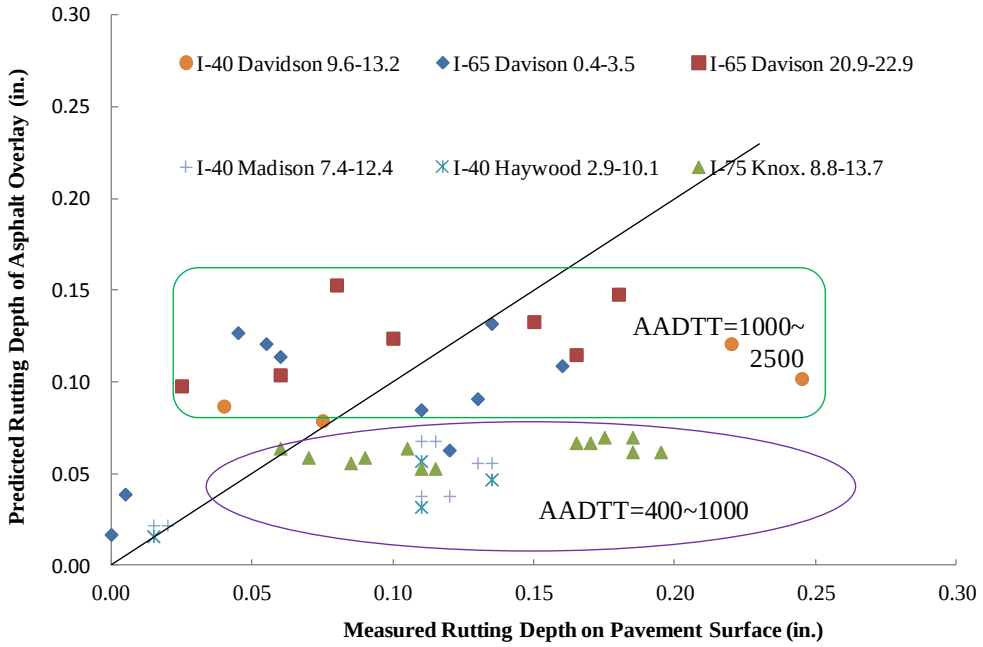

Figure 5.4 Measured rutting versus predicted rutting of asphalt overlay in the national calibrated model on PCC pavements

Assume the local coefficients β_{r2} and β_{r3} are the same with national default value, 1.0. Microsoft Solver was used to minimize the SEE between the measured and the predicted rutting values through changing β_{r1}. For the group with high traffic volume, the local coefficient β_{r1} was determined as 1.0. The comparison between the measured and predicted rutting values was shown in Figure 5.5. It indicates that the national calibrated rutting transfer function provides sound prediction on the asphalt overlay on PCC pavements with heavy volume traffic and there is no local calibration needed on this

group. However, for the group with low traffic volume, the national calibrated model predicted the rutting depth values poorly comparing to the measured ones, as shown in Figure 5.6. With the Microsoft Excel Solver, the β_{r1}.was determined as 2.20, which could minimize the SEE from 0.08in. to 0.04in.

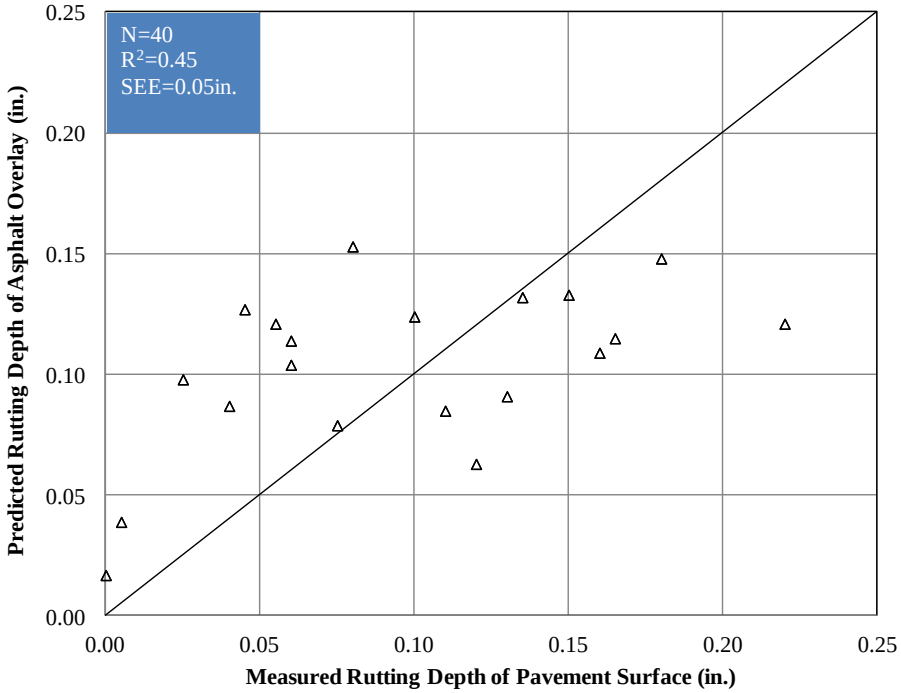

Figure 5.5 Comparison of measured and predicted rutting of the asphalt overlay on PCC pavements with heavy traffic volume

Due to the source limit, the validation on the rutting transfer function in this part was not conducted. This task would be done when similar pavement sections are available in the PMS database.

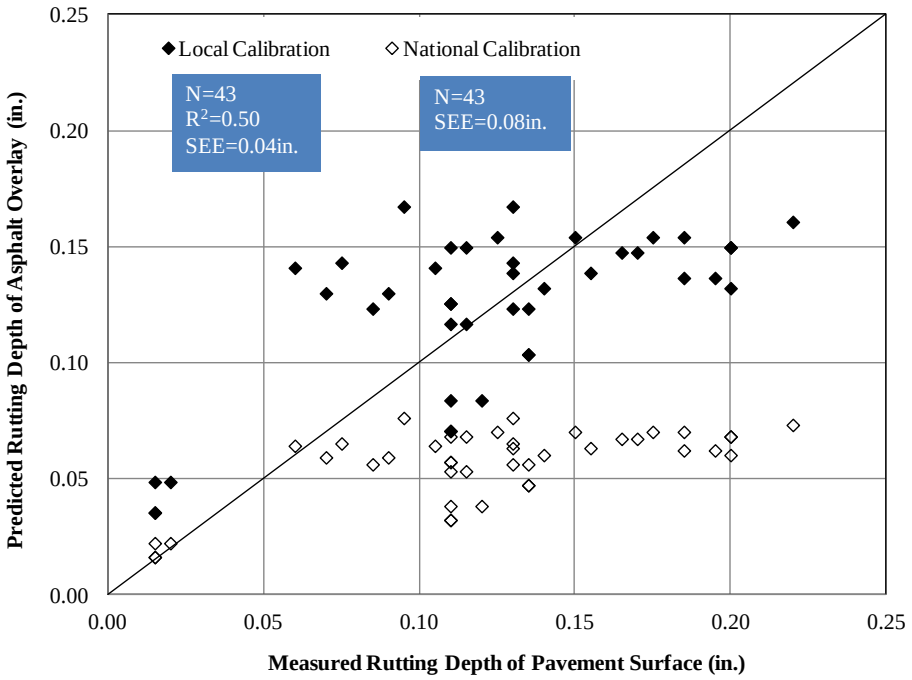

Figure 5.6 Comparison of measured and predicted rutting of the asphalt overlay on PCC pavements with low traffic volume

5.7 Calibration on Rutting Transfer Function for Asphalt Overlay on Asphalt Pavements

Since the asphalt overlay on asphalt pavements has not been nationally calibrated, the asphalt overlay pavement sections in this part were assumed as new asphalt pavements. All the selected overlays were thicker than 4 inches. Actually, the asphalt overlay pavements and the new asphalt pavements use the same rutting transfer functions in the MEPDG. There were totally 14 pavement sections were selected in this part, as shown in

Figure 5.7. The detailed information was listed in Table 5.2, including pavement structure, materials, and traffic.

Two sections, I-40 in Cumberland County and I-75 in Anderson County, were randomly selected to be left for the validation. The rest 12 pavement sections were used in the local calibration procedure.

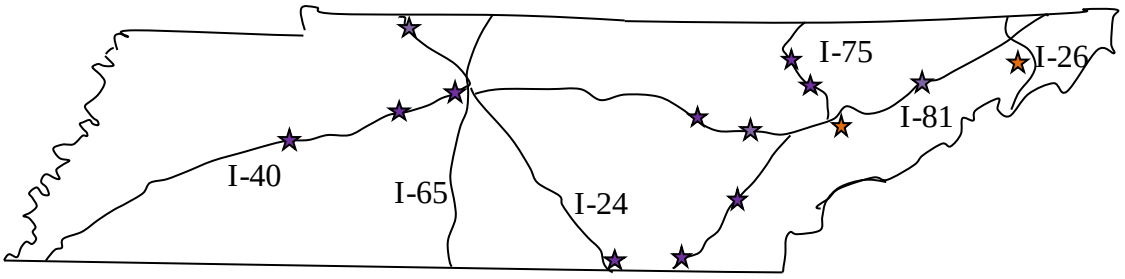

Figure 5.7 Asphalt pavement sections for local calibration on rutting models

Table 5.2 New asphalt pavements and asphalt overlay on asphalt pavements for local calibration on rutting model

Highway	County	Milestone	AADTT	Overlay (cm)	Existing AC/PCC (cm)	Crushed Stone (cm)
I_40	Knoxville	0-6.9	250	--	31.1Asphalt Surface+8.9Asphalt Base	20.3
SR_36	Washington	14.4-15.1	380	--	17.8Asphalt Surface+8.9Asphalt Base	20.3
I_81	Greene	6.0-12.3	520	13.3Asphalt Surface	5.7Asphalt Surface+26.7Asphalt Base	7.6
I_40	Roane	15.7-22.9	600	3.2GrD+6.4GrB+7.6GrA	18.4Asphalt Surface+17.8Asphalt Base	25.4
I_40	Benton	0-8	750	7.6Asphalt Surface+7.6Asphalt Base	25.4Asphalt Base	20.3
I_75	Campell	27-30.4	750	7.6Asphalt Surface +15.2 Asphalt Base	25.4Asphalt Base	20.3
I_40	Dickson	9.1-17.8	820	8.3Asphalt Surface +27.9Asphalt Base	17.8Asphalt Base	20.3
I_75	McMinn	10.9-13.4	870	11.4Asphalt Surface	5.7Asphalt Surface+17.8Asphalt Base	20.3
I_40	Cumberland	6.4-13.5	950	3.2Asphalt Surface +7.6Asphalt Base	6.4Asphalt Surface+31.8Asphalt Base	20.3
I_40	Davidson	0-4.69	1100	13.3Asphalt Surface	Milled Asphalt Surface off	35.6
I_75	Anderson	8.3-10.2	1150	8.3Asphalt Surface +10.2Asphalt Base	17.8Asphalt Base	20.3
I_24	Montgomery	11.7-17.2	1370	3.2Asphalt Surface +12.1Asphalt Base	19.7Asphalt Surface+8.9Asphalt Base	12.7
I_24	Marion	1.2-6.3	820	3.2Asphalt Surface+15.2Asphalt Base	4.4Asphalt Surface+8.9Asphalt Base	20.3
I_75	Hamilton	8.5-15.6	1300	6.4Asphalt Surface+6.4Asphalt Base	7.0Asphalt Surface+10.8Asphalt Base	35.6

Figure 5.8 provides the comparison of the measured rutting and the predicted rutting from national calibrated model. It indicates the national calibrated rutting transfer functions over predict total rutting. Similar conclusions have been claimed by researchers (Velasquez, et al., 2009, Zhou, et al., 2012). As analyzed above, significant variance exists between the strain states in asphalt layers on the two pavement structures, i.e., the asphalt overlay on PCC pavements and flexible pavements. Therefore, the local calibrated coefficients obtained on asphalt overlay on PCC pavements could not be utilized in the flexible pavements. The Microsoft Excel Solver was utilized to minimize SEE and the local coefficients β_{r1}, β_{BS}, and β_{SG} were reaches as 1.33, 0.12, and 0.68, respectively. These local coefficients made the SEE decrease from 0.08in. (national calibration) to 0.05in. It can be seen that the local calibrated rutting transfer functions conduct better prediction than the national calibrated ones. The scatter of data is due to the measuring error of the field rutting depth.

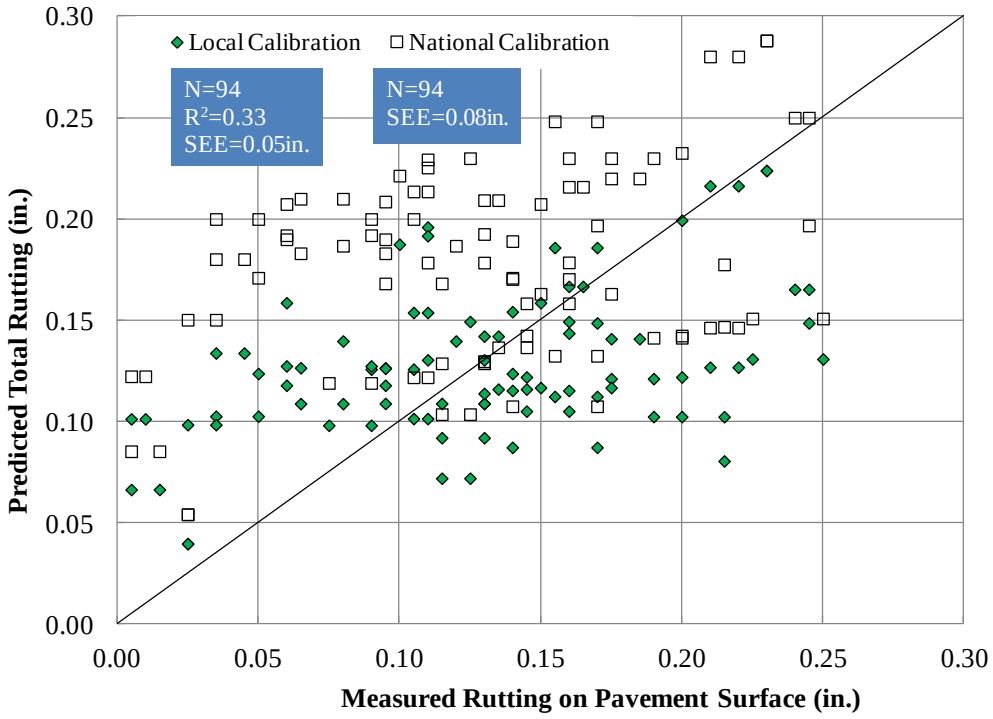

Figure 5.8 Comparison of measured and predicted rutting of asphalt pavements

.

The local calibrated rutting transfer functions were validated through the two pavement sections, I-40 in Cumberland County and I-75 in Anderson County. The comparison of predicted and measured rutting was shown in Figure 5.9. It indicates that the local coefficients proposed above are proper for the rutting transfer functions.

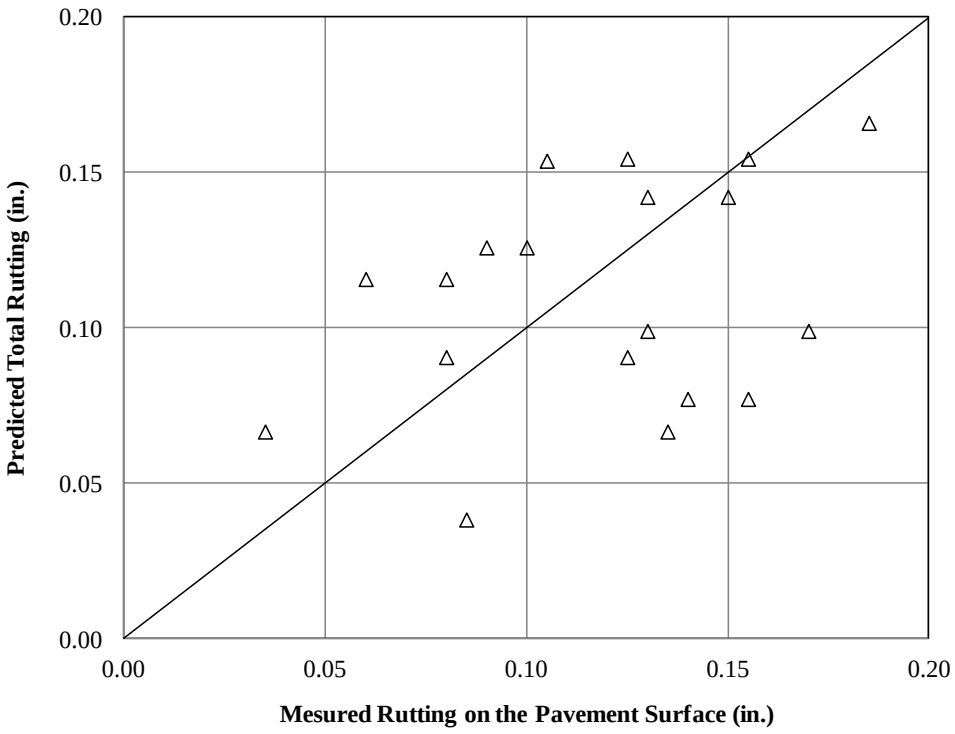

Figure 5.9 Predicted v.s. measured rutting on the pavement sections for validation

5.8 Conclusions

The local calibrations on the rutting transfer functions were conducted for Tennessee conditions. Sections from two main types of pavements, asphalt overlay on PCC pavements and asphalt overlay on asphalt pavements, were selected from PMS, as well as basic information and the measured rutting data. The local calibrations were conducted by minimizing the difference between the predicted and the measured rutting. The conclusions can be drawn as follows:

- It is found that the vertical compressive strains in asphalt layers from flexible pavements and from asphalt overlay on PCC pavements are varied from each

other. Individual local calibration is recommended on the each pavement structure on the rutting transfer function for asphalt layers.

- The current MEPDG should elaborately describe the variation of vertical compressive strain in asphalt layer, especially in the depth from 1in. to 3in. under surface from increasing sublayers during calculation in the rutting transfer function.
- The national calibrated rutting transfer function under predicted rutting of asphalt overlay on PCC pavements with low traffic, while over predicted the total rutting on the asphalt pavements.
- Local calibrations offered better agreements between the predicted and the measured rutting. The local coefficients for the two main types of pavements were summarized in Table 5.3.
- The measured data in PMS are very scattered, it is recommended that carefully data mining should be conducted prior to use.

Table 5.3 Local coefficients on the rutting transfer functions in Tennessee

Pavement Type		Asphalt Layer	Base	Subgrade
Asphalt Overlay on PCC Pavements	AADTT (0-1000)	β_{r1}=2.20, β_{r2}=1, β_{r3}=1	β_{BS}=0	β_{SG}=0
	AADTT (1000-2500)	β_{r1}=1, β_{r2}=1, β_{r3}=1	β_{BS}=0	β_{SG}=0
Asphalt Pavements		β_{r1}=1.33, β_{r2}=1, β_{r3}=1	β_{BS}=0.12	β_{SG}=0.68

5.9 References

Applied Research Associates, Inc. (2004). "NCHRP 1-37A: Guide for the Mechanistic-Empirical Design for New and Rehabilitated Pavement Structures." Transportation Research Board, Washington, DC.

Applied Research Associates, Inc. (2009). "NCHRP 1-40B: User Manual and Local Calibration Guide for the Mechanistic-empirical Pavement Design Guide and Software." Transportation Research Board, Washington, DC.

Applied Research Associates, Inc. (2011). "NCHRP 1-40D: Technical Assistance to NCHRP and NCHRP Project 1-40A: Versions 0.9 and 1.0 of the M-E Pavement Design Software." Transportation Research Board, Washington, DC.

Darter, M. I., Titus-Glover L., and Von Quintus, L. V. (2009). "Implementation of the Mechanistic-Empirical Pavement Design Guide in Utah: Validation, Calibration, and Development of the UDOT MEPDG User's Guide." Utah Department of Transportation Research Division.

Glover, L. T. and Mallela, J. (2009). "Guide for Implementing NCHRP 1-37a Design Procedures in Ohio: Volume 4-MEPDG Models Validation & Recalibration." Applied research Associates, Inc., the Ohio Department of Transportation, and Federal Highway Administration.

Jannant G., Yuan X.-X., and Shehata, M. (2013). "Local Calibration of MEPDG Distresses Models for Flexible Pavements Using Ontario's Long-Term PMS Data." Transportation Research Record, 2303.

Kang, M. and Adams T.M. (2007). "Local Calibration for Fatigue Cracking Models Used in the Mechanistic-Empirical Pavement Design Guide." Department of Civil and

Environmental Engineering. University of Wisconsin, Madison Proceedings of the 2007 Mid-continent Transportation Research Symposium, Ames, Iowa.

Khazanovich, L., Tompkins, D., Saxena, P., Harvey, J.T., and Wu, R. (2013). "Mechanistic-Empirical Pavement Design to Mitigate Rutting in Asphalt Overlays of Concrete Pavements Using MEPDG and CalME." Transportation Research Record, 3258.

Kim, Y. R., Jadoun, F. M., Hou, T., and Muthadi, N. R. (2007). "Local Calibration of the MEPDG for Flexible Pavement Design." Final report to the North Carolina Department of Transportation.

Li, J., Pierce, L. and Uhlmeyer, J. (2010). "Updating the Pavement Design Catalog for the Washington State Department of Transportation Using 1993 AASHTO Guide, mechanistic-Empirical Pavement Design Guide, and Historical Performance", Transportation Research Record, 2776, 124-129.

Li, J., Uhlmeyer, J.S., Mahoney, J.P., and Muench, S.T. (2009). "Calibration of the Flexible Pavement Portion of the Mechanistic-Empirical Pavement Design Guide for the Washington State Department of Transportation." Transportation Research Record, 2121, 73-83.

Mallela, J., Glover L.T., Darter M.I., Von Quintus, H., Gotlif. A., Stanley M., Suri Sadasivam. (2009). "Guidelines for Implementing NCHRP 1-37A M-E Design Procedures in Ohio: Volume 1- Summary of Findings, Implementation Plan, and Next Steps." Applied Research Associates, Inc. 100 Trade Centre Drive, Suite 200. Champaign, IL 61820.

Mamlouk, M.S. and Zapata, C.E. (2010) "Necessary Assessment of Use of State Pavement Management System Data in Mechanistic-Empirical Pavement Design Guide Calibration Process," Record Vol. 1, No. 2153, Journal of the Transportation Research Board, Washington, DC.

Schram, S., and Abdelrahman, M. (2006). "Improving prediction accuracy in mechanisticempirical pavement design guide." Rigid and Flexible Pavement Design, No. 1947, pp. 59-68 59-68.

Velasquez, R., Hoegh, K., Yut, I., Funk, N., Cochran, G., Marasteanu, M. and Khazanovich, L. (2009). "Implementation of the MEPDG for New and Rehabilitated Pavement Structures for Design of Concrete and Asphalt Paveemnts in Minnesota." Final Report to Minnesota Department of Transportation.

White, T.D., Haddock, J.E., Hand, A.J.T., and Fang, H. (2002). "contributions of Pavement Structural Layers to Rutting of Hot Mix Asphalt Pavements." National Cooperative Highway Research Program, Transportation Research Board, National Research Council, National Academy Press, Washington, D.C.

Zhou, C., Huang, B., Shu, X., and Dong., Q. (2013) "Validating MEPDG with Tennessee Pavement Performance Data."Journal of Transportation Engineering-Asce, Vol. 139, No. 3, 2013, pp. 306-312.

Von Quintus, H.L. and Schwartz, C.W. (2003). "Experimental Plan for Calibration and Validation of Hot Mix Asphalt Performance Models for Mix and Structural Design."National Cooperative Highway Research Program 9-30, National Research Council.

Von Quintus, H.L. (2013). "User Manual and Local Calibration Guide for the Mechanistic-Empirical Pavement Design Guide and Software." National Cooperative Highway Research Program 1-40B, National Research Council.

PART 6 SUMMARY AND FUTURE RESEARCH

6.1 Summary on Research Topics

This study is the start of the transition of pavement design in Tennessee from AASHTO 1993 to new MEPDG in Tennessee. A comprehensive literature review was firstly conducted to see the latest research on this transfer in other states. Key properties of several pavement materials that greatly influence pavement performance in MEPDG were studied through modeling and laboratory investigation. Then the MEPDG software version 1.1 with the national default values and national calibrated models was verified with the PMS database including pavement information and measured distresses/IRI data in Tennessee. Finally, the rutting transfer functions in MEPDG were calibrated and validated according to local conditions in Tennessee. Conclusions in this study were summarized as follows:

Concrete CTE values were found to be very sensitive to concrete pavement performance. A database for concrete CTE values in Tennessee was established through laboratory investigation. A concrete CTE prediction model was developed based on micromechanics and validated through laboratory test data. The differences between measured and predicted CTE values on cement paste and cement concrete are no more than 5% and 15%, respectively. The aggregate type was found to be the most important factor that affects concrete CTE while aggregate gradation slightly affects concrete CTE. With the water cement ratio varied from 0.32 to 0.44, the concrete CTE was found no obvious change.

A database of soil resilient modulus was established for MEPDG input Levels 1 and 2 utilizing the triaxial cyclic test results of fourteen soils in Tennessee. Because of the complexity and difficulty in laboratory approach, an alternate method was proposed to evaluate soil resilient modulus. The coefficients in the generalized model for soil resilient modulus were regressed from physical properties and validated. The impact of the seasonal variation of soil resilient modulus due to moisture change on pavement performance was investigated. And it was found that seasonal variation of soil resilient modulus greatly decreases fatigue life and increases rutting depth of asphalt pavements. It is recommended that the seasonal changes in soil resilient modulus and the coefficients of the generalized model should be covered in MEPDG software in pavement design and analysis.

Utilizing the PMS database in Tennessee, the national calibrated transfer functions in MEPDG were verified. It was found that the national default MEPDG overpredicts total rutting in asphalt pavements. Also traffic was found to be an important factor affecting predicted pavement roughness in MEPDG. The MEPDG design was relatively conservative for the design of low-traffic level highway pavements. MEPDG was not sensitive enough to reflect the variations in climate, traffic, and materials when predicting PSI for the some highway pavement sections in Tennessee.

The local calibrations on the rutting transfer functions were conducted for two main types of pavements, asphalt overlay on PCC pavements and asphalt overlay on asphalt pavements according to local conditions in Tennessee. It is found that the vertical

compressive strains in asphalt layers from flexible pavements and from asphalt overlay on PCC pavements are varied from each other. The current MEPDG should elaborately describe the variation of vertical compressive strain in asphalt layer, especially in the depth from 1in. to 3in. under surface from increasing sublayers during calculation in the rutting transfer function. The national calibrated rutting transfer function under predicted rutting of asphalt overlay on PCC pavements with low traffic, while over predicted the total rutting on the asphalt pavements. Local coefficients of rutting transfer functions were reached by minimizing the difference between the predicted and the measured rutting. Local calibrations were validated to offer better agreements between the predicted and the measured rutting. It is observed that the measured data in PMS are very scattered, carefully data mining is recommended prior to use.

6.2 Future Research

Since traffic was found to be a very important input that affects pavement performance prediction in MEPDG, the load spectrum information should be established in the main interstate highways in Tennessee through weigh-in-motion facilities.

The PMS database requires further data cleaning and modification. Information of distresses such as longitudinal cracking, fatigue cracking on asphalt pavements or faulting on concrete pavements were not available and should be collected in future. The gap of measured data before and after new measurement equipments adopted should be eliminated to keep the development of pavement distresses follows a reasonable trend.

In order to obtain a high confidence level on local calibrations, more pavement sections should be collected from PMS database and the recalibration should be carried out, especially when new version of MEPDG software is issued.

APPENDICES

Appendix A: Calibrated Parameters for PSI Curves

Contract No.	Location	Company	Compressive Strength (MPa)	Elastic Modulus (GPa)	CTE (10^{-6}/°C)	
			28d	28d	28d	60d
CNK 914	Harrison Oak Ridge	APAC	23.5	24.0	9.65	9.99
			23.6	23.1	9.32	9.54
			23.5	23.1	8.67	8.65
CNK 014	Morristown	IMI	19.7	18.6	10.74	7.61
			20.1	21.6	9.32	8.35
			20.4	19.6	9.74	8.34
CNK 811	Spring Hill	IMI	23.0	19.2	7.99	7.83
			19.4	19.3	7.04	6.43
			20.5	23.5	7.28	7.30
PIN# 113411.00	Nashville	IMI	21.2	18.5	6.68	7.03
			20.0	20.5	6.43	6.59
			25.0	21.5	6.30	6.14
CNK 067	Memphis	APAC	19.7	18.8	8.65	8.44
			20.5	20.6	8.81	8.79
			20.8	20.2	8.26	8.27
CNJ 232	Chattanooga	Sequatchie	20.1	19.8	10.04	-
			21.9	21.2	10.12	10.02
			20.7	20.6	10.26	9.32
CNK 244	Blountville	Summers Taylor	21.3	20.8	9.15	-
			20.5	18.9	8.59	8.53
			20.5	19.6	8.02	8.69
CNJ 060	Sparta	IMI	19.8	20.5	8.76	8.80
			20.6	21.2	8.57	8.62
			22.7	21.8	8.86	-

VITA

Changjun Zhou was born in China in 1983. He entered Harbin Institute of Technology, Harbin, China in 2003 and received his Bachelor's Degree in Civil Engineering in 2007. He studied as a master student in the School of Transportation Science and Engineering in Harbin Institute of Technology from 2007 to 2009, where his research interest concentrated on the pavement structure and materials and finite element analysis. Mr. Zhou entered the Department of Civil and Environmental Engineering in The University of Tennessee at Knoxville (UTK) to pursue the PH. D. degree in August 2010. During his stay in UTK, he extended his research area to material property modeling and pavement design and analysis.